

Mechanics of the Annulus Fibrosus Lamellae Under Physiologic Loading Conditions:
Do Interlamellar Connections Matter?

A DISSERTATION
SUBMITTED TO THE FACULTY OF
UNIVERSITY OF MINNESOTA
BY

Tina M. Nagel

IN PARTIAL FULFILLMENT OF THE REQUIREMENTS
FOR THE DEGREE OF
DOCTOR OF PHILOSOPHY

Victor H. Barocas, Adviser

September 2014

© Tina M. Nagel 2014

Acknowledgements

The past five years have been a journey developing my skills, experience, and self. I have crossed paths with so many influential people during this time; I am blessed for that.

Although ultimately I was unable to complete my main experiments with human tissue, cadaver tissue obtained from donors through the University of Minnesota Anatomy Bequest Program was instrumental in allowing me to accomplish my dissertation. From this amazing resource, I had access to some of the healthiest donor tissue available in the country. The dissection technique to accomplish this work required approximately two years of practice and as a result, numerous donated spines. Science aside, I was honored to learn from each and every donor. I want to thank each donor as well as their loved ones for pursuing donation for scientific advancement.

In place of human tissue, I used porcine tissue obtained from the University of Minnesota Visible Heart Lab, (VHL). Twice a week the VHL was generous to allow Amy and me (mostly Amy) to harvest the porcine spines. Their staff was always helpful to assist us.

To complete my mechanical and biochemical experiments, I received help from extremely knowledgeable University of Minnesota staff. After initial testing, I found that the current grips used for mechanical testing were insufficient. Conrad Lindquist worked with me to create an elegant, effective solution that continues to be used and developed. Sandy Johnson guided me through three biochemical assays over the course of a few

months. During that time, I honed my lab techniques, but I also had the opportunity to learn and spend time with someone that is wise in the lab and in life.

One of the reasons I joined the Victor Barocas lab (and the David Nuckley group) was because of the wonderful, supportive group members. Present and former members have been so supportive and helpful. Arin, thank you for teaching me so much in the cadaver lab space. Hallie, Colleen, Inka, and Rohit, I will miss sitting in the office with you (Spence, I still miss having you in the office). Hallie, thank you for being a great mentor and friend. I appreciated all the time you took to help me and provide advice in mechanical testing and so many other areas. Your presence really helped to push me to the end. Faisal and Victor Lai, I always appreciated your sage advice. Sara, without you teaching me the entire controls book in a semester, I would not have passed my qualifying exams. Sarah and Vahhab, I will miss chatting with you while working in the lab space. Mike, it was wonderful to have you as my right-hand man for four years. Thank you for your help dissecting and your hard work to get the lap modeling going. Amy and Julia, I will miss coming to chat with you in your corner. Amy, I have so enjoyed all of our time in the lab and out of the lab. It was always so great to have another lady who enjoyed working in the cadaver lab as much as I did. Thick and thin, we saw it together. I know you will do great things in orthopaedics, and I am proud to have shared this journey with you.

I need to thank my committee, especially Joan and Sue. I appreciated your support, insight, and guidance along the way. Sue, it was a pleasure and a great learning

experience to be a teaching assistant in your class. Joan, I appreciated our time at ORS each year, and your mentorship along the way.

I also need to thank Victor and David for their leadership and support. From the beginning, you took the time to mentor me academically and professionally. I appreciate that you let me discover research paths I was interested in and provided great insight into new directions. Victor, thank you for believing in me and taking me into the group, when I did not have a lab. David, thank you for the professional development and mentorship as well as the hours you spent assisting me in honing my dissecting technique.

I am so thankful to Jennifer, Kathryn, Kelsey, Bob, and everyone I saw biweekly on Fridays. You were instrumental in helping me to maintain and really learn how to take care of myself during stressful times. Without you, I would not have made it through.

As one of the first in my family to attend graduate school, these experiences have not been easy to explain, but Becki, you always understood with little explanation. You have always been there to listen, support, and provide advice. I knew I could always count on you.

My parents deserve the utmost thanks. They supported the engineer and scientist in me since I was just a little girl. I grew up being encouraged to have limitless goals. They also instilled in me the passion and drive to work hard in everything I do. In addition to their moral support, they were wonderful and understanding when I was on deadlines. I am so appreciative for the countless leftovers and free laundry.

Eric, you give me so much encouragement and support. Having you with me in the last portion of this journey has been crucial. I am extremely blessed to have you in my life.

Dedication

“Take pride in how far you have come and have faith in how far you can go.”

~Christian Larson

Eric, I dedicate this thesis to you. You provided me endless encouragement, for which I am eternally grateful.

Abstract

During healthy function, the spine provides the body with stability, strength, and flexibility. Unfortunately, spinal injuries such as annular tears are prevalent in human spines after age 10 (Boos et al. 2002), and at some point in their lives, about 75% of individuals experience low back pain (Andersson 1999). There are many hypotheses related to the origin of pain, but it is often attributed to injury and/or degeneration of the intervertebral disc (IVD) in the lower, lumbar spine (Andersson 1999). While the vertebral bodies are rigid structures, the IVD is a flexible, composite structure of two main components; the nucleus pulposus (NP) and the annulus fibrosus (AF), which is a fibrous structure that surrounds the NP with largely concentric layers containing highly aligned collagen fibers. There are connections that traverse between layers (C. A. Pezowicz, Robertson, and Broom 2006). The organization and composition of the lamellae allow the IVD and thus the spine to exhibit multi-axial motion including flexion, extension, and lateral bending, common to many activities of daily living.

The purpose of this dissertation was to assess the influence of the interlamellar connection through pre-failure and failure mechanics of discrete AF lamellae by creating a physiologically relevant test method to deform single and multiple AF lamellae and evaluate the kinetic response using a validated structural model.

Vertebral kinematics were quantified from human *in vivo* flexion. Average intervertebral strains were found to be symmetric during the flexion sequence but intervertebral angles were not, suggesting a physiologic decoupling of the two.

A structural model was validated for use to characterize AF lamellae. Through parameter sensitivity analysis and calculating confidence intervals of the fitted parameters, it was found that the fitted parameters were more robust when using both surface displacements and grip forces.

Single and multiple AF lamellae were characterized using the biaxial protocol generated from the analysis of vertebral kinematics. Single lamella samples produced significant in-plane shear force and moments, while multiple lamellae samples did not, after accounting for the number of lamellae. This suggests isolated single lamellae experience complex loading in biaxial tension but the AF as a whole reduces this response. Parameters fitted from the structural model were not statistically different between single and multiple lamellae samples.

This work suggests the interlamellar connection is mechanically significant in shear rather than a planar biaxial context. AF lamellae in shear were found to withstand significant displacement prior to failure as well as carry a non-zero load during the sliding phase. This response suggests a preventative feature within the AF region to resist and mitigate damage due to axial rotation. Although the model used was unable to characterize the shear stress of the experimental data in its present form, further improvements to the model such as more anatomically accurate interlamellar layer may improve the capabilities of the model.

The work accomplished in this dissertation forms a base for further assessment of discrete AF lamella(e) and interlamellar connections. Using porcine tissue, experiments performed within Chapters 4 and 5 should be continued to increase the sample size and

strengthen possible trends seen within this work. With these tools, these experiments should also be performed with a larger sample size using healthy human cadaver tissue. It would also be interesting to use these tools to assess human cadaveric tissue from the degenerative spectrum. The shear testing showed the interlamellar connection to be mechanically significant in that context, but the test configuration as well as the simplistic modeling did not elucidate whether this mechanical significance originates from a fibrous connection or a matrix material. Further testing and modeling should work towards determining the connection to attribute the mechanical significance.

Table of Contents

Acknowledgements.....	i
Dedication.....	v
Abstract.....	vi
List of Tables.....	x
List of Figures.....	xi
List of Abbreviations and Parameter Definitions.....	xiii
Chapter 1 – Introduction.....	1
Chapter 2 – Characterization of <i>in vivo</i> vertebral kinematics in flexion.....	10
Chapter 3 – Structural model verification and validation.....	25
Chapter 4 – Assessing discrete annulus fibrosus lamellae using physiologic loading.....	43
Chapter 5 – Assessing mechanical interlamellar interaction via shear lap.....	62
Chapter 6 – Conclusions and Future Work.....	78
Bibliography.....	81
Appendices.....	95
Appendix A – Directions for structural model use.....	95
Appendix B – Directions For Biaxial Annulus Fibrosus Lamella(e) Sample Dissection.....	165
Appendix C – Directions for use of JR3 load cells.....	170
Appendix D – Quantitative T2* (T2 star) Relaxation Times Predict Site Specific Proteoglycan Content and Residual Mechanics of the Intervertebral Disc Throughout Degeneration.....	192

List of Tables

Table 1.1. Intervertebral Kinematic Literature (<i>in vitro</i> Testing Conditions)	6
Table 1.2 Intervertebral Kinematic Literature (<i>in vivo</i> Testing Conditions)	7
Table 2.1. Subject Demographics	20
Table 2.2. Description of Vertebral Calculations	21
Table 3.1. Tissue Characteristics and Testing Protocols	36
Table 3.2. Representative Experiment Parameter Values	36
Table 4.1. Biochemical and Mechanical Data	53
Table 5.1. AF Lap Strength Summary Data	71

List of Figures

Figure 1.1. Spinal Anatomy (Adapted from “3D Spine, Primal Interactive Human, Anatomy.tv”)	8
Figure 1.2. Image of Representative Interlamellar Connection Cross-Section (Adapted from (C. A. Pezowicz, Robertson, and Broom 2006)	9
Figure 2.1. a. Representative Fluoroscopic Frame with Labeled Anatomy. Vertebral margin points labeled with circles (representative origin at the superior, posterior point of S1), and computed angles shown. b. Representative profile of the Lower Lumbar Angle as a Function of Position, Raw Points and Filtered Data	22
Figure 2.2. Peak Green Strains on the Anterior and Posterior Margins	23
Figure 2.3. Intervertebral Margin Motion Decoupled into Anterior –Posterior Translation and Axial Displacement	23
Figure 2.4. Average Posterior Margin Green Strains in Flexion and Extension Phases ..	23
Figure 2.5 Intervertebral Angle Contribution During Flexion and Extension (filtered using a low-pass Butterworth filter with a cutoff frequency of 250 Hz)	24
Figure 3.1. Lamella of the Annulus Fibrosus	37
Figure 3.2. Sensitivity of Force (F) and Displacement (U) Error to Model Parameters ...	38
Figure 3.3. Parameter Error Using Simulated Data Perturbed with White Gaussian Noise	39
Figure 3.4. Representative Experiment Grip Force Data Fitted with the Simple Structural Model	40

Figure 3.5. Representative Experiment Parameter Estimates with Each Fitting Approach Based on the Ratio of Parameter Value to the Width of the Confidence Region (CR)	41
Figure 4.1. Dissection and Testing of Annulus Fibrosus Lamellae	54
Figure 4.2. Single Annulus Fibrosus Lamella Behavior	55
Figure 4.3. Single Annulus Fibrosus Lamella Force Behavior Separated Into Axial and Circumferential Axes	56
Figure 4.4. Mechanical Properties of Annulus Fibrosus Lamellae in Loading Conditions Based on Flexion	57
Figure 4.5. Single Annulus Fibrosus Lamella Shear Force Behavior	58
Figure 4.6. Single Annulus Fibrosus Lamella In-Plane Moment Behavior	59
Figure 4.7. Representative Single Annulus Fibrosus Lamella Experimental and Modeled Surface Displacements	60
Figure 4.8. Multiple Annulus Fibrosus Lamellae Behavior – Experiment and Predicted Model from Single Lamella Data	61
Figure 5.1. Shear Lap Sample Geometry	72
Figure 5.2. FEBio Representative Mesh Geometry	73
Figure 5.3. Representative Shear Lap Load Curve	74
Figure 5.4. Representative Shear Lap Surface During Experiment	75
Figure 5.5. Shear Lap Surface Displacements at Maximum Strain Prior to Failure	77

List of Abbreviations and Parameter Definitions

Abbreviations¹

A	Anterior
AF	Annulus Fibrosus
BOTH	Finite element modeling compared to force and displacement data
DISP	Finite element modeling compared to displacement data alone
FORCE	Finite element modeling compared to force data alone
I	Inferior
IVD	Intervertebral Disc
L3-L4	Motion segment between lumbar vertebrae 3 and 4
NP	Nucleus Pulposus
P	Posterior
S	Superior

Parameter Definitions¹

A	Fiber stiffness (N/mm)
B	Fiber non-linearity
κ	Spread of fiber distribution
θ	Mean fiber alignment (°)

¹ This list is not intended to be exhaustive.

Chapter 1 – Introduction

During healthy function, the spine provides the body with stability, strength, and flexibility along its entire length, anatomically defined by three regions: cervical, thoracic, and lumbar. Unfortunately, spinal injuries such as annular tears are prevalent in human spines after age 10 (Boos et al. 2002), and at some point in their lives, about 75% of individuals experience low back pain (Andersson 1999). The related health care costs represent an immense economic burden (Gore et al. 2012). There are many hypotheses to the origin of pain, but it is often attributed to injury and/or degeneration of the intervertebral disc (IVD) in the lower, lumbar spine (Andersson 1999), as described below.

The spine is a series of joints, or motion segments, consisting of a vertebral body, intervertebral disc, and adjacent vertebral body, Figure 1.1. While the vertebral bodies are rigid structures, the IVD is a flexible, composite structure of two main components; the nucleus pulposus (NP) resides in the center as a gelatinous, pressurized region that distributes compressive loading, and the annulus fibrosus (AF) is a fibrous structure that surrounds the NP with largely concentric layers containing highly aligned collagen fibers,

oriented at $\pm 30^\circ$ from the horizontal. The AF is composed largely of Type I collagen, water, and proteoglycans (e.g. Brickley-Parsons and Glimcher 1984; P. Adams and Muir 1976). The biochemical composition varies more strongly radially than circumferentially (Skaggs et al. 1994). An anatomical study has shown that by placing lamellae in radial tension physical interlamellar connections appear. Figure 1.2 shows a representative interlamellar connection. The organization and composition of the lamellae allow the IVD and thus the spine to exhibit multi-axial motion including flexion, extension, and lateral bending common to many activities of daily living.

Whole Spine Kinematics

Kinematics of the lumbar vertebrae have been well studied in flexion (Tables 1.1-2). Cadaveric and *in vivo* experiments typically report segmental rotation (Gatton and Percy 1999; Hayes et al. 1989; Allison M. Kaigle, Holm, and Hansson 1997; A M Kaigle, Wessberg, and Hansson 1998; M. Percy, Portek, and Sheperd 1984; Kanayama et al. 1996; Okawa et al. 1998; Takayanagi et al. 2001; Teyhen et al. 2007), with a few experiments also reporting intervertebral strains (Stokes 1987; O'Connell, Vresilovic, and Elliott 2011; M. J. Percy and Tibrewal 1984). Takayanagi *et al.* (Takayanagi et al. 2001) took fluoroscopic video of healthy males performing flexion. They reported intervertebral margin anterior-posterior translation and segmental angular rotation but not segmental intervertebral margin strains or segmental axial displacement, leaving an incomplete assessment of segmental intervertebral strains. Another study took radiographs of healthy subjects at neutral and full flexion to calculate disc margin strains (M. J. Percy and Tibrewal 1984). With only the endpoints of motion examined, the complex motion of the IVD throughout flexion was neglected. To date, the full pathway

of lumbar kinematics and intervertebral deformation throughout flexion has not been reported.

Motion Segment Kinematics

Stemming from the multi-axial usage of the spine, the IVD as a whole has been characterized along multiple axes. The IVD has been well characterized *in vitro* within the motion segment in multiple different loading configurations such as flexion-extension (M.A. Adams and Dolan 1991), axial compression (Nachemson, Schultz, and Berkson 1979; Shea et al. 1994; Beckstein et al. 2008), and torsion (Elliott and Sarver 2004; Abumi et al. 1990; Haughton et al. 2000; Beckstein, Espinoza Orias, and Cloyd 2007). Testing in modes relevant to activities of daily living has elucidated the viscoelastic nature of the IVD as well as the limits of healthy motion.

Multiple Lamellae Kinetics

The multi-axial response of the AF tissue is less well understood. Extensive work has been performed to understand multiple AF lamellae in uniaxial tension (Ebara et al. 1996; Acaroglu et al. 1995; Fujita, Duncan, and Lotz 1997; Guerin and Elliott 2006; Huyghe and Drost 2004; Malgorzata and Pezowicz 2013), but much less work has been performed to understand multiple AF lamellae in biaxial tension (O'Connell et al. 2010; Gregory and Callaghan 2011) to replicate multi-axial loading *in vivo*. The biaxial studies showed that the AF produces a nonlinear, anisotropic response, where the response of the circumferential direction is 1-2 orders of magnitude larger than the axial direction. To understand better the response of the annulus and the interlamellar connections, excised annulus fibrosus tissue has been tested extensively in shear. One previous study (Fujita et

al. 2000) has examined blocks of AF in shear and found the shear modulus was regionally dependent. Another study (Gregory et al. 2011) examined the interlamellar connections and shear directly by dissecting lamellae to the shear lap geometry: two adjacent lamellae delaminated with the exception of the lap region, which maintains their physiologic attachment. Gregory *et al.* dissected annulus from porcine cervical spines, tested, and analyzed the data using a 1-D model, which demonstrated the mechanical importance of the interlamellar connections.

Single Lamella Kinetics

At the single lamella scale, some work has been performed in uniaxial tension (Skaggs et al. 1994; Holzapfel et al. 2005; Gregory and Callaghan 2011; C. Pezowicz 2010) and less in biaxial tension (Bass et al. 2004; Gregory and Callaghan 2011). This testing also showed single AF lamella to have a nonlinear, anisotropic response, but it was found that uniaxial testing was not sufficient to predict biaxial behavior, which produced much higher stresses. Tensile properties were also found to vary more strongly radially, likely due to structural and biochemical differences. The aforementioned work used human cadaveric as well as porcine lumbar IVDs. Due to limited availability of healthy, human cadaveric spines, porcine spines provide a suitable alternative anatomically (Busscher, Ploegmakers, et al. 2010) and biomechanically (Busscher, van der Veen, et al. 2010), acknowledging that the functional demands on the porcine spine are very different from those on the human spine due to their quadruped gait. Further biaxial testing of single and multiple AF lamellae is necessary to understand the multi-axial function of the multi-scale structure that is the IVD. The fibers in AF lamellae are

anisotropic and aligned off-axis, so biaxial tension such as in the *in vivo* stress state could generate an in-plane shear force and moment within a lamella from the resistance to fiber rotation.

The spine is a largely mechanical system which allows activities of daily living to be possible but is also susceptible to injury, thus physiologic mechanical testing in pre-failure and failure modes is crucial to gain a better understanding of the AF harvested from the IVD. To do so, this dissertation aims to assess the influence of interlamellar connections of discrete AF lamellae by:

- 1) Generating a test method that replicates an activity of daily living in AF lamellae by quantifying *in vivo* lumbar vertebral kinematics (Chapter 2),
- 2) Verifying and validating a structural model to describe and quantify planar lamellar mechanics obtained from biaxial testing (Chapter 3),
- 3) Quantifying single and multiple AF lamellae kinetics using the physiologically relevant test method obtained in Chapter 2 and the structural model from Chapter 3 (Chapter 4), and
- 4) Quantifying AF lamellae kinetics in the shear lap geometry to understand the delamination failure mode and mechanical interlamellar interaction (Chapter 5) through surface strains and finite element modeling.

Table 1.1. Intervertebral Kinematic Literature (*in vitro* Testing Conditions)

Method	Data Type ^a	Motion Segment(s)	Motion Type	Data Reported	Reference
Digital Strain Indicators	C	L1-L5	Flexion (eccentric compression)	Load – deflection curves	(Lin, Liu, and Adams 1978)
Stereophotogrammetry	C	T12-L5	Flexion/ Extension (6.5°, eccentric compression)	Surface fiber strains	(Stokes 1987)
Magnetic Resonance Imaging	E	L3-L5	Flexion (5°, eccentric compression)	Axial, radial, and shear strains	(O’Connell, Vresilovic, and Elliott 2011)

^aC = Continuous Data Collection, E = Data Collected at Motion Endpoints

Table 1.2 Intervertebral Kinematic Literature (*in vivo* Testing Conditions)

Method	Data Type ^b	Motion Segment(s)	Motion Type	Data Reported	Reference
External Three-Dimensional Position Sensors	C	L1-S1	Standing Flexion	Proportion of inter sensor angle	(Gatton and Percy 1999)
Lateral Radiographs	E	L1-S1	Standing Full Flexion/ Full Extension	Anterior and posterior disc height changes	(M. J. Percy and Tibrewal 1984)
	E	L1-S1	Sitting Full Flexion/ Full Extension	Segmental angle and anterior-posterior translation	(Hayes et al. 1989)
Neutral Lateral Radiograph, Displacement Transducers, and a Potentiometric Goniometer	C	L3-L4	Prone Flexion (60°)/ Extension (50°)	Segmental angle, anterior-posterior translation, and axial displacement	(Allison M. Kaigle, Holm, and Hansson 1997) ^c
	C	L2-L5	Standing Full Flexion/ Full Extension	Same as (Allison M. Kaigle, Holm, and Hansson 1997)	(A M Kaigle, Wessberg, and Hansson 1998)
Biplanar Fluoroscopy	C	L1-S1	Standing Full Flexion/Full Extension	Same as (Allison M. Kaigle, Holm, and Hansson 1997)	(M. Percy, Portek, and Sheperd 1984)
Single Plane Fluoroscopy	C	L3-S1	Standing Full Flexion/ Full Extension	Same as (Hayes et al. 1989)	(Kanayama et al. 1996)
	C	L2-L5	Standing Flexion	Segmental angle	(Okawa et al. 1998)
	C	L2-S1	Sitting Flexion	Same as (Hayes et al. 1989)	(Takayanagi et al. 2001)
	C	L3-S1	Standing Flexion	Segmental angle	(Teyhen et al. 2007)
	C	L3-S1	Standing Full Flexion (29°)	Proportion of segmental angle and margin anterior-posterior translation and axial Green strains	Present Study

^bC = Continuous Data Collection, E = Data Collected at Motion Endpoints

^cDomestic pigs used

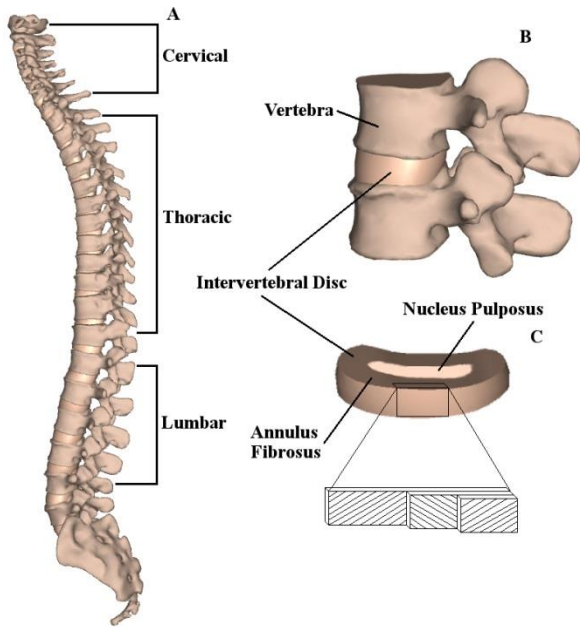


Figure 1.1. Spinal Anatomy (Adapted from “3D Spine, Primal Interactive Human, Anatomy.tv”). A. Sagittal plane vertebral column. B. Motion segment. C. Intervertebral disc with exploded annulus fibrosus lamellae. Collagen fiber bundles alternate at $\pm 30^\circ$ from the horizontal between lamellae.

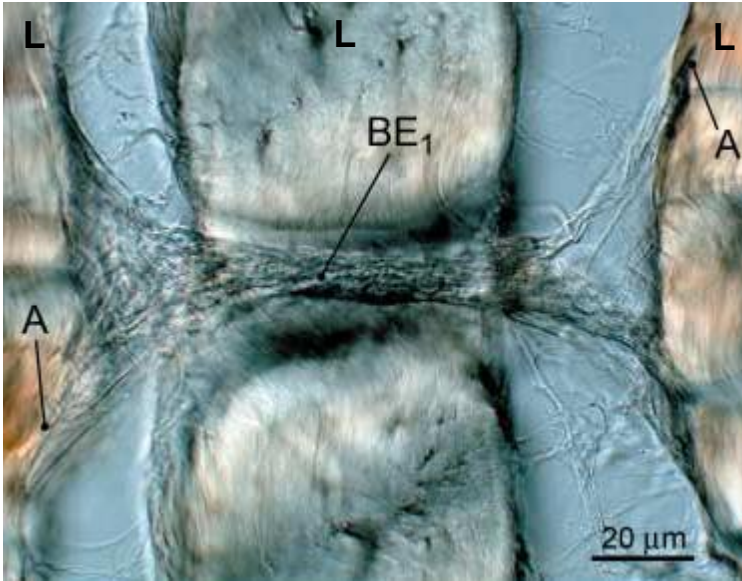


Figure 1.2. Image of Representative Interlamellar Connection Cross-Section (Adapted from C. A. Pezowicz, Robertson, and Broom 2006). Lamellae were placed in radial tension to visualize the interlamellar connection (BE₁). Cross-sections of three lamellae are shown and labeled (L). In this case, the interlamellar connection traverses through a lamella connecting three adjacent lamellae (A).

Work described here is reprinted with permission.

Nagel et al. "Quantification of Continuous in vivo Flexion-Extension Kinematics and Intervertebral Strains" European Spine Journal. 2014. 23. 754-761.

Chapter 2 – Characterization of *in vivo* vertebral kinematics in flexion

Introduction

Much work has been done *in vitro* to characterize the disc mechanically, both whole sample and isolated annulus fibrosus / nucleus pulposus (Nachemson, Schultz, and Berkson 1979; Skaggs et al. 1994; Iatridis et al. 1997). The annulus has been tested at strains ranging from 2.5 to 50% in uniaxial tension (Skaggs et al. 1994; Ebara et al. 1996; Fujita, Duncan, and Lotz 1997; Elliott and Setton 2001; Wagner and Lotz 2004; Holzapfel et al. 2005; Guerin and Elliott 2006) and from 1.25 to 15% in equibiaxial extension (Bass et al. 2004; O'Connell, Sen, and Elliott 2012). The wide range of strains utilized in these experiments makes the results difficult to interpret within a functional context. Furthermore, incorporating physiologic strains into tissue testing would ensure the clinical relevance of materials testing of the intervertebral disc.

Ideally, physiologic strains would be determined from *in vivo* three-dimensional kinematics of intervertebral discs during activities of daily living, such as spinal flexion. MRI is capable of visualizing soft tissue but does not allow for real time scans during subject movement. Fluoroscopy can image in real time but cannot detect soft tissue and is

constrained by patient radiation exposure limits. Due to these imaging limitations, physiologic disc annulus fibrosus strains have not been reported in the lumbar spine literature. Many studies have focused on planar vertebral motion, using adjacent vertebrae as approximations of intervertebral disc margins, as discussed previously (Chapter 1).

Therefore, the objective of this study was to characterize the *in vivo* kinematic response of lower lumbar motion segments and intervertebral margin strains throughout a flexion cycle.

Materials and Methods

Fifteen healthy volunteers were recruited to perform flexion, which was captured by fluoroscopic video. This study was exempt from IRB approval as a category 4 study. Subjects were excluded for musculoskeletal disease, abdominal or pelvic surgery, low back pain in the previous three years, or an Oswestry Disability Index above 5%. Sex, age, and body mass index (BMI) of subjects are shown in Table 2.1.

Subjects, having been placed in a device to fix the pelvis, were instructed to practice bending forward as far as possible and returning to neutral at least three times. Then, the subjects were imaged performing flexion and extension. Sagittal images of the lumbar spine (L3-S1) were recorded continuously during flexion at 30 Hz using digital fluoroscopic video (12 inch image intensifier, OEC 9800 GE, Fairfield, CT).

The fluoroscopic videos were randomized, and all data were analyzed by a single investigator. Six data sets were removed due to indistinct anatomy. Video frames were analyzed at 10 Hz using Image J (NIH, Bethesda, MD) to take the pointwise

measurements shown on the vertebral margins in Figure 2.1A. The data were then analyzed using Matlab (Mathworks, Natick, MA) following the methods of Takayanagi *et al.* (Takayanagi et al. 2001). Briefly, pointwise measurements were used to create local coordinate systems with the origin at the point $(p_{x_{S,P}}, p_{y_{S,P}})$ for each motion segment (L3-L4, L4-L5, and L5-S1). The origin represents the most superior (S) and posterior (P) point on the inferior vertebra of the motion segment. This local coordinate system was then used to calculate the lower lumbar angle, anterior and posterior margin strain, axial displacement, anterior-posterior (A-P) translation, and intervertebral angle as described in Table 2.2. A low-pass Butterworth filter with a cutoff frequency of 2 Hz was applied to the calculated data, as shown in Figure 2.1B.

In this work, Green strain was used rather than linearized strain, often used for bone and other small-deformation systems. The Green strain is commonly used in soft-tissue biomechanics (see, e.g.(O’Connell et al. 2007; Bass et al. 2004; Michalek, Gardner-Morse, and Iatridis 2012)) to quantify deformation due to its independence from rigid body rotation. The linear strain (i.e., $(l - L)/L$, where l is the final and L is the initial length) has non-zero rigid body rotation; if the rigid body rotations are small, linear strain remains similar to the Green strain. However, if rigid body rotations are not small, the linear strain becomes an inaccurate measure, and the Green strain must be used. The Green strain is given by

$$GS = \frac{1}{2} \left(\frac{l^2 - L^2}{L^2} \right) \quad (1)$$

In the limit of small deformations and rotations, the Green strain becomes identical to the linear strain.

Statistical analysis was performed using two-tailed independent sample t-tests which assumed equal variances. Observer error was estimated by calculating the standard deviation between intervertebral angles calculated by four observers using one segment from one subject in a single frame.

Results

The peak flexion range-of-motion across L3-S1 was $29 \pm 2.9^\circ$, and the local segmental peak angular displacements were $6.1 \pm 1.5^\circ$ (L3-L4), $9.0 \pm 2.1^\circ$ (L4-L5), and $7.3 \pm 1.1^\circ$ (L5-S1) (mean \pm 95% CI). The local segmental angular displacements do not sum to the flexion range-of-motion across L3-S1, because each measurement was taken at its local maximum, which do not necessarily correspond with peak global flexion range-of-motion, as shown in (Kanayama et al. 1996).

In flexion, posterior intervertebral strains were tensile (+) in nature and those on the anterior margin were compressive (-). L4-L5 had the largest anterior and posterior intervertebral margin strains, -29% and 65% respectively, which was significantly larger than the posterior margin strain at L5-S1, 29% ($p < 0.001$, Figure 2.2). The smallest anterior and posterior intervertebral margin strains occurred at L5-S1, -24% and 29% respectively. It is emphasized that these results are *margin* strains, that is changes in the bone-to-bone distance along the anterior or posterior margin, not actual intervertebral disc strains; the intervertebral margin strains may be interpreted as an upper bound on the intervertebral disc strains.

As expected, at the superior vertebra of each motion segment, flexion involved anterior and inferior displacement of the anterior margin and anterior and superior displacement of the posterior margin. Decomposing the intervertebral margin

displacement into A-P translation and axial displacement showed that displacements varied by level (Figure 2.3). The L4-L5 anterior intervertebral margin produced the greatest axial displacement (compression). At the posterior margin, L4-L5 produced the most axial displacement (tension) which was significantly larger than L5-S1 level ($p < 0.001$). Furthermore, the L3-L4 spinal level produced posterior margin axial displacements that were significantly larger than L5-S1 ($p = 0.008$). Posterior margin A-P translation accounted for about a third of the decomposed motion at L3-L4 and L4-L5.

The posterior margin Green strains were averaged across the nine subjects and fitted with 4th order polynomials, as shown in Figure 2.4. Across the flexion phase, L3-L4 and L5-S1 displayed similar strains, but L4-L5 produced larger strains, culminating in strains four times larger than the other two segments measured.

Intervertebral angle contributions to the summed L3-S1 segment angular displacement were averaged across the nine subjects and filtered with a low-pass Butterworth filter with a cutoff frequency of 250Hz (Figure 2.5). In the early flexion phase, L3-L4 contributes the largest amount, followed by L4-L5. As the flexion phase progresses, the contribution from L4-L5 and L5-S1 increase. At full flexion, L4-L5 contributes the largest amount to the total amount of angular displacement, 37%. At the start of the extension phase, L5-S1 continues to increase in contribution. At 30% extension, L5-S1 begins to contribute less and L3-L4 more. These spinal levels also exhibited a different peak contribution time throughout the flexion-extension sequence where the median peak contribution of each segmental angle to the sum of the segmental angles is: L3-L4, 89% α , L4-L5, 98% α , L5-S1, 100% α . This pattern has been seen in previous flexion literature (Kanayama et al. 1996). However, the data herein illustrate

angle contributions which are not symmetric about the full flexion point (100% α).

Extracting data at $\pm 70\%$ α showed significant differences in the L3-L4 A-P translation ($p = 0.032$) and L4-L5 posterior margin strain ($p = 0.021$), axial displacement ($p = 0.022$), and A-P translation ($p = 0.038$).

Interobserver error was estimated by calculating the standard deviation of the measured segmental angle in one sample by four observers. This standard deviation was small, 2.81° with respect to the magnitude of the angular displacement measured (9.77°).

Discussion

This work identified the time history of Green strains across lumbar vertebrae throughout a flexion extension cycle to upright standing. These strain profiles demonstrate the relative strains which presumptively affect the intervertebral disc tissues during a physiologic motion. These data also illustrate the natural human variability between spinal levels and between healthy subjects. To contextualize the results herein, other research efforts aimed at uncovering the intervertebral strains will be examined and compared.

Pearcy and Tibrewal (M. J. Pearcy and Tibrewal 1984) reported percentage changes in disc height on the anterior and posterior margins at the full flexion endpoint. Calculating the Green strains from their published data shows that the data of the present study are similar. On the posterior margin, L4-L5 had 69% Green strain (present study 65%), and L5-S1 had 39% Green strain (present study 29%), with the exception of the L3-L4 which is lower, 51% and 71% respectively. Differences could be the product of Pearcy and Tibrewal's use of an all-male population and/or differences in the magnitude of lower lumbar angle, which was not reported in Pearcy and Tibrewal.

More recently, Takayanagi *et al.* (Takayanagi et al. 2001) reported segmental angular displacement and segmental anterior-posterior translation in flexion-extension. The present study found these outcomes to be similar among levels as opposed to being larger at L3-L4 and L4-L5. Both measurements were similar in L3-L4, 6.5° and 3.2 mm (present study 6.1° and 3.0 mm), and larger in L4-L5, 4.8° and 2.3 mm (present study 9.0° and 3.6 mm), and L5-S1, 2.5° and 0.5 mm (present study 7.3° and 3.2 mm). The present study produced larger magnitudes likely due to subjects starting in a standing rather than seated position.

Additional studies have reported segmental angular displacement. Teyhen *et al.* (Teyhen et al. 2007) reported segmental angular displacements as a percent of maximum segmental angular displacement at 35% of total flexion. The present study found similar trends but larger magnitudes. Okawa *et al.* (Okawa et al. 1998) reported segmental angular displacement as the angle from the inferior surface of the vertebrae from the horizontal. Reporting the present study data with this method finds similar trends but again larger magnitudes. These studies (Teyhen et al. 2007; Okawa et al. 1998) do not report flexion range-of-motion, so it is possible that the present study flexion range-of-motion was higher.

The present study found intervertebral margin motion was mainly composed of axial displacement, but a significant amount of motion was produced by anterior-posterior translation. This result agrees with previous literature (A M Kaigle, Wessberg, and Hansson 1998), which found 4 mm of anterior-posterior translation on average when considering L2-L5. The present study found 3.27 mm of anterior-posterior translation on average considering L3-S1. This result also agrees with (M. Pearcy, Portek, and Sheperd

1984), which found 2 mm (L3-L4), 2 mm (L4-L5), and 1 mm (L5-S1) of anterior-posterior translation at the centroid and with (Hayes et al. 1989), which found 2.5 mm (L3-L4), 3.0 mm (L4-L5), and 1.3 mm (L5-S1) of anterior-posterior translation at the centroid averaged for flexion and extension. The present study found 2.98 mm (L3-L4), 3.63 mm (L4-L5), 3.21 mm (L5-S1). The present study found higher magnitudes than in (Hayes et al. 1989), as a result of measuring subjects in standing rather than sitting flexion, and in (M. Pearcy, Portek, and Sheperd 1984) which does not report flexion range-of-motion, so again, it is possible that the present study flexion range-of-motion was higher.

Furthermore, the sum of the decomposed motion, axial displacement and anterior-posterior translation, was larger on the anterior margin than the posterior margin. This result is likely due to the posterior elements that resist flexion: supraspinous and infraspinous ligaments, the facet capsular ligaments, and the ligamentum flavum. There is no resistance on the anterior margin to flexion.

The average posterior margin Green strains had the largest magnitude at L4-L5 in the flexion phase. L3-L4 and L5-S1 had similar margin Green strains throughout the flexion phase. The pattern follows published magnitudes of segmental rotation in flexion, where L4-L5 is the largest, $15.3 \pm 1.6^\circ$, then L5-S1, $12.5 \pm 1.9^\circ$, then L3-L4, $9.8 \pm 3.5^\circ$ (Kanayama et al. 1996).

The intervertebral angle contributions to the summed L3-S1 segment angular displacement followed the same patterns during spinal flexion but displayed hysteresis over the course of the returning extension movement. In flexion, L3-L4 made the dominant contribution, then L4-L5, then L5-S1. This result agrees with previous literature

(Gatton and Pearcy 1999). A-P translation, posterior margin strain, and axial displacement compared between the flexion and extension phases suggest that the kinematic response of the flexion phase is different from the extension phase. Differences between the flexion and extension phases have been previously reported in *in vitro* studies through the neutral zone parameter [e.g., 24]. The intervertebral angles displayed a non-symmetric response between flexion and extension, which is also visible in other measurements at L3-L4 and L4-L5. Interestingly though, the average posterior margin Green strains were symmetric about the full flexion point revealing a decoupling of margin strains and angular displacements.

Typical human subject and sample size limitations must be considered when digesting the results of this study. Only 2D sagittal plane fluoroscopic images were captured, which likely led to errors based upon the 3D nature of spinal motion. Furthermore, intervertebral disc margins were not visible on the fluoroscopic images. As a result, at the neutral position, pre-strain on the anterior margin and slack on the posterior margin could not be assessed. Our results must therefore be viewed as relative to neutral position rather than relative to the unloaded state of the tissue (see further discussion of this issue in (M.A. Adams and Hutton 1986)).

The challenge of placing margin points on the same segment across the course of the flexion movement created some within subject errors. The pelvis of each subject was fixed, but it is possible that the data included some out of plane motion. As each subject performed flexion, anatomical features of the vertebral margins moved in and out of view, which at times created difficulty in choosing the same margin point. Although all

subjects reported to be in good health, it is possible that varying levels of disc health were represented in the sample.

Conclusion

The L4-L5 spinal unit exhibited the largest amount of anterior and posterior margin strain. The presumptive strains in the intervertebral disc during *in vivo* lumbar flexion are due to segmental angular rotation and linear translations, which together represent physiologic intervertebral disc loading. Peak intervertebral angular displacement occurred at approximately 75% of the total segment (L3-S1) motion, during the extension phase. As the Green strains across the intervertebral margins are symmetric about the flexion-extension activity and the angles are not, these two measures appear physiologically decoupled. As a result, x-rays at the end points of the flexion-extension motion do not capture the complexity of intervertebral motion. From an engineering perspective, the strain data gives an approximation of the physiologic strains which could be used to evaluate intervertebral disc replacements and other therapies. In addition, non-symmetric loading should be considered in segment testing.

Table 2.1. Subject Demographics

Subject #	Age	Sex	BMI
1	32	M	22
2	38	M	24
3	18	F	25
4	22	M	26
5	21	M	25
6	29	F	26
7	26	F	22
8	48	F	27
9	46	M	27
10	23	F	26
11	21	M	23
12	19	M	26
13	36	F	30
14	18	F	29
15	19	M	28

Table 2.2. Description of Vertebral Calculations^a

Name	Description	Calculation
Anterior margin, \mathbf{D}_A	Anterior margin vector.	$(px_{S,A} - px_{I,A}, py_{S,A} - py_{I,A})$
Posterior margin, \mathbf{D}_P	Posterior margin vector.	$(px_{S,P} - px_{I,P}, py_{S,P} - py_{I,P})$
Superior x-axis, \mathbf{x}_S	Superior x-axis vector with origin at $(px_{S,P}, py_{S,P})$.	$(px_{S,P} - px_{S,A}, py_{S,P} - py_{S,A})$
Superior y-axis, \mathbf{y}_S	Superior y-axis vector with origin at $(px_{S,P}, py_{S,P})$.	$[0,0,1] \times \mathbf{x}_S$
Inferior x-axis, \mathbf{x}_I	Inferior x-axis vector with origin at $(px_{S,P}, py_{S,P})$.	$(px_{I,P} - px_{I,A}, py_{I,P} - py_{I,A})$
Superior distance, D_S	Magnitude of superior x-axis vector.	$\ \mathbf{x}_S\ $
Lower lumbar angle, α	Calculated as the angle between the inferior L3 and superior S1 vertebral margin points.	$\cos^{-1}(\mathbf{x}_{S,S1} \cdot \mathbf{x}_{I,L3})$
Disc margin angle, β	Calculated as the angle between the inferior and superior vertebral margin points of the given motion segment.	$\cos^{-1}(\mathbf{x}_S \cdot \mathbf{x}_I)$
Margin height, \mathbf{d}_u	Calculated as the distance between the inferior and superior vertebral points of the given margin (anterior or posterior) of a motion segment.	$(px_S - px_I, py_S - py_I)$
Margin strain	Calculated as the Green strain using the neutral margin height as the original length and the minimum anterior margin height as the deformed length.	$0.5 * ((\mathbf{d}_{u,current}^2 - \mathbf{d}_{u,neutral}^2) / \mathbf{d}_{u,neutral}^2)$
Axial displacement	Calculated as the distance moved perpendicular to the superior margin of the inferior vertebra relative to the average disc margin height.	$\mathbf{d}_u \cdot \mathbf{y}_S$
Anterior-Posterior (A-P) displacement	Calculated as the distance moved parallel to the superior margin of the inferior vertebra relative to the average disc margin height.	$\mathbf{d}_u \cdot \mathbf{x}_S$

^aDirectionality was defined as inferior (I), superior (S), anterior (A), and posterior (P) relative to each vertebra (L3-S1).

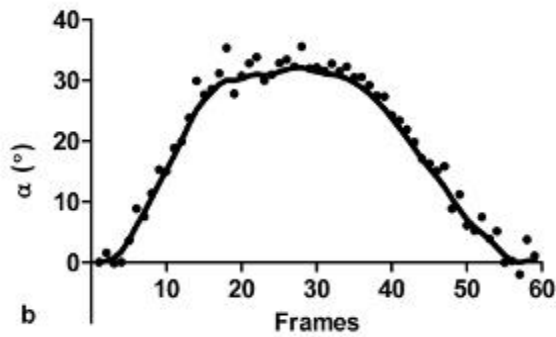
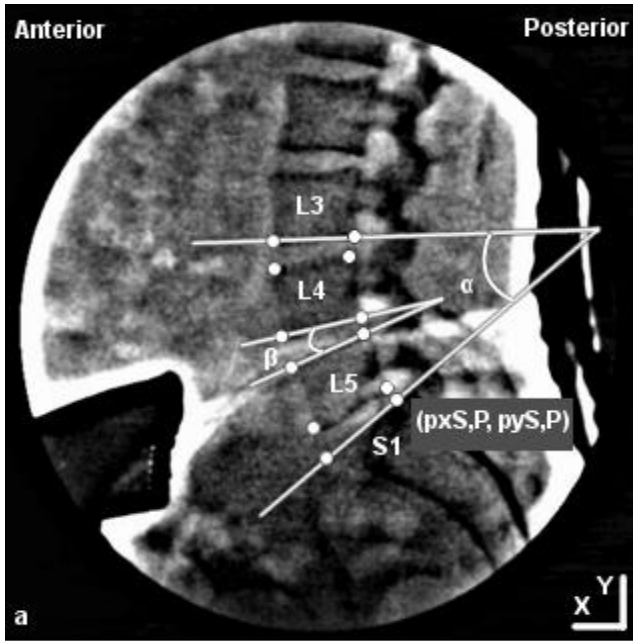


Figure 2.1. a. Representative Fluoroscopic Frame with Labeled Anatomy. Vertebral margin points labeled with circles (representative origin at the superior, posterior point of S1), and computed angles shown. b. Representative profile of the Lower Lumbar Angle as a Function of Position, Raw Points and Filtered Data

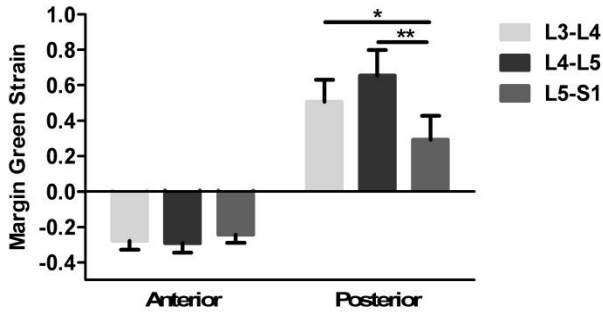


Figure 2.2. Peak Green Strains on the Anterior and Posterior Margins (mean \pm 95% CI, * $p < 0.05$, ** $p < 0.001$)

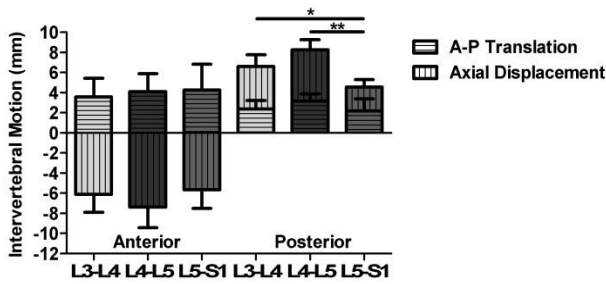


Figure 2.3. Intervertebral Margin Motion Decoupled into Anterior –Posterior Translation and Axial Displacement (mean \pm 95% CI, * $p < 0.05$, ** $p < 0.001$)

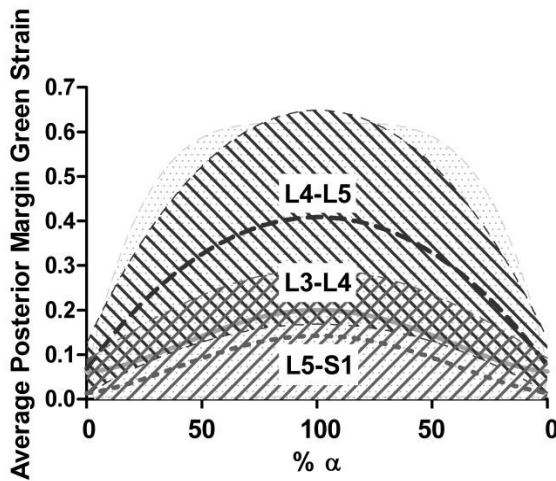


Figure 2.4. Average Posterior Margin Green Strains in Flexion and Extension Phases.

95% confidence intervals shown as filled regions (L3-L4 speckled, L4-L5 left slant, L5-S1 right slant). Data were fitted with 4th order polynomials

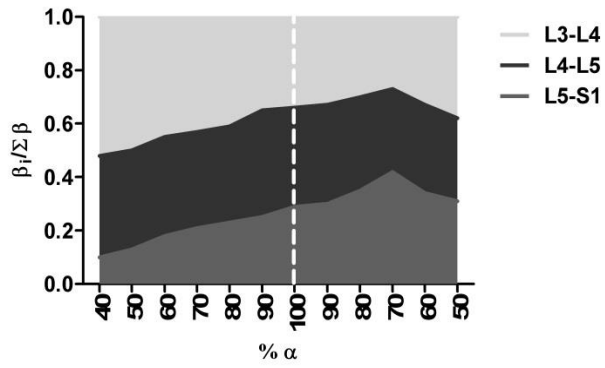


Figure 2.5. Intervertebral Angle Contribution During Flexion and Extension (filtered using a low-pass Butterworth filter with a cutoff frequency of 250 Hz). Dotted line represents full flexion; area to the left of the dotted line is neutral to full flexion and to the right is flexion to upright neutral

Work described here is reprinted with permission.

Nagel et al. "Combining displacement field and grip force information to determine mechanical properties of planar tissue with complicated geometry" Journal of Biomechanical Engineering. 2014. 136. 114501-114506.

Chapter 3 – Structural model verification and validation

Introduction

Soft-tissue characterization using planar biaxial testing and nominal stress-strain curves usually relies on certain conditions²:

- The sample should have a shape, (e.g., square or cruciform) that tends to produce homogeneous strain fields in the central region.
- If the sample is fibrous, the fiber orientation should be known and aligned with the axes of the test system.
- Strain should be measured far from any rigid boundary, such as a grip or attachment to bone.

These criteria are often met (e.g., Fung 1973; M S Sacks and Gloeckner 1999; Waldman and Lee 2002; Waldman, Sacks, and Lee 2002; Jacobs et al. 2013; Miller, Connizzo, et al. 2012; Miller, Edelstein, et al. 2012), but for some tissue types, meeting one or more criteria is impossible. The tissue may, for example, be too small to allow isolation of a sample that is large enough for biaxial testing and is shaped to create a

² For further information on strain uniformity and boundary conditions see (Eilaghi et al. 2009; Sun, Sacks, and Scott 2005).

homogeneous strain region in the center. Aligning the material axes does not allow a biaxial test to generate planar shear strain (Michael S. Sacks 2000). Furthermore, if the material axes are improperly aligned, the variation in tissue response will increase, which could hinder elucidation of complex behaviors such as coupling between the two directions (Michael S. Sacks 2000). Other groups (e.g. Michael S. Sacks 2000) have used biaxial testing to good effect for off-axis fibrous samples. This is only effective, however, when the fiber orientation is known. When fiber orientation is unknown and/or the objective is to determine the fiber orientation, as in the current study, force-stretch data alone is insufficient. It also may be undesirable or even impossible to remove the tissue from bone, which restricts one's ability to align the tissue fiber direction with the testing apparatus and leads to inhomogeneity of the strain field. An example of these challenges is found in the annulus fibrosus of the intervertebral disc, particularly if one seeks to do single lamella experiments. Although some single lamella experiments have been performed in uniaxial (Holzapfel et al. 2005; Skaggs et al. 1994; C. Pezowicz 2010) and biaxial modes (Bass et al. 2004; Malgorzata and Pezowicz 2013), testing with intact bone (Holzapfel et al. 2005; C. Pezowicz 2010; Bass et al. 2004; Malgorzata and Pezowicz 2013) is attractive both because of direct relevance to *in vivo* loading and because of minimized tissue damage. Figure 3.1 shows a lamella of annulus fibrosus attached to axial vertebral bone. This geometry is not conducive to a homogeneous strain field, and the principal fiber direction does not align with the axes of the testing apparatus.

Sample geometries that produce inhomogeneous strain fields pose a considerable challenge to the investigator, but the advent of image-correlation-based methods for tracking motion over the entire tissue during testing (Elliott and Setton 2001; Gaudette et

al. 2001; Doehring, Kahelin, and Vesely 2009; Quinn and Winkelstein 2010; Raghupathy et al. 2011; Keyes et al. 2011; Witzenburg et al. 2012; Li et al. 2012) present new opportunities. The approach of simulating the experiment and then iterating over the model parameters to determine a best fit has been used in elastography (Barbone and Oberai 2007; Pellot-Barakat et al. 2004) as well as indentation (Kim and Srinivasan 2005) and can be applied to tissue testing as well. In this study, we demonstrate the use of combined displacement field data, grip force-stretch data, and finite-element modeling to determine tissue properties from a biaxial test.

Methods

Fitting Procedure - Model

The model of choice for the current study is a simple structural model for fibrous tissue (Raghupathy and Barocas 2009) whose parameters correspond roughly to fiber stiffness, A , fiber nonlinearity, B , preferred fiber orientation direction, μ , and fiber spread, κ (note that these parameters are representative of the fiber architecture but do not necessarily correlate with a specific fiber measurement, and, particularly in complex, multicomponent tissues, the meaning of the parameters cannot be related directly to the tissue architecture or properties of constituents). The fiber population is taken to be distributed according to a bidirectional von Mises distribution (1), and the tension in a fiber is taken to be exponential in its Green strain (2). The model equations are as follows:

$$f(\theta; \kappa, \mu) = \frac{1}{\pi I_0(\kappa)} \exp(\kappa \cos[2(\theta - \mu)]), \quad \theta \in [0, \pi) \quad (1)$$

$$S_f = A(\exp[B(\lambda_f^2 - 1)] - 1) \quad (2)$$

$$S_{ij} = \int_0^\pi S_f(\theta) n_i(\theta) n_j(\theta) f(\theta) d\theta \quad (3)$$

In (1-3), $f(\theta)$ is the probability of a fiber oriented in direction θ , I_0 is the modified Bessel function of the first kind and order 0, and λ_f^2 is the squared fiber stretch given by $C_{ij} n_i(\theta) n_j(\theta)$, where C_{ij} is the right Cauchy-Green tensor and $n_i(\theta)$ is the unit vector in direction θ . S_{ij} is the tension in the tissue. This model was chosen for convenience and familiarity, and it was treated as a representative anisotropic model.

Fitting Procedure - Algorithm

The four parameters in the model (A, B, μ, κ) were fit to experimental results by minimizing the error in the two-term objective function, φ :

$$\varphi = SSE_{Grip\ Forces}(A, B, \mu, \kappa) + w * SSE_{Nodal\ Displacements}(A, B, \mu, \kappa) \quad (4)$$

The first term in the objective function, $SSE_{Grip\ Forces}$, represents the sum of squared errors between the model and experimental grip force-stretch data at incremental extensions. A finite-element (FE) simulation (written in C++) was used to solve for the stress and displacement fields over the planar, two-dimensional domain of the sample using equations (1-3) as previously described in (Raghupathy and Barocas 2009), at incremental grip extensions. For the FE model, the domain of each experimental sample was taken from a video frame and meshed using Abaqus (Simulia, Providence, RI) with an average of 306 linear quadrilateral elements per sample. The second term in the function, $w * SSE_{Nodal\ Displacements}$, represents the sum of squared errors between the FE

model and experimental nodal displacement fields for each sample mesh, scaled by weighting factor, w . The weighting factor was calculated based on the errors from the initial guess to balance the grip force-stretch and nodal displacement field errors. Model displacement fields were taken from the FE nodes, excluding grip nodes. Experimental displacements were calculated for each sample using its FE mesh and digital image correlation (DIC) as previously described (Raghupathy et al. 2011).

The two-term objective function (4) was minimized using Newton-Raphson iteration (with trust region control) using an analytical Jacobian (Draper and Smith 1981). Analytical expressions were provided for the Jacobian and numerical approximations for the Hessian. Further explanation of the parameter determination scheme is given in the flow chart provided in Appendix A.

Confidence regions for each parameter were calculated using a linearized form of the model with the simplification that the other three parameters were assumed known, shown in equations (5-6) (Knapp et al. 1997).

$$(\psi_i - \hat{\psi}_i)^T \hat{Z}_{ij}^T \hat{Z}_{ij} (\psi_i - \hat{\psi}_i) \leq 4 \left(\frac{\varphi}{[n - 4]} \right) F(4, n - 4, 1 - \alpha) \quad (5)$$

$$\text{where } \hat{Z}_{ij} = \frac{\delta \varepsilon_j}{\delta \psi_i} \quad (6)$$

ψ_i is the set of parameters, where all terms in the expression with a hat represent those related to the fitted parameter set. Z_{ij} represents the linear approximation of the

error of the predictor variables (grip force-stretch data, nodal displacement field data) while incrementing one parameter and holding the remaining three parameters constant for each grip stretch increment, j . n represents the total number of observations from the predictor variables at each grip stretch increment. F represents the F-statistic, where α is the 0.05 confidence level. All computations were carried out on a single core at the University of Minnesota Supercomputing Institute.

Simulated Experiments

Simulated data sets were created using a forward simulation with previously fitted parameters (Nagel et al. 2011)³ to assess the performance of the method.

- Parameter values were varied $\pm 15\%$ to assess sensitivity of φ to the different parameters. Parameter sensitivity was defined as:

$$\text{Parameter Sensitivity} = \text{Param} \cdot \frac{d\varphi}{d\text{Param}} \quad (7)$$

- The initial guess of each parameter was varied $\pm 15\%$ to assess the robustness of the fitted parameters.
- The effect of noise was assessed by fitting parameters to data perturbed with white Gaussian noise, varying SNR between 2.5 and 100.

³ This parameter set is from a previous test of a different annulus fibrosus lamella sample, fitted prior to improving the technique as shown in the current study.

Representative Experiments

Three representative tissue types were tested. Superficial pectoralis major (SPM) represents highly aligned tissue with fibers oriented with the test axes. Facet capsular ligament (FCL) represents highly aligned tissue with fibers oriented with the test axes and a small sample with rigid boundaries. A lamella from the annulus fibrosus (AF) represents highly aligned tissue with fibers oriented off-axis and a small sample with rigid boundaries. All samples were obtained from the University of Minnesota Anatomy Bequest Program and approved by institutional review. The tissues used and testing protocol are detailed in Table 3.1. The SPM was dissected to a cruciform shape. The FCL was dissected from a right L3-L4 motion segment. The thin membrane covering the FCL was removed, and the facet capsule was isolated from the motion segments with ligament attachments to the superior and inferior articular facets intact. The ligamentum flavum and trabecular bone within the facet joints were removed to create a planar bone-ligament-bone configuration. AF, from the anterior region of a L3-L4 intervertebral disc, was dissected to a single lamella with axial vertebral attachments, using a technique similar to that of (Bass et al. 2004). More detailed dissection instructions are given in Appendix B. Sandpaper was attached to sample arms with cyanoacrylate glue.

To obtain the displacement field, each sample was speckled with Verhoeff's stain (Sigma-Aldrich, St. Louis, MO) to provide image texture over the sample domain while it was filmed (Canon Rebel T2i, Melville, NY) during the experiment. Still images taken from the filmed experiments were used to calculate the displacement field of the sample

(using a custom DIC code⁴) at incremental extensions. Further detail to obtain the displacement field by this method, has been described in literature (i.e. Raghupathy et al. 2011).

Each sample was attached to an Instron-Sacks biaxial tester, and a preload was applied. Samples were preconditioned for 8 cycles and tested in equibiaxial extension, a common loading configuration. Images and grip force-stretch data were acquired for each test, and the grip force-stretch data were zeroed with respect to the preload. Levels of preload and maximum grip stretch were chosen to stretch each tissue outside of its toe region and thus produce a significant non-linear response. The structural model was used to fit parameters to each data set, and parameter confidence regions were calculated as described in the Algorithm section.

Results

Simulated Experiments

Sensitivities of the error in simulated force-stretch data and displacement field to the parameter values are shown in Figure 3.2. Arm force-stretch data (F_1 , F_2) and nodal displacement field data (U_1 , U_2) were taken from a single node, showing how their values changed by adjusting the parameter values. The subscript refers to the direction of the measurement. The arm force-stretch data are more sensitive to the parameters μ , A , and B than to κ . Horizontal nodal displacement field data (U_1) were more sensitive to the parameter κ , and vertical nodal displacement field data (U_2) were more sensitive to the

⁴ This code is available for licensing at http://license.umn.edu/technologies/20130022_robust-image-correlation-based-strain-calculator-for-tissue-systems. There is no charge for an academic license.

parameters κ and μ , where greater sensitivity to the parameters leads to more accurate parameter estimation.

Parameters κ , μ , and B were largely unaffected by noise, and the error in A was less than 5% for signal to noise ratios greater than 10 (Figure 3.3). For all initial guesses studied, the fitting based on both grip force-stretch data and nodal displacement field data converged to the correct result (within 8%).

Representative Experiments

Parameters were fit to experimental data using three approaches: grip force-stretch data alone (FORCE), nodal displacement field data alone (DISP), and grip force-stretch and nodal displacement field data simultaneously (BOTH). Figure 3.4 shows grip force-stretch data on the arm along or closest in alignment to the fiber axis of each tissue type, for the experiments (points) and the BOTH fit (lines). The four-parameter model fits the grip force-stretch data well. Parameter values for the BOTH approach of each tissue are shown in Table 3.2. The FCL and annulus fibrosus lamella parameters denote strong alignment and a highly nonlinear response.

Figure 3.5 shows the ratio of the parameter magnitude to width of its 95% confidence region for each fitting approach. A high ratio indicates a precise estimate, and a low ratio indicates a high degree of uncertainty. The FCL and AF lamella data show three of the four parameters are described more precisely using the BOTH approach rather than FORCE or DISP. For all parameters, the ratio is consistently greater than one using the BOTH approach, whereas the FORCE and DISP approaches were less precise. In all tissues evaluated, DISP described κ , μ , and B poorly.

Discussion

Simulated and experimental data were used to evaluate a regression scheme using grip force-stretch and nodal displacement fields, which allowed robust fitting with low sensitivity to noise and initial guess and tight confidence regions. This combined approach produced unique parameter sets that accurately described the tissue tested. In general, the BOTH approach generated tighter confidence regions than the magnitude of the parameter, whereas the FORCE and DISP approaches often produced broad confidence regions, making the parameter less precisely determined in each tissue type and parameter. Although one direction of the nodal displacement data (U_2) is more sensitive to κ , it was not sensitive enough to present in the confidence regions from the tissues tested.

The fitted representative experimental data were consistent with previous studies. Moduli and stiffness were calculated from the fitted data for direct comparison to published data. While the lack of published data on biaxial passive mechanics of superficial pectoralis major prevents direct comparison, passive inflation testing has been performed on rat diaphragm, which is also a large, wide-span skeletal muscle (Boriek, Rodarte, and Reid 2001). Moduli along the fiber direction in the in the SPM of the current study (0.77 MPa) were comparable to those in (Boriek, Rodarte, and Reid 2001) (0.92 MPa). Few tensile tests have been performed on isolated facet capsular ligaments, but one comparable study (Quinn and Winkelstein 2010) of preconditioning in uniaxial tension measured the elastic modulus along the fibers (1.33 ± 0.49 MPa). In the current study, the average tangent elastic modulus along the fibers (calculating the stiffness from both arms along the fibers) is within range (1.08 MPa). Additionally, some tensile tests of

single annulus fibrosus lamella have been performed in biaxial tension. One such study (Bass et al. 2004) reports an axial tangent modulus (16 MPa) about twice that calculated in the current study (9.88 MPa).

In the current study, we used our previous structural model for convenience and familiarity, but any anisotropic model would be suitable to apply this method. For example, Flynn, Cormac, and Rubin have proposed a three-parameter strain energy density model based on total dilatation, an orthotropic invariant, and a measure of the elastic distortional deformation (Flynn and Rubin 2014). Sun and Sacks have published a planar soft tissue seven parameter generalized Fung-elastic constitutive model with two restrictions for numerical stability (Sun and Sacks 2005). Other constitutive equations have been published with application to tissue from, e.g., anterior cruciate ligament (Wan, Hao, and Wen 2013), abdominal aortic aneurysm tissue (Martufi and Christian Gasser 2013), and healthy renal artery (Avril et al. 2013).

This evaluation has some limitations. The approach described herein assumes the tissue properties are homogeneous. We have shown previously (Raghupathy and Barocas 2010) that inhomogeneous tissue properties can be determined through inverse modeling through partitioning. Performance of the current model could be modified following (Raghupathy and Barocas 2010) to account for tissue property inhomogeneity, but that might require significantly more complex experiments. It is possible that in the simulated experiments the range of initial guesses and noise used were not large enough to evaluate the capabilities of the method. Also, fitted representative experimental data were obtained from a single experiment of each tissue type. The robustness of fitting would be

evaluated further by fitting repeated experiments of a tissue or experiments using different loading configurations.

For an isotropic material, grip force-stretch data could be sufficient to specify the model, and the techniques described herein would be unnecessary. For more complex geometries and orientations, however, more information is needed to define the model parameters robustly. This comes at a moderate computational cost to generate the Jacobian and Hessian. The combination of force-stretch and displacement field data for an equibiaxial test is a good option, especially when fiber direction is not known or controlled.

Table 3.1. Tissue Characteristics and Testing Protocols

	SPM	FCL	AF Lamella
Alignment	On Axis	On Axis	Off Axis
Donor	76F	60M	65M
Preload (N)	0.2	1	2
Preconditioning (grip stretch)	1.50	1.14	1.15
Grip Strain Rate (%/s)	1	1	1
Maximum Grip Stretch	1.50	1.14	1.15

Table 3.2. Representative Experiment Parameter Values

Tissue Type	Parameters			
	κ	μ	A (N/mm)	B
SPM	0.135	124.812°	4.683	1.616
FCL	2.777	0.144°	0.225	9.751
AF Lamella	4.000	22.500°	0.144	9.750

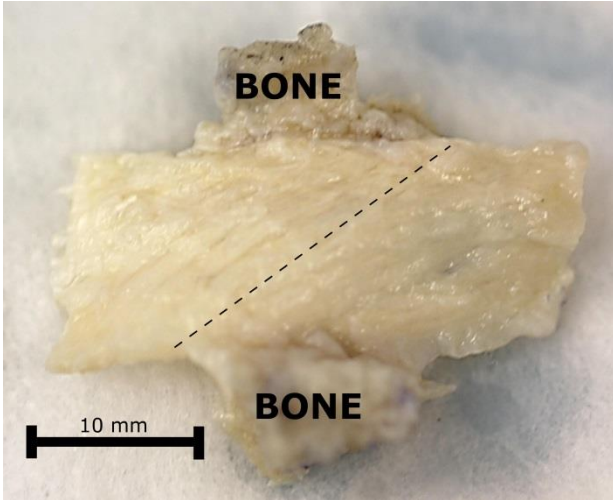


Figure 3.1. Lamella of the Annulus Fibrosus. The sample is attached to bone, labeled, and is anisotropic with fibers aligned 30° from the horizontal testing axis, along the dotted line. The dissected tissue is too small to be removed from the bone and cut to align the fibers to the direction of pull for biaxial testing.

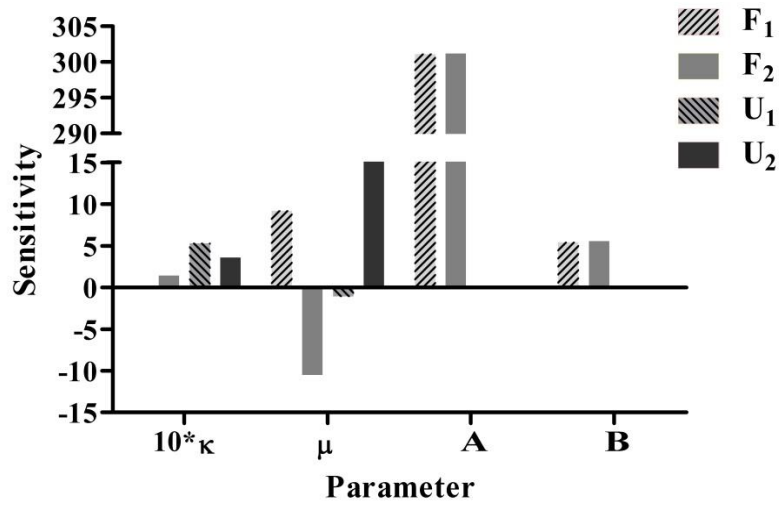


Figure 3.2. Sensitivity of Force (F) and Displacement (U) Error to Model Parameters.

The parameter κ has been multiplied by 10 for visual clarity. Sensitivities of nodal measurements in the 1 and 2 directions are different due to the anisotropy of the model. A and B affect grip force but have less influence on the displacements, whereas displacements are more sensitive to μ and κ .

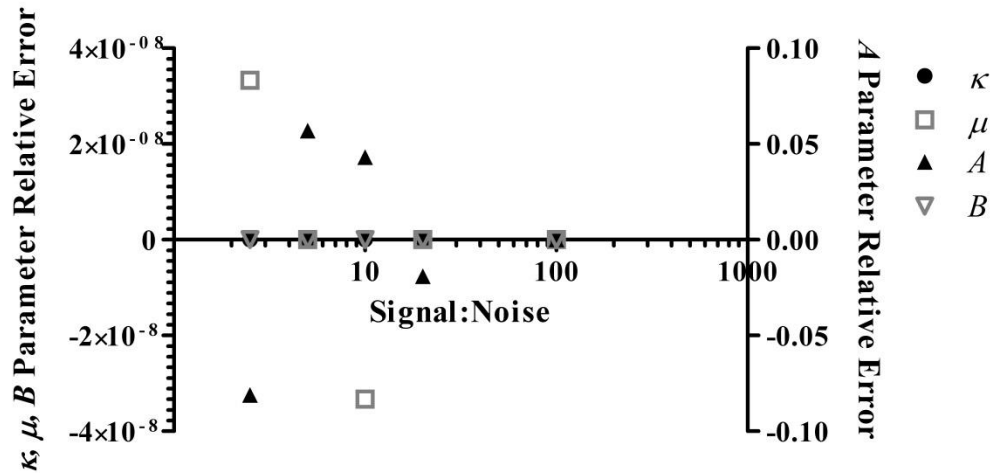


Figure 3.3. Parameter Error Using Simulated Data Perturbed with White Gaussian Noise. Relative error for the fitted parameter is shown for each parameter: κ (●), μ (□), A (▲), and B (▽). Parameters, κ , μ , and B are plotted on the left axis and parameter A is plotted on the right. Parameters κ , μ , and B are largely unchanged by the noise, and the relative error for A was less than 5% for signal to noise ratios greater than 10.

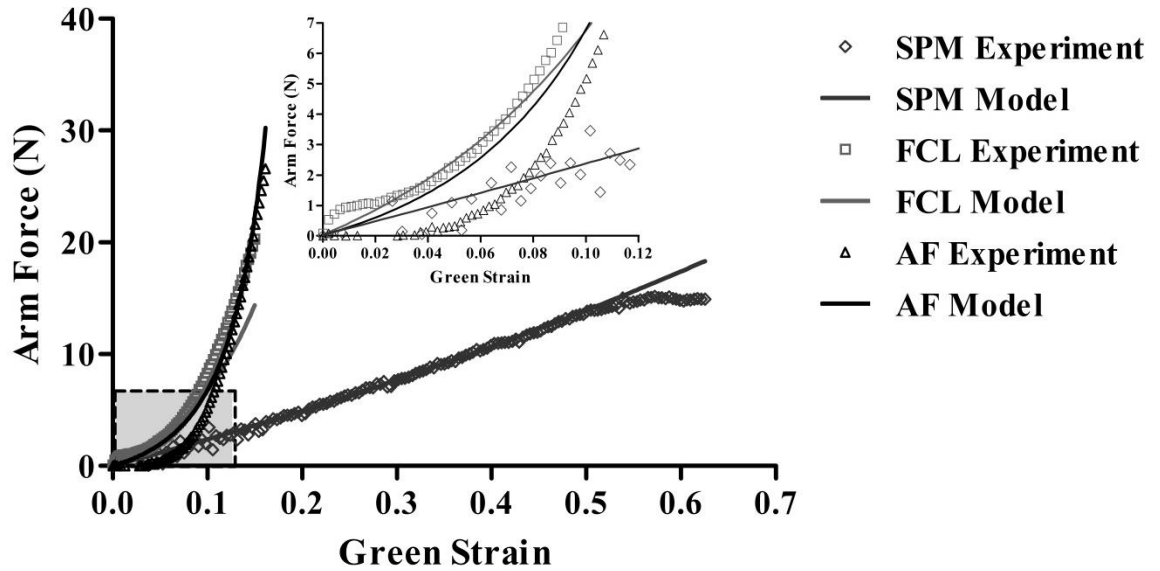


Figure 3.4. Representative Experiment Grip Force Data Fitted with the Simple Structural Model. Based on Grip Force and Nodal Displacement Data. A single arm along or near the fiber axis is shown for each tissue type: superficial pectoralis major (\diamond), facet capsular ligament (\square), and annulus fibrosus lamella (\triangle). Data at low Green strains are inset to better visualize the facet capsular ligament and annulus fibrosus lamella data. Each data set is fitted well considering all four grip forces as well as nodal displacements are fitted simultaneously.

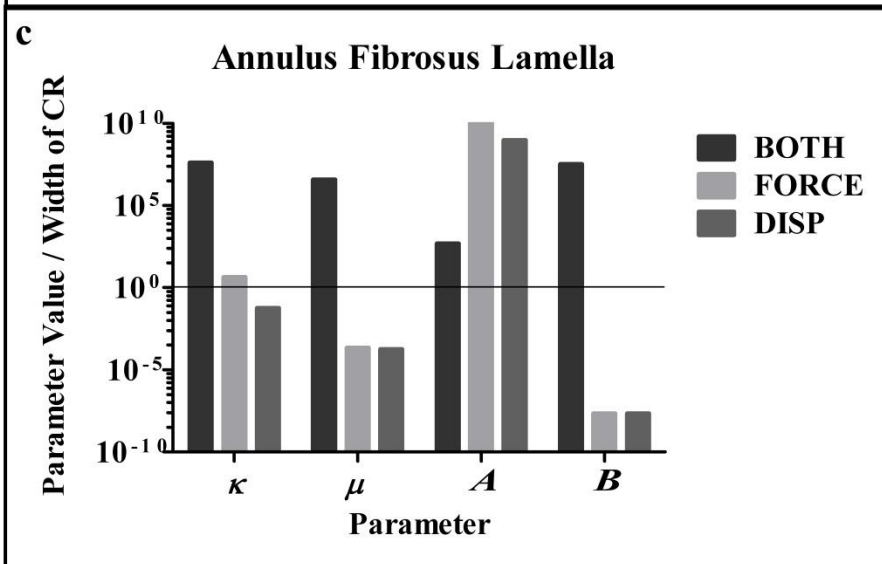
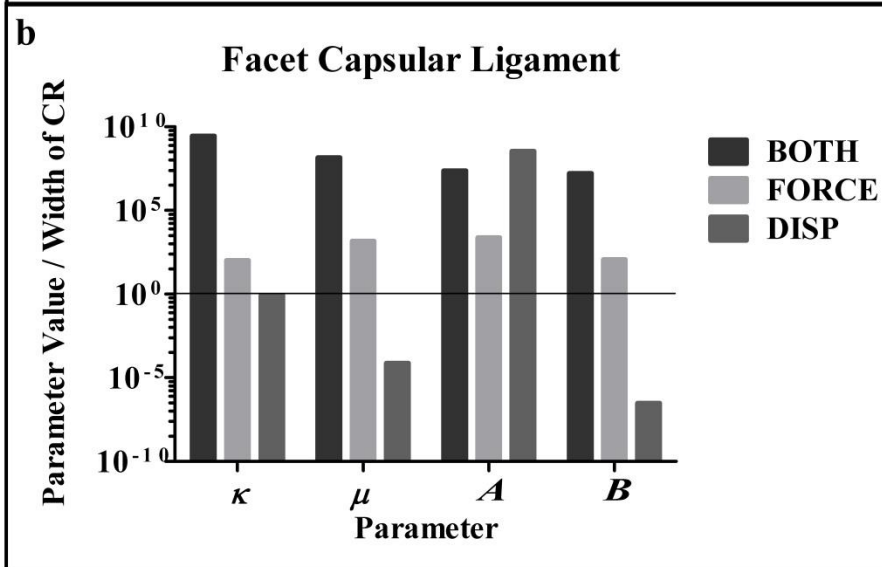
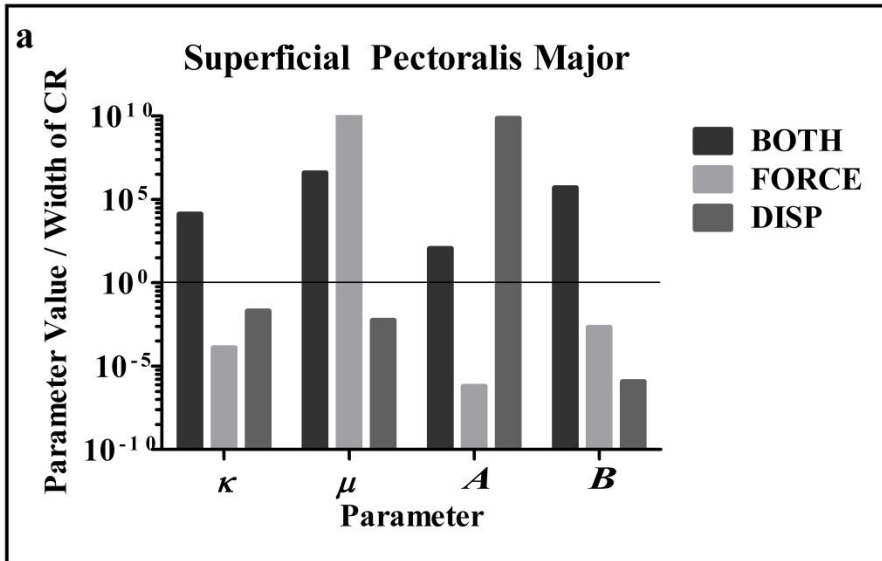


Figure 3.5. Representative Experiment Parameter Estimates with Each Fitting Approach Based on the Ratio of Parameter Value to the Width of the Confidence Region (CR). The fitting approaches shown refer to the data used to inform the model: grip forces and nodal displacements (BOTH), grip forces alone (FORCE), and nodal displacements alone (DISP). The tissue data fitted are a) superficial pectoralis major (SPM), b) facet capsular ligament (FCL), and c) annulus fibrosus (AF) lamella. The horizontal line represents the location where the fitted parameter value is equivalent to the width of the CR. Fitted parameters above the line are a more precise estimate than those below. The BOTH approach consistently fits three of the four parameters more precisely than the other approaches in the facet capsular ligament and the annulus fibrosus lamella. The BOTH approach has a ratio larger than 1 for each parameter in each tissue type as opposed to the FORCE and DISP approaches.

Chapter 4 – Assessing discrete annulus fibrosus lamellae using physiologic loading

Introduction

To the authors’ knowledge, neither shear force or in-plane moment generated by either single or multiple AF lamellae in biaxial tension has been reported.

Therefore, this work seeks to characterize AF lamellae through a physiologically relevant (multi-axial) mechanical test and biochemical assay, by (1) measuring both normal and shear in-plane forces and the in-plane moment and (2) quantifying differences between single and multiple lamellae in the anterolateral region.

Materials and Methods

Sample Preparation

Fresh six to eight month old porcine lumbar spines were obtained from the University of Minnesota Visible Heart Lab. Three L3-L4 segments were harvested for the current study and stored at -20°C until dissection.

The dissection was conducted so as to ensure that the tissue remained hydrated with isotonic saline. All segments were dissected and tested within one week of thawing and stored at 4°C in saline between dissection and testing. After the tissue had thawed, excess musculature and other tissue were removed to expose the intervertebral disc and adjacent vertebrae. Rangeurs were used to remove all trabecular bone from the inferior and superior vertebrae. The outer tissue and AF lamellae were dissected away from the disc to reveal a single lamellar surface a minimum distance of 20mm in circumferential length on two portions of the anterior surface, as shown in Figure 4.1a, to produce two samples from one disc: anterolateral right, single-lamella and anterolateral left, multiple-lamella. To maintain a physiologic attachment, 10mm wide sections were marked on adjacent vertebrae at the center of each sample. A small rotating saw was used to cut at the marked positions, and all remaining cortical bone was removed except for 10mm sections adjacent to each sample. Each sample was dissected using a scalpel to reveal a single lamellar surface. Multiple-lamella samples were less than ten lamellae thick. More detailed dissection instructions are given in Appendix B. Near each sample, two 5x5x5mm cubes were removed and placed in pre-weighed vials for biochemical analysis. Thus, two samples from six discs were dissected and tested, for a total of twelve samples. A representative single lamella sample is shown in Figure 4.1b.

Mechanical Testing

Sandpaper (Grade 4130, 3M, Maplewood, MN) was attached to the sample axial vertebral attachments and circumferential annulus fibrosus arms using cyanoacrylate glue. The outer annular surface of each sample was speckled with Verhoeff's stain (Sigma-Aldrich, St. Louis, MO) for continuous displacement tracking via image correlation (Raghupathy et al. 2011).

The prepared samples were mounted in a custom, rigid grip attached to an Instron-Sacks biaxial tester (Instron, Norwood, MA), shown in Figure 4.1c. The sample was submerged in saline bath. The load cells (JR3 Inc., Woodland, CA) used in this study measure six degrees of freedom, three forces and three moments. The coordinate system is shown in Figure 4.1c. Only in-plane forces and moment will be used in this study. From here on, the normal force is in the direction perpendicular to the edge of the sample, the shear force is in the direction parallel to the edge of the sample, and the in-plane moment is counter-clockwise as viewed from above the sample (i.e., looking in from the outside of the IVD).

Each sample was given a preload of 0.5 N. Then, the sample was strained in the circumferential direction, held, and strained in the axial direction using the protocol shown in Figure 4.1d. This protocol reflects 20% of the average L4-L5 posterior intervertebral strain in the axial direction obtained from lumbar vertebral kinematics in flexion (Chapter 2: Nagel, Zitnay, et al. 2014). The amount of average *in vivo* strain used was less than that measured to account for IVD curvature and anatomical differences between the porcine and human spine (Busscher, Ploegmakers, et al. 2010). The *in situ* pre-strain in the circumferential direction was selected to ensure biaxial stretch during the

protocol but not failure. The sample surface was recorded on video during testing using a Canon Rebel T2i camera (Canon USA, Inc., Melville, NY) for continuous displacement tracking.

Data Analysis

Surface displacements were calculated using a custom in-house digital image correlation code (Raghupathy et al. 2011). Surface displacements and in-plane force and moment data were used in a structural model (Chapter 3: Nagel, Hadi, et al. 2014) to fit parameters to describe the sample's fiber distribution dispersion, κ , mean fiber alignment, μ , fiber stiffness, A , and degree of fiber non-linearity, B . To represent the alternating fiber alignment between adjacent lamellae, multiple-lamella sample mean fiber alignment was fit to a positive (μ_1) and negative (μ_2) mean fiber alignment, accounting for the number of layers corresponding to each alignment. The fiber population is taken to be distributed according to a bidirectional von Mises distribution (1), and the second Piola-Kirchhoff stress in a fiber is taken to be exponential in its Green strain (2). The model equations are as follows:

$$f(\theta; \kappa, \mu) = \frac{1}{\pi I_0(\kappa)} \exp(\kappa \cos[2(\theta - \mu)]), \quad \theta \in [0, \pi) \quad (1)$$

$$S_f = A(\exp[B(\lambda_f^2 - 1)] - 1) \quad (2)$$

$$S_{ij} = \int_0^\pi S_f(\theta) n_i(\theta) n_j(\theta) f(\theta) d\theta \quad (3)$$

In (1-3), $f(\theta)$ is the probability of a fiber oriented in direction θ , I_0 is the modified Bessel function of the first kind and order 0, and λ_f^2 is the squared fiber stretch given by

$C_{ij}n_i(\theta)n_j(\theta)$, where C_{ij} is the right Cauchy-Green tensor and $n_i(\theta)$ is the unit vector in direction θ . S_{ij} is the total second Piola-Kirchoff stress in the tissue.

Multiple fiber distributions were accounted for in fitting multiple-lamella samples (total stress, S_T) by computing the total second Piola-Kirchoff stress for each fiber orientation, μ_1 and μ_2 , multiplying by the given number of layers at each orientation, m_1 and m_2 , and summing the two products, shown in (4).

$$S_T = m_1 S_{ij}|_{\mu_1} + m_2 S_{ij}|_{\mu_2} \quad (4)$$

Biochemical Analysis

Assay samples were dried at 60°C to a constant dry weight (~96 hours). Hydroxyproline content was determined using a previously reported method (Stegemann and Stalder 1967), except for the omission of lyophilization and normalized by dry weight ($\mu\text{g}/\mu\text{g}$).

Statistical Analysis

Statistical comparisons were made between single and multiple lamellae samples and between axial and circumferential directions among samples harvested from the same disc. Repeated measures ANOVA was performed, rejecting the null hypothesis at $\alpha < 0.05$.

Results

Three porcine L3-L4 IVDs were harvested to dissect and test an anterolateral single and anterolateral multiple lamellae sample from each motion segment. Each was tested biaxially with a protocol reflecting the IVD in flexion, obtained from (Chapter 2: Nagel, Zitnay, et al. 2014).

Biochemical content assayed is shown in Table 4.1. Statistical differences were not present between the single and multiple lamellae samples in both hydroxyproline (collagen I) content ($p = 0.235$) and water content ($p = 0.192$) among each disc tested.

Figure 4.2 shows the typical normal force during the experiment with the corresponding structural model fit. Once the circumferential displacement reached the maximum value, it was held prior to the commencement of the axial displacement. During this region, the load decreased slightly. Over the course of the protocol, the circumferential axis maintained a higher load. The load on each axis tapered near the peak applied axial grip displacement.

Figure 4.3 shows the typical normal force during the experiment plotted against the respective grip strain; for reference, the grip strain protocol is shown at the bottom (Fig. 4.3). At the beginning of the protocol, the circumferential axis is displaced, increasing the circumferential load. At the same time, the axial axis load is increasing, even though it is not being displaced. Then, the circumferential axis is held while the axial axis is displaced. The axial axis load steadily increases as does the circumferential axis load.

Figure 4.4 summarizes the average peak in-plane forces and in-plane moment measured with 95% confidence intervals and provides the reference orientation (Fig.

4.4A). The in-plane forces and moment for the multiple-lamella samples were normalized to the number of lamellae in each sample for this figure only. Even though the stretch was greater in the axial direction, the single-lamella experiments showed significantly ($p = 0.0059$) higher normal forces in the circumferential direction (Fig 4.4 B). Importantly, however, the shear forces for the single-lamella experiments were much larger on the circumferential grips ($p = 0.011$, Fig. 4.4 C), indicating an axial force that could be contributing to the overall state of the material and emphasizing the role of off-axis forces. Likewise, the large moment acting on the circumferential grips is indicative of a complex stress field (Fig. 4.4 D).

For the multiple-lamella experiments, all forces and moments on the circumferential grips were greatly reduced in comparison to the single-lamella circumferential data in comparison to the multiple-lamella axial data (Fig. 4.4 B-D). The lack of moment is readily attributed to the symmetry of the lamellae, but the lack of net force was surprising and will be addressed further in the Discussion section. The multiple-lamella experiments showed significant axial forces and moments with a high degree of sample-to-sample variability.

Biaxial test data, including grip normal forces and surface displacements, were fit to the structural model. Table 4.1 shows the fitted parameters for the single- lamella and multiple-lamella data. Single-lamella parameters μ and B had less variation among the three samples. Multiple-lamella parameter sets showed the same trend. The average spread of the fiber distribution showed moderate strength, and the high B value reflects the nonlinear nature of the tissue. As a result, the normal force was fit well (Fig. 4.2). While the model was not fit to the shear force or the in-plane moment, the model

capability can be evaluated by comparing the model prediction of the shear force and in-plane moment to the experimental data (Fig. 4.5-6). The model shear force followed the trend of the experimental data but underestimated the magnitude. The model in-plane moment neither reached the magnitude nor captured the trend of the experimental data. The surface displacements between the experiment and the model are compared in Figure 4.7. The model captured both the shape and magnitude of the surface displacements in the axial axis. The circumferential axis model data did not fit the experimental data nearly as well as the axial axis, but the circumferential axis did capture the general trend and magnitude of the surface displacements.

Discussion

Porcine lumbar IVDs were dissected and tested biaxially using a protocol based on measured vertebral motion during flexion in healthy, human subjects. Anterolateral single and multiple-lamella samples were tested to obtain surface displacements, in-plane forces, and in-plane moment. The normal force showed a strong non-linear response as evidenced by the force curve as well as the fitted B parameter. Although the axial axis was being displaced during the majority of the protocol, the circumferential axis, for both single and multiple lamellae samples, had a higher load. This response is consistent with preferential fiber alignment toward the circumferential axis and also suggests significant cross-coupling between the stresses along the two axes.

In single-lamella samples, large shear forces and in-plane moments were present. The average circumferential shear force was similar to the average circumferential normal force. The shear force and moment are as one would expect given the off-axis,

anisotropic nature of the fibers in the lamella. As the lamella is displaced biaxially, the fibers tended to rotate into the direction of pull. This fiber rotation was evidenced by resultant calculations, not shown, where the resultant orientation rotated into the dominant direction of pull, the axial direction, which may generate the shear force and in-plane moment.

Single lamellae also generate larger magnitude in-plane shear forces and moment than multiple lamellae. After normalizing by the number of lamellae in each sample, the average shear force and moment become negligible in the circumferential axis. Physiologically negligible shear force and moments seem reasonable, else there would be significant forces and additional bending generated in the lamellae during flexion. Interlamellar connections have been shown to be present anatomically in radial tension but are not visible when the tissue is unloaded (C. A. Pezowicz, Robertson, and Broom 2006). From a mechanical standpoint, negligible shear forces and moment suggest there is an interlamellar attachment which decreases the shear force and moment present in isolated single lamellae.

Collagen I and water content were measured in tissue harvested near the samples mechanically tested. Comparing among discs, we found no statistically significant difference between single and multiple lamellae. Similar biochemical content among samples from the same disc suggests the single and multiple lamellae samples were taken from the same radial location within the annulus, since AF biochemical content has greater variation radially than circumferentially (Skaggs et al. 1994). The collagen and water content measured are also within range of previously published literature of annulus tissue from the outer anterior region (Skaggs et al. 1994).

Normal force and surface displacement data were used to characterize the tissue with a structural model. Parameter sets from single and multiple lamellae samples harvested from the same IVD were slightly dissimilar ($0.302 \leq p \leq 0.851$, Table 4.1). The mean fitted fiber alignment for both single and multiple lamellae samples is within the published anatomical range (Marchand and Ahmed 1990). Parameter sets from the single-lamella samples were also used to predict the behavior of the multiple-lamella samples from the same IVD, taking into account the number of layers. The experimental and predicted data are shown in Figure 4.8. Comparing the sum of squared error between the fitted and predicted data did not show a significant difference ($p = 0.147$); in other words, the error between the multiple-lamella data and the predicted data from the single lamella parameters was not significantly different from the error between the multiple-lamella data and the best-fit multiple-lamella model of those data. The similarity between the single-lamella and multiple-lamella samples is not surprising in the biaxial test, which naturally imposes similar deformations on all layers of the multiple-lamella sample; one would expect larger differences during crack propagation or loading with large interlamellar shear, such as the lap test (Gregory et al. 2011; Driscoll et al. 2013).

Overall, single lamella data showed larger magnitude in-plane shear forces and moments than the multiple lamellae data. This effect suggests isolated single lamellae generate a complex load response to biaxial tension, but in a larger context of the AF, the in-plane shear forces and moments may be redistributed. In addition, using a structural model to describe the tissue response to a protocol mimicking an activity of daily living showed single and multiple-lamella parameter sets did not show a significant difference.

Table 4.1. Biochemical and Mechanical Data (mean \pm 95% confidence interval)

		Anterolateral Single-Lamella	Anterolateral Multiple-Lamella	p-value
Biochemical Content	Collagen I (% dry weight)	68.6 \pm 29.1	94.6 \pm 56.2	0.235
	Hydration (% water/dry weight)	74.8 \pm 4.0	82.1 \pm 9.2	0.192
Fitted Material Parameters	κ	3.01 \pm 2.17	2.20 \pm 1.84	0.386
	μ ($^\circ$)	28.33 \pm 3.27	26.67 \pm 6.53	0.423
	A (N/mm)	0.11 \pm 0.07	0.07 \pm 0.03	0.302
	B	10.83 \pm 2.25	11.00 \pm 3.39	0.851

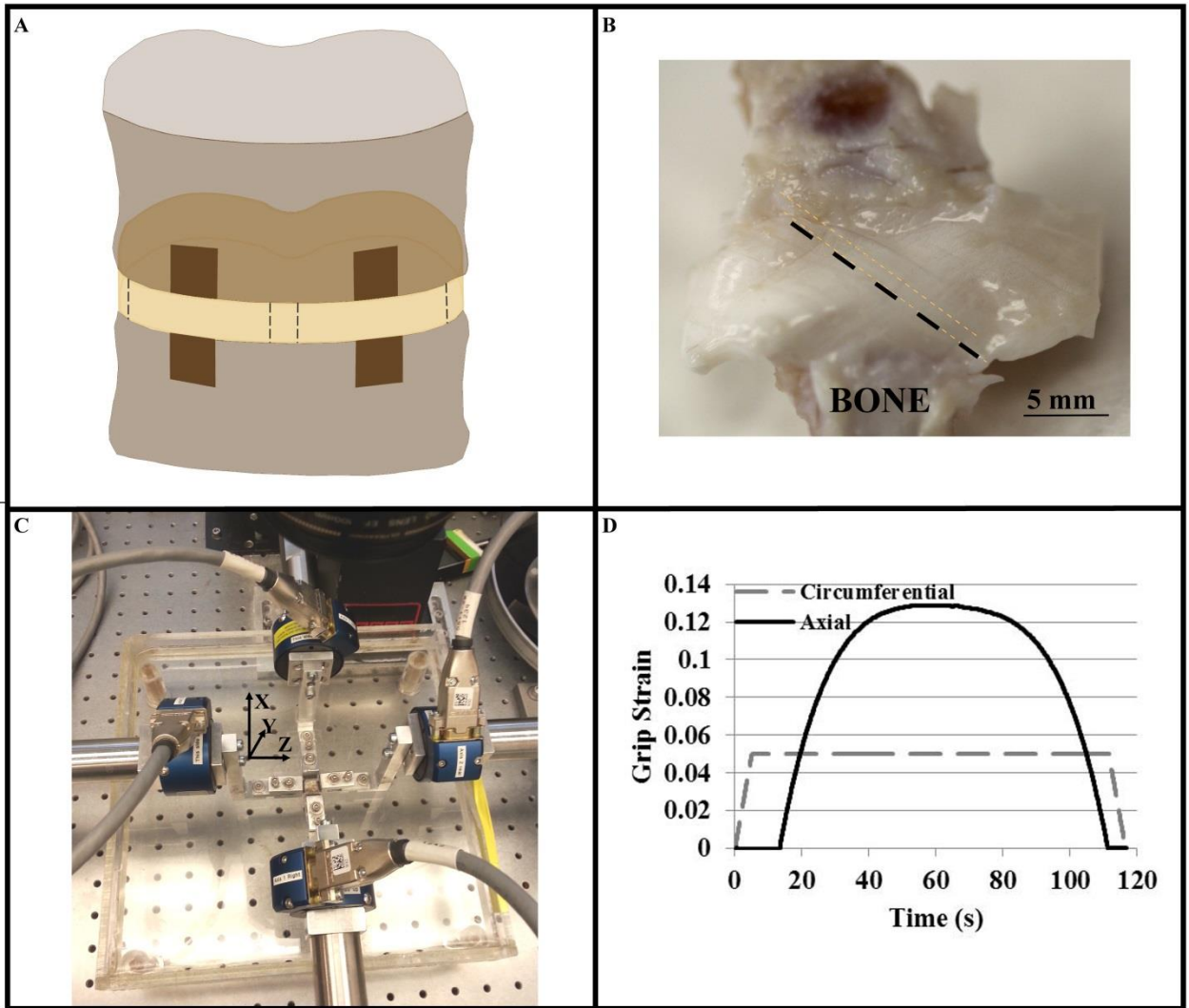


Figure 4.1. Dissection and Testing of Annulus Fibrosus Lamellae. A. Dissection geometry shown in motion segment. B. Representative annulus fibrosus multiple-lamella sample with axial vertebral attachments labeled and fiber alignment noted with a dotted line. C. Biaxial tension test set-up. D. ‘Flexion’ mechanical testing protocol.

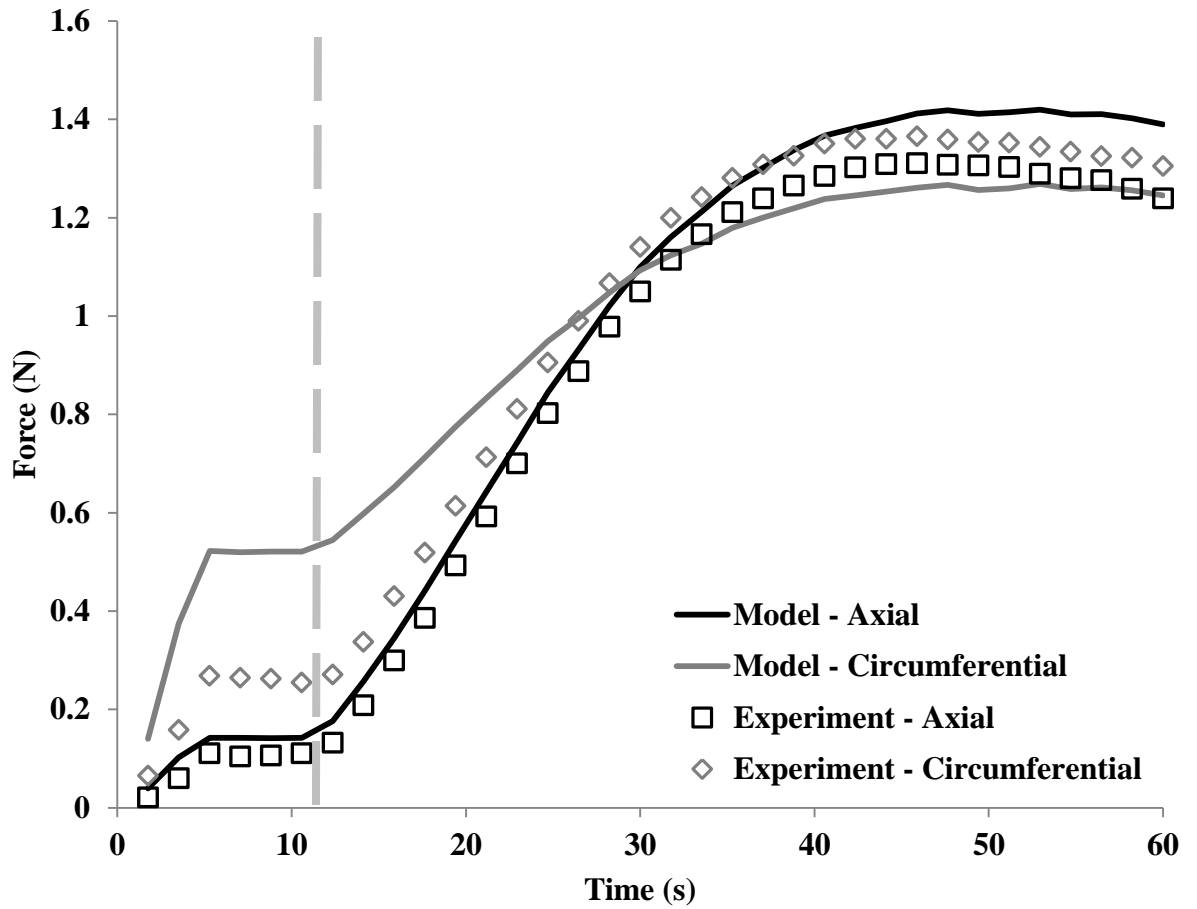


Figure 4.2. Single Annulus Fibrosus Lamella Behavior. A representative single-lamella sample normal force is shown with the modeled data. The vertical grey line denotes the point at which axial displacement begins.

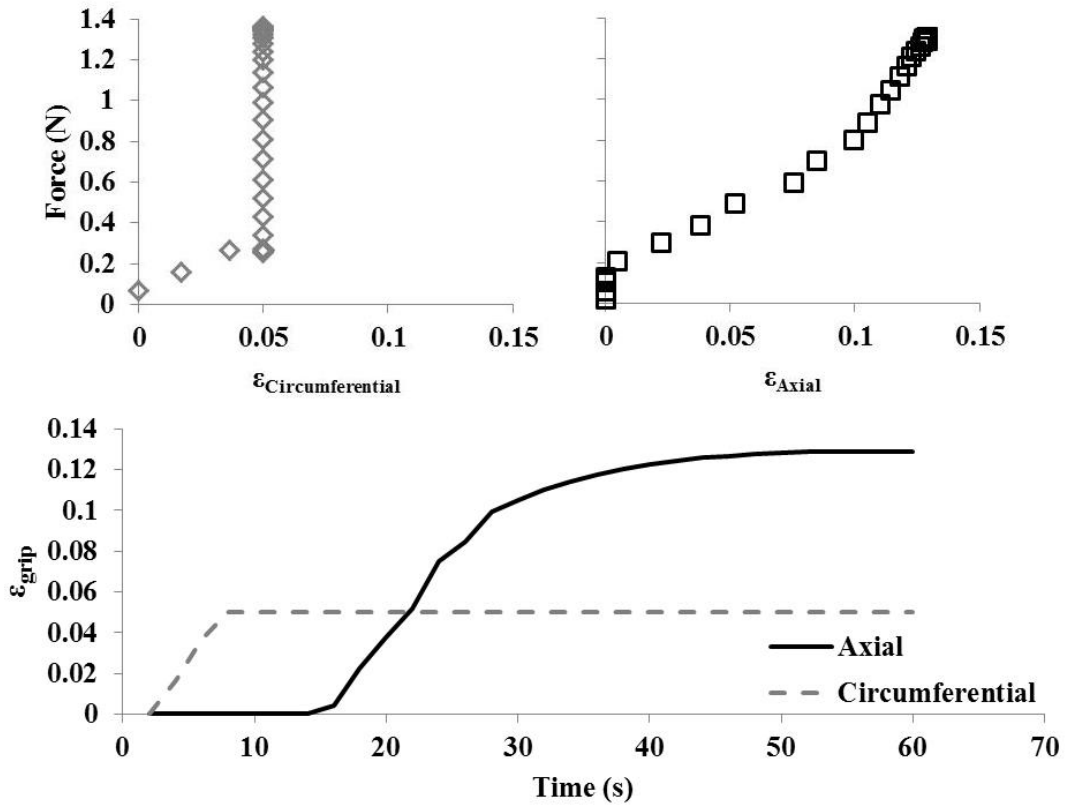


Figure 4.3. Single Annulus Fibrosus Lamella Force Behavior Separated Into Axial and Circumferential Axes. The top panels show the grip force vs. the grip strain (circumferential grip strain at left and axial grip strain at right). For reference, the loading protocol is shown in the bottom panel, grip strain vs. time.

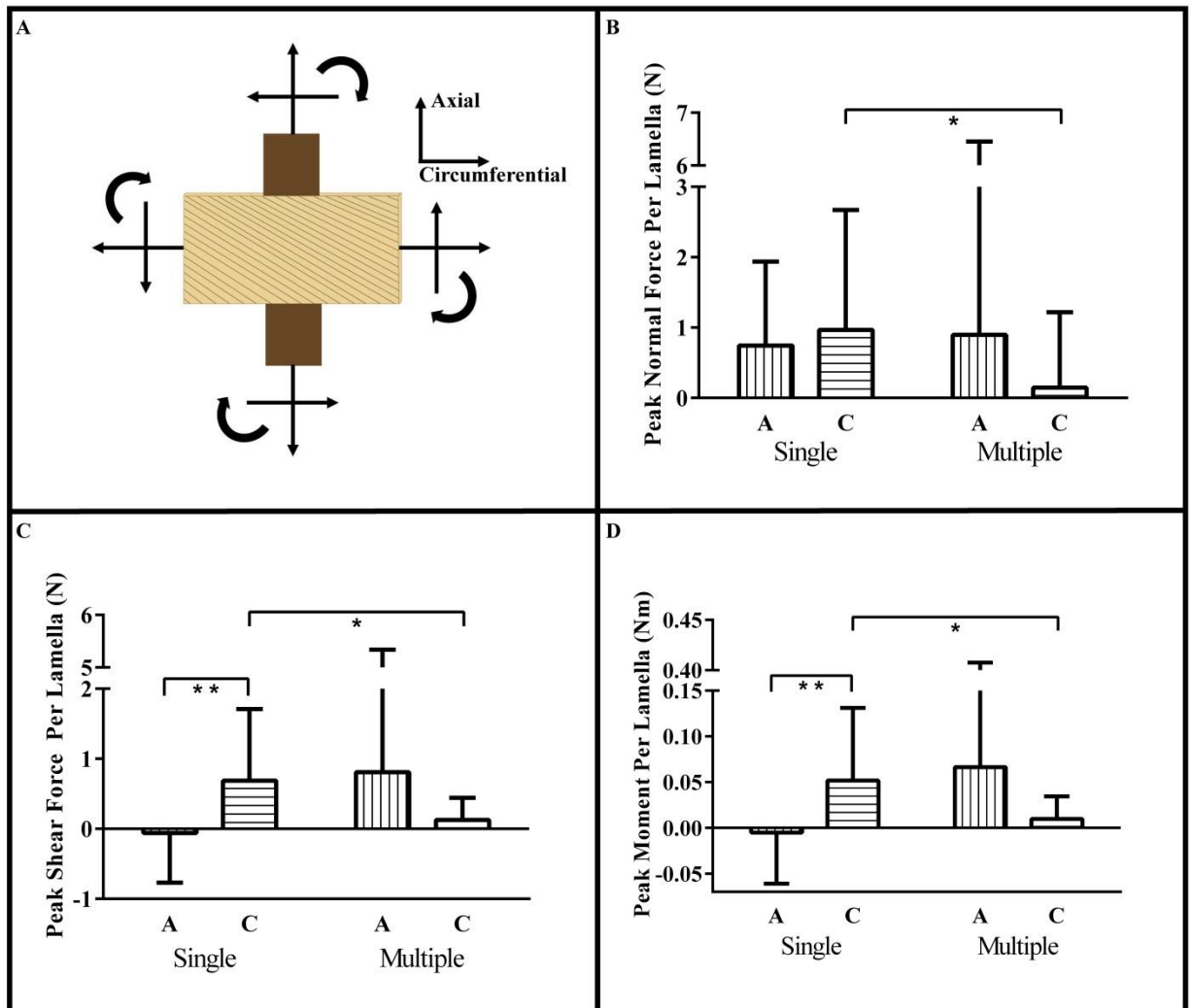


Figure 4.4. Mechanical Properties of Annulus Fibrosus Lamellae in Loading Conditions Based on Flexion. A. Positive sign convention of in-plane forces and moment. B. Peak normal force. C. Peak shear force. D. Peak in-plane moment. Panels B-D display the mean and 95% confidence intervals of anterolateral single lamella (n=3) and anterolateral multiple lamellae (n=3) samples. Multiple lamellae data were normalized to the number of lamellae in each sample. Vertical lines represent the axial axis and horizontal lines the circumferential axis. Paired t-tests were used to compare single to multiple lamellae samples (* $p < 0.05$) and axial to circumferential data (** $p < 0.01$).

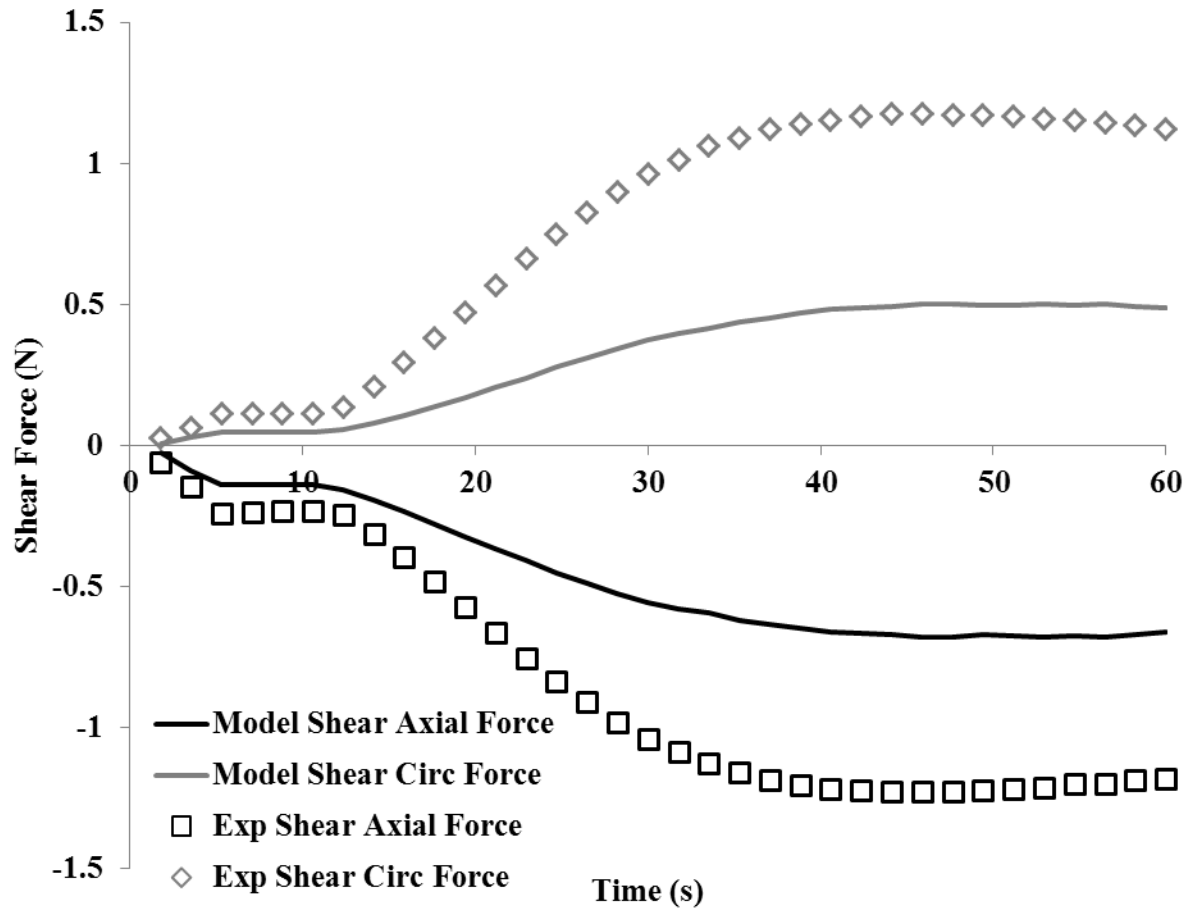


Figure 4.5. Single Annulus Fibrosus Lamella Shear Force Behavior. A representative single-lamella sample shear force is shown with the modeled data.

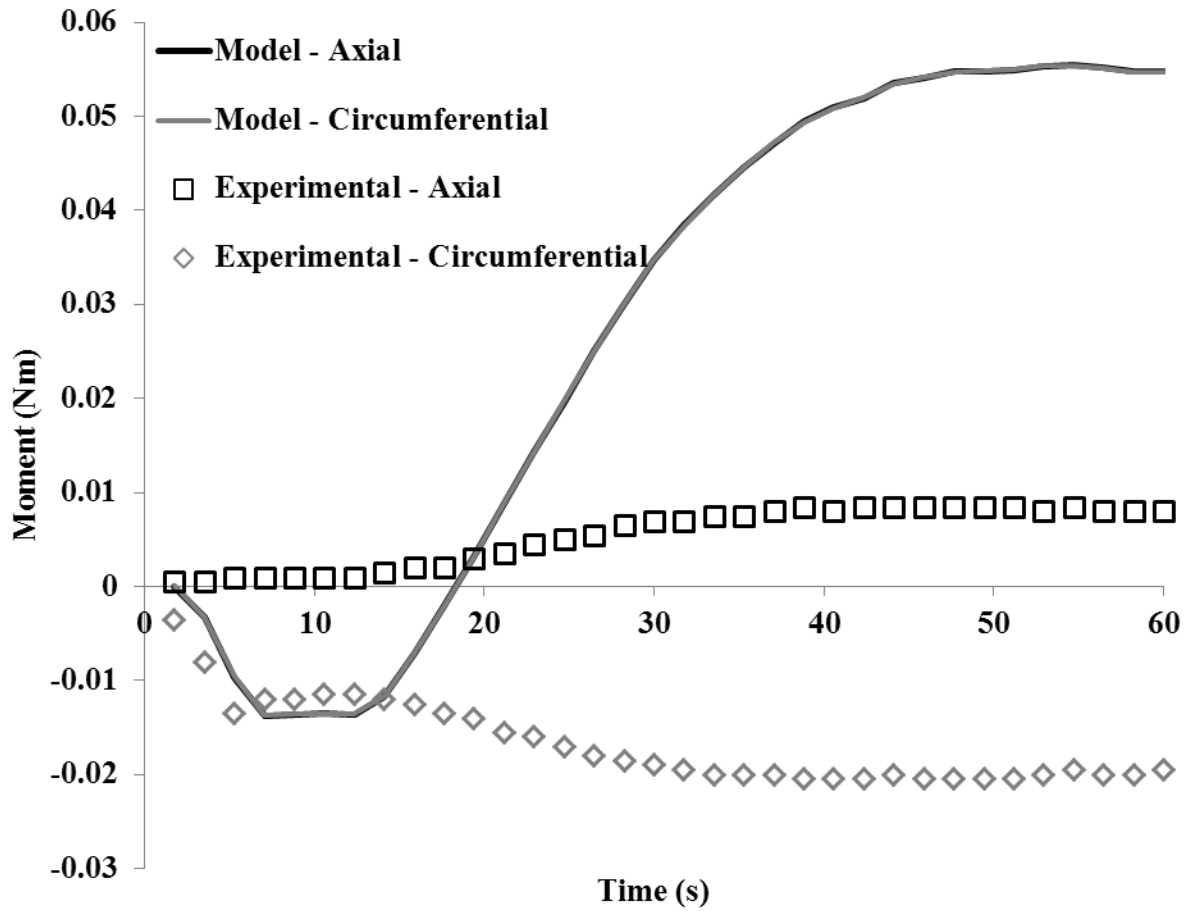


Figure 4.6. Single Annulus Fibrosus Lamella In-Plane Moment Behavior. A representative single-lamella sample shear force is shown with the modeled data.

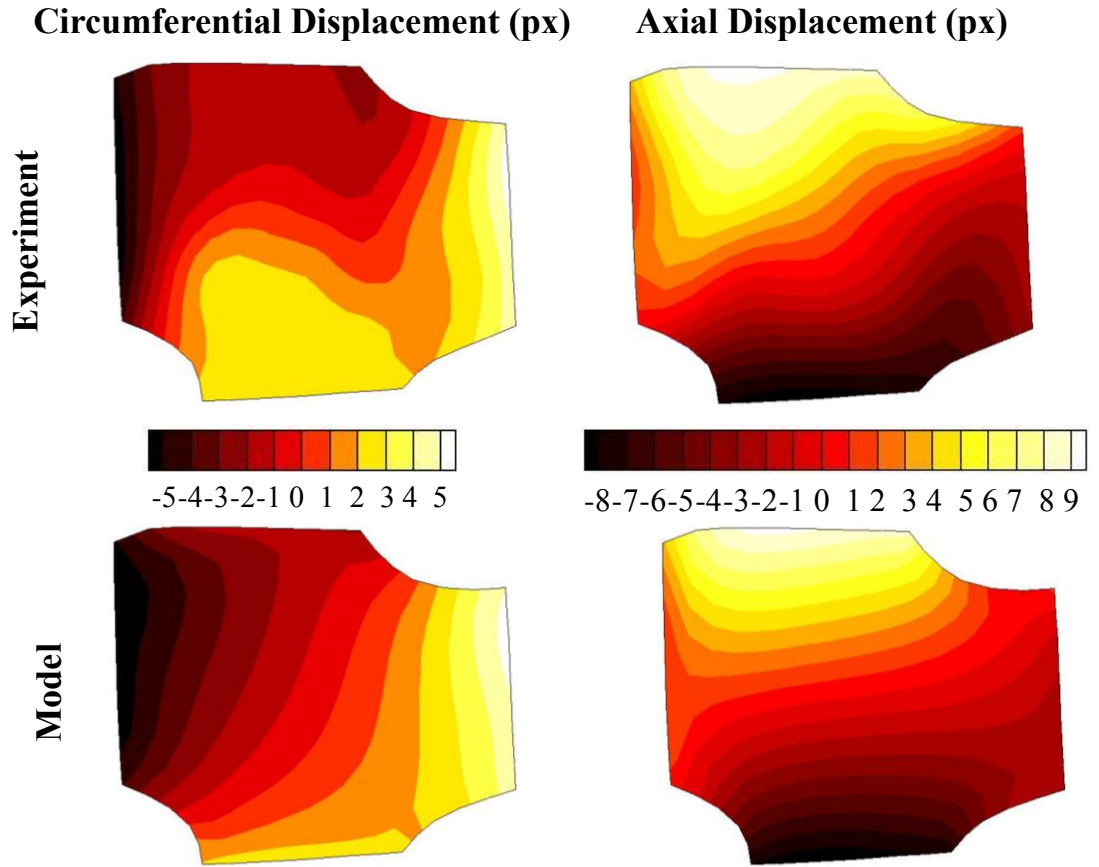


Figure 4.7. Representative Single Annulus Fibrosus Lamella Experimental and Modeled Surface Displacements. Circumferential (left column) and axial (right column) displacements are shown calculated from the continuous displacement tracking (top row) and from the model (bottom row).

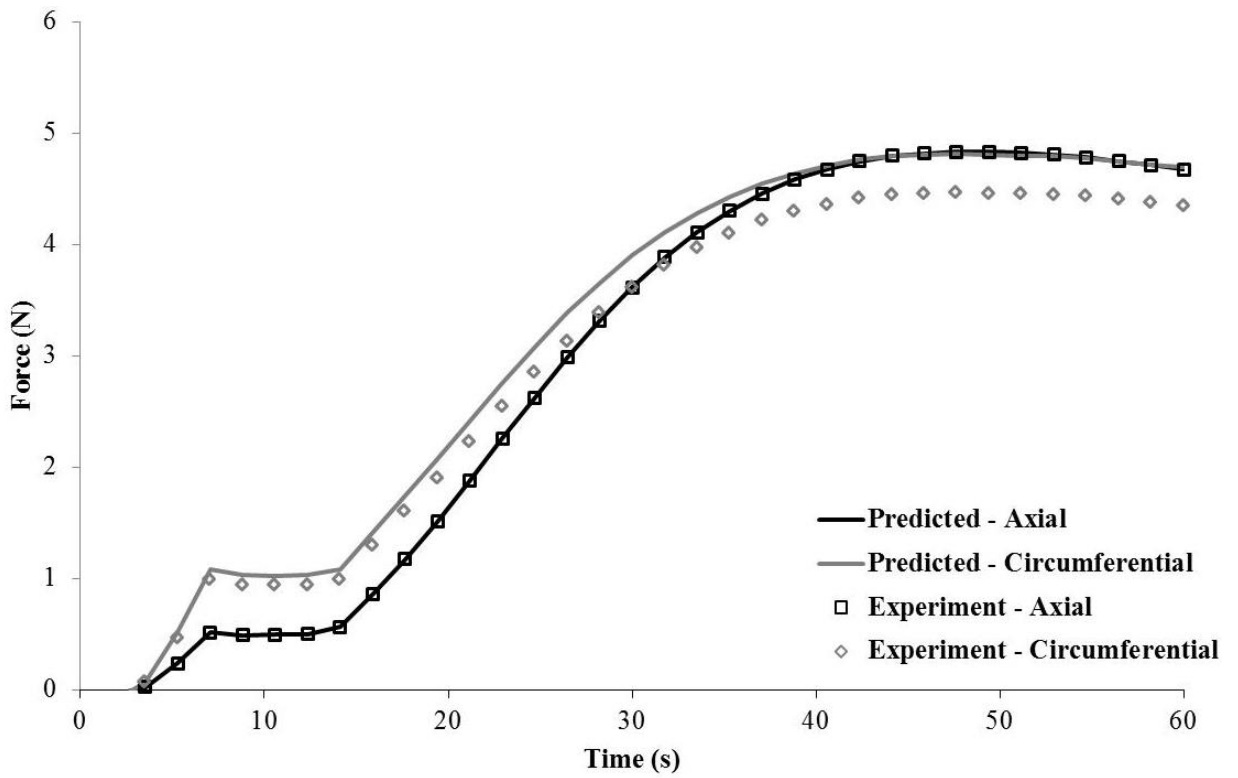


Figure 4.8. Multiple Annulus Fibrosus Lamellae Behavior – Experiment and Predicted Model from Single-Lamella Data. The diamonds and squares show the experimental data for the axial and circumferential arms, respectively. The grey and black solid lines show the model from the single-lamella sample, accounting for the orientation and number of lamellae.

Chapter 5 – Assessing mechanical interlamellar interaction via shear lap

Introduction

In healthy IVDs, adjacent AF lamellae are connected, resisting shear from axial rotation. If degeneration or damage occurs, however, it is possible that AF lamellae would delaminate. Little work has been published to understand delamination of isolated adjacent lamellae. Delamination and mechanics of an interlamellar connection can be studied directly using the shear lap geometry (Fig. 5.1A). One published article (Gregory *et al.* 2011) loaded porcine cervical IVDs in axial compression, isolated AF lamellae from the anterior and posterior margins in the shear lap geometry and displaced the lamellae at 2%/sec to failure. The authors observed significant sample narrowing prior to an initial failure then sliding phase where the two lamellae slid apart maintaining a non-zero load, before ultimately failing completely. Uniform strain was observed in the lap region while strain in the arm regions was four times larger than in the lap region. The lamellae were loaded at a fairly quick rate and strain tracked using changes in the color on the surface. This approach could lead to miscalculations in the strain due the rate as

well as the fact that the largely white AF does not vary greatly in color. The shear lap test was also modeled with a two-dimensional finite element model as a homogeneous, isotropic, linear elastic material. This modeling effort revealed shear stresses were concentrated at the edges of the lap region and trended to zero in the center of the lap region. The modeling approach used homogeneous, isotropic, linear elastic plates for the lamellae as well as linear strains. While this approach maintains focus on the interlamellar connection, this approach neglects key, well-documented anatomical features that likely have a large influence on the result such as being non-linear and anisotropic (Nerurkar *et al.* 2010). In addition, much information may be lost by utilizing a two-dimensional geometry rather than a three-dimensional geometry. Therefore, the objective of this study was to assess the mechanics of interlamellar AF connections in the lumbar region using a non-linear, three-dimensional finite element model.

Methods

Sample Preparation

Three fresh, porcine lumbar spines were harvested from six to eight-month-old swine, obtained from the University of Minnesota Visible Heart Lab. Tissue was harvested, dissected, and tested according to United States animal welfare regulations and guidelines. From each spine, the L4-L5 motion segment (intervertebral disc and adjacent vertebrae) was excised and stored at -20°C until dissection. Prior to dissection and testing, each motion segment was thawed and stored at 4°C. Excess tissue was removed from the anterior intervertebral disc surface. To benefit from the *in vivo* pre-stress, which aids in the identification of the interlamellar region, the motion segment was kept intact

while a scalpel was used to reveal the top surfaces of the shear lap geometry. First, an intact single lamella surface (lamella 1, Fig. 5.1A) was revealed by peeling and cutting away the overlying lamellae. Second, at the end of the lamellar surface, lamella 1 was delaminated from part of the length of the next medial lamella (lamella 2) and cut away using dissection scissors. Third, from the same end, lamella 2 was delaminated from the adjacent lamella across the entire length of lamella 2 to remove the lamellae from the motion segment. Fourth, from the opposing end, the lamella 1 was delaminated from part of the surface of lamella 2 and cut away. The desired lap region was less than half the length of each arm.

Mechanical Testing

Sandpaper (Grade 4130, 3M, Maplewood, MN) was attached to the arms with cyanoacrylate glue. Verhoeff's stain was speckled on the surface for continuous displacement tracking. The arms were connected to custom grips for testing on a custom Instron-Sacks biaxial tester with 500N load cells (Instron, Norwood, MA). The shear lap samples were displaced to failure at 0.1mm/s. The tests were videotaped for continuous displacement tracking using a Canon Rebel T3i camera(Canon USA, Inc., Melville, NY).

Experimental Data Analysis

Using an in-house digital image correlation code (Raghupathy et al. 2011), surface displacements were calculated over a finite element mesh. These displacements

were converted to strains which were averaged over the arm and overlap regions for comparison to the computational model.

Computational Modeling

A three-dimensional, three-layer finite element model of the shear lap test was constructed using the open-source finite element software FEBio version 2.0 (www.febio.org, Maas et al. 2012). The model simulated shear delamination of two adjacent lamellae. The purpose of this model was not to capture the complex mechanics of the lamella (e.g. O’Connell *et al.* 2012), but rather to examine how relative stiffness of the interlamellar and lamellar components affect the strain field in the lap versus the arm regions, an effect that could be compared directly to the experimental data. A secondary purpose of the model was to elucidate the kinematics of isolated lamellae in shear.

The model consisted of two lamellae and an interlamellar layer, as shown in Fig. 5.1B. The mesh was composed of 2,150 hex8 elements and 2,296 nodes, with 48 nodes in the lap region (counted from one lamellar surface). Model parameters were taken from (Skaggs et al. 1994; Holzapfel et al. 2005), and each layer was assumed to be incompressible. The lamellae were modeled as a fiber-reinforced composite (uncoupled solid mixture) with fibers aligned at $\pm 30^\circ$ from the horizontal. The fibers were modeled using the fiber-exponential power law; the fiber strain energy density is given by Equation 1, and the fiber orientation in the reference configuration is given by Equation 2.

$$\underline{\underline{\Psi}} = \frac{\xi}{\alpha\beta} \left(\exp \left[\alpha \left(\underline{\underline{I}}_n - 1 \right)^\beta \right] - 1 \right) \quad (1)$$

$$\underline{\underline{N}} = \sin\varphi \cos\theta \underline{\underline{e}}_1 + \sin\varphi \sin\theta \underline{\underline{e}}_2 + \cos\varphi \underline{\underline{e}}_3 \quad (2)$$

The fibers were modeled with an elastic modulus, ξ , of 100 MPa, model parameter 1, α , of 1, model parameter 2, β , of 2, azimuthal angle, θ , of $\pm 30^\circ$, and the polar angle from the z-axis, φ , of 90° . The matrix was modeled as a Mooney-Rivlin material. The uncoupled strain energy density is given by Equation 3.

$$\underline{\underline{W}} = c_1 \left(\underline{\underline{I}}_1 - 3 \right) + c_2 \left(\underline{\underline{I}}_2 - 3 \right) + \frac{k}{2} (\ln J)^2 \quad (3)$$

The matrix was modeled with a bulk modulus, k , of 0.22MPa, Mooney-Rivlin coefficient 1, c_1 , of 1, and Mooney-Rivlin coefficient 2, c_2 , of 0 to enforce incompressibility. The interlamellar layer was modeled as a homogenous, isotropic, neo-Hookean solid. The strain energy density is given by Equation 4.

$$\underline{\underline{W}} = \frac{E}{2(1+\nu)} \left(\frac{1}{2} \left[\underline{\underline{I}}_1 - 3 \right] - \ln J + \left[\frac{\nu}{1-2\nu} \right] [\ln J]^2 \right) \quad (4)$$

The interlamellar layer was modeled with a range of Young's moduli, E , (1, 10, 50 MPa), a Poisson's ratio, ν , of 0.49, and a density of 1.

The shear lap geometry was deformed such that layer 2 was pulled away from the fixed layer 1. A prescribed displacement of -5mm in the x-direction over 100 steps was given to all nodes on the far left edge of layer 2; these nodes were given fixed displacement constraints in the y and z-directions. All nodes on the far right edge of layer 1 were given a fixed displacement in all directions. The interlamellar layer was connected to the bottom surface of layer 1 and the top surface of layer 2 in the lap region using a tied contact boundary condition to connect the non-conforming surfaces.

Post Processing

Average surface strains in the lap region and arm region were calculated and plotted to determine the relationship between the two in the model and the experimental.

Then, using mechanical property values from literature (Skaggs et al. 1994; Holzapfel et al. 2005) and finite element modeling in FEBio, multiple values of interlamellar layer elastic moduli (1, 10, 50 MPa) were used to calculate the surface strains in a shear lap test. These modeled surface strains were used to calculate the relationship between the lap region and arm region strains and compared to the experimental data.

Results

Porcine lumbar intervertebral disc AF lamellae were dissected to a shear lap geometry. A representative force/displacement curve is shown in Figure 5.2. The force trace began with a short toe region, a linear region, initial failure to start the sliding phase, and a plateau region during the remaining sliding phase. The key quantities identified in Figure 5.2 are summarized in Table 5.1. Toe and peak displacements were similar among samples, but load and modulus calculations had more variation. In comparison to the relative size of the samples, the average peak displacement was large, 2.60 mm (38.9% of original length). The capital letters marked in Figure 5.2 correspond to the surface displacement fields and sample photographs in Figure 5.3. Over the course of the experiment, the specimen width narrowed, and the strain in the arm was much greater than the strain in the lap region, and the strain in the lap region was inhomogeneous.

Average surface strains in the lap region and arm region were calculated and plotted to determine the relationship between the two in the model and the experimental data (Fig. 5.3, 0.643:1 lap:arm model). These data showed the lap to arm strain ratio increased as the interlamellar modulus decreased. The model in the given state was capable of converging with moduli greater than or equal to 1 MPa.

Comparing the experimental surface strains to the modeled surface strains showed similar trends in the direction of pull. Both the experimental and modeled surface strains showed inhomogeneous and large magnitudes of strain in each component, and narrowing largely occurred from one edge rather than symmetrically.

Discussion

Considering the loading characteristics and surface strains in this study of porcine AF lamellae in the shear lap configuration, a prior study performed using porcine cervical AF lamellae (Gregory et al. 2011), found similar trends. The samples in this study reached higher loads (T_{Toe} , Current: 0.23N/mm, Gregory *et al.*: 0.06 N/mm; T_{Peak} , Current: 2.53 N/mm, Gregory *et al.*: 0.30 N/mm; $T_{Plateau}$, Current: 0.34 N/mm, Gregory *et al.*: 0.14 N/mm) and larger displacements (δ_{Toe} , Current: 1.06 mm, Gregory *et al.*: 0.95 mm; δ_{Peak} , Current: 2.60, Gregory *et al.*: 2.08 mm). Although the load-displacement data in the current study was higher, the current study data is within range of the prior study due to the large variation in data. Similar to the previous study, the current study also saw sample narrowing prior to an initial failure and then a sliding phase with a non-zero load. The prior study observed arm strains to be four times larger than those in the lap region; the current study observed arm strains to be one and a half times larger than the lap strains. This difference is likely due to the differences in surface strain tracking. The current study utilizes a custom code which tracks the pattern on the material surface, which is made more distinct and unique by adding Verhoeff's stain, while the previous study utilizes the natural color of the surface to track movement. It is possible that error could be incurred from water moving on the surface or varying reflections of light. In

terms of the modeling utilized, the current model and the model from the previous study both produced largely homogeneous strains in the lap region.

The prior study, however, did not report strains in the direction perpendicular to pull (y-direction) as well as shear strains (xy-direction). In the anterior-posterior direction, both the model and the experiment in the current study showed asymmetric narrowing attributed to the anisotropic and off-axis collagen fiber orientation within the lamellae. The model however, did not capture the shear strains well. The model showed largely homogeneous shear strains, while the experiment showed inhomogeneous strains across the surface.

In comparison to the experimental data, the FEBio model displayed similar trends in surface strains. The FEBio model, however, did not show the pronounced strain inhomogeneity (in the x and xy –directions) seen experimentally, which must have resulted from a combination of lamellar tissue inhomogeneity, interlamellar matrix inhomogeneity, and local failure events. It has been shown (C. A. Pezowicz, Robertson, and Broom 2006) that the lamellae are connected by short fibers as well as other material.

The FEBio model was limited in characterizing the shear stress of the shear lap configuration due to not being able to converge on interlamellar elastic moduli less than 1 MPa. The lap and arm strains calculated at 1, 10, and 50 MPa suggest the modulus of the interlamellar region was likely much lower than 1 MPa. This interlamellar modulus estimate was two orders of magnitude lower than the modulus of the lamellae along the fibers (Skaggs et al. 1994; Holzapfel et al. 2005). Intuition suggests, the interlamellar modulus would be more similar in stiffness due to the extensibility possible prior to initial failure. The model would likely be more accurate if a more realistic interlamellar

connection were defined to approximate the anatomy seen in (C. A. Pezowicz, Robertson, and Broom 2006).

In conclusion, porcine lumbar AF lamellae in the shear lap configuration showed connected lamellae withstood significant displacement prior to failure as well as carried significant load during the sliding phase. Significant asymmetric narrowing was seen in samples prior to initial failure as well as in the non-linear model. The current non-linear model constitutes a first-step towards understanding delaminating AF lamellae as well as the mechanical significance of the interlamellar connection. Physiologically, this response suggests a preventative feature within the IVD to resist or mitigate damage in spinal axial rotation, which produces shear within the AF.

Table 5.1. AF Lap Strength Summary Data. The location at which each mechanical property was calculated is shown in Figure 5.1. Load data is divided by sample width.

Mechanical Property	Symbol	Mean \pm Standard Deviation
Load at the end of the toe region	T_{Toe}	0.23 ± 0.20 N/mm
Displacement at the end of the toe region	δ_{Toe}	1.06 ± 0.47 mm
Peak load prior to initial failure	T_{Peak}	2.53 ± 2.44 N/mm
Displacement at peak load prior to failure	δ_{Peak}	2.60 ± 0.52 mm
Peak load prior to plateau region	T_{Max}	2.69 ± 2.36 mm
Elastic modulus	M	6.57 ± 8.68 MPa
Load at plateau region	T_{Plateau}	0.34 ± 0.26 N/mm

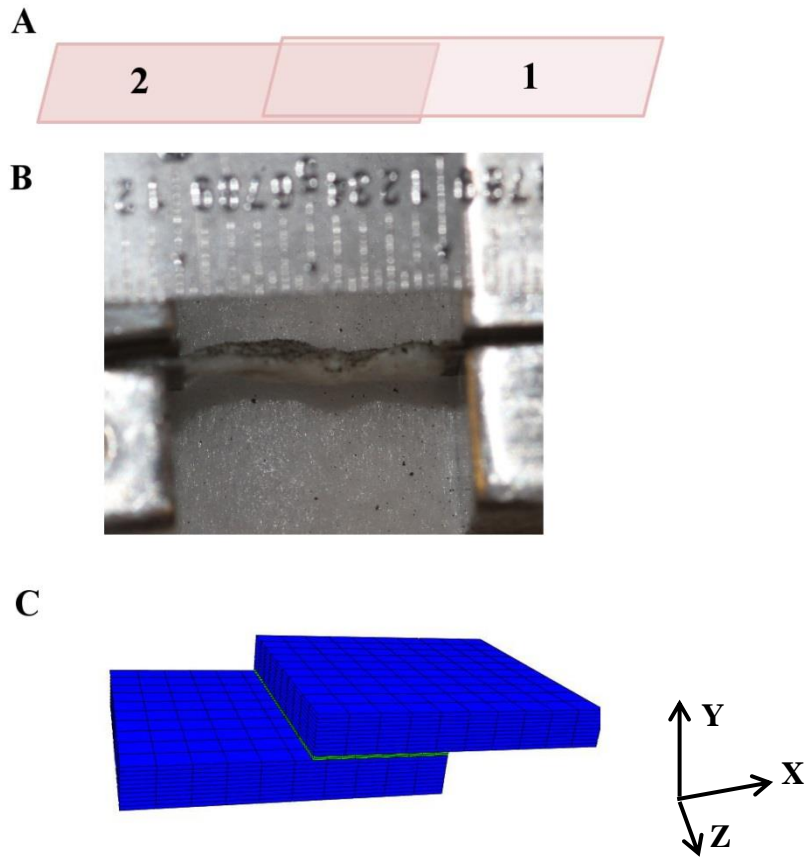


Figure 5.1. A. Shear Lap Geometry. B. Image of Representative Lap Sample from the Side. C. FEBio Representative Mesh Geometry with Coordinate System.

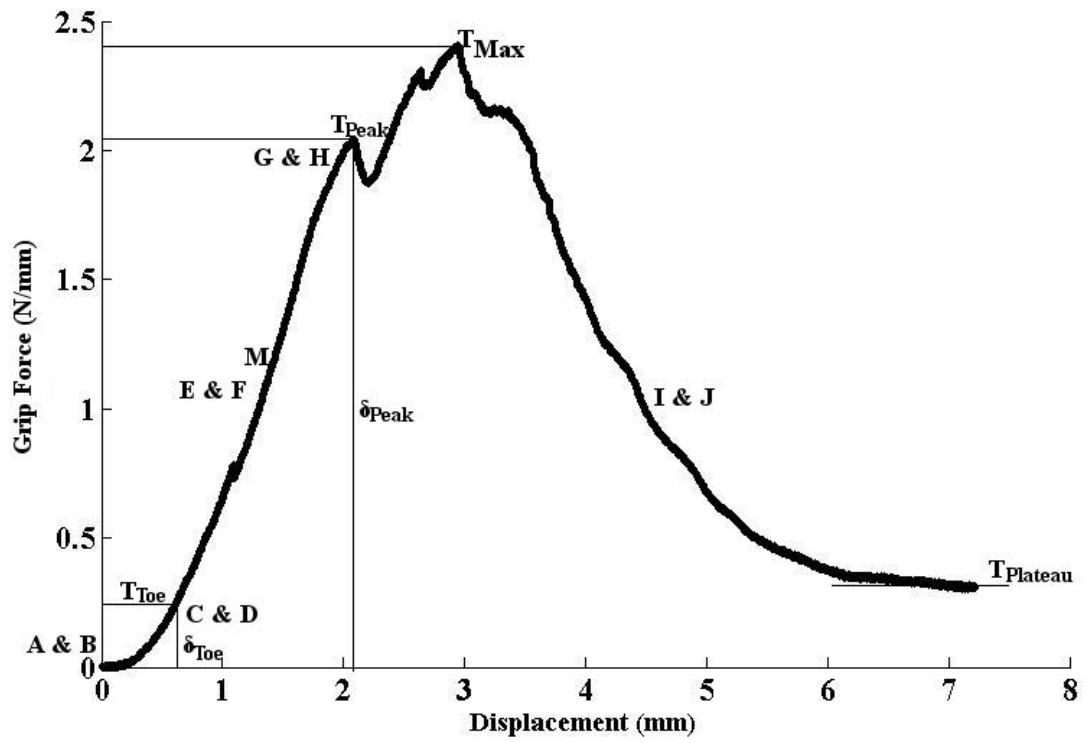


Figure 5.2. Representative Shear Lap Load Curve. Locations marked with letters are visualized in Figure 5.4. The quantities defined by lines and labeled are summarized in Table 5.1.

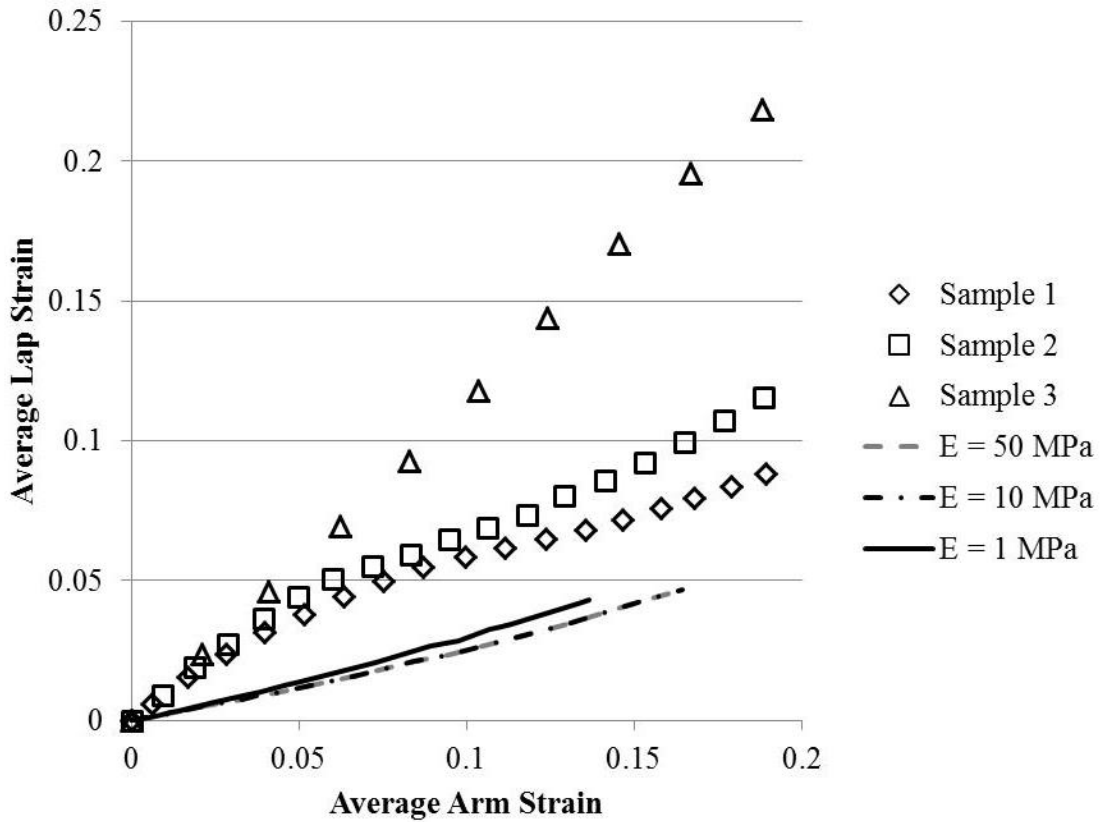
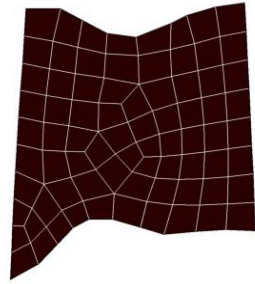
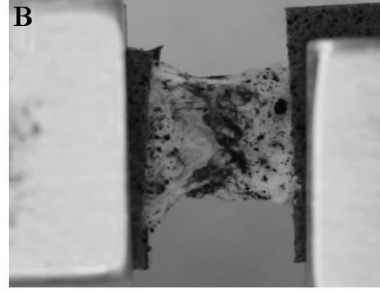


Figure 5.3. Utilizing Average Lap and Arm Strain to Evaluate Model Interlamellar Stiffness. Lap and arm surface strains were averaged and plotted over the course of the experiment for each sample tested, prior to failure. Modeled lap and arm surface strain were plotted to evaluate how the interlamellar stiffness influences the lap and arm strain.

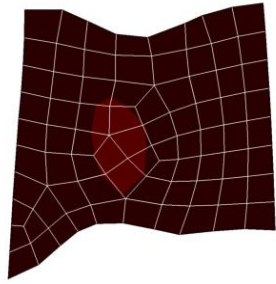
A



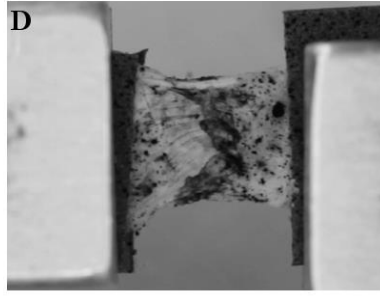
B



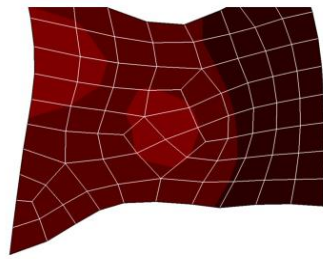
C



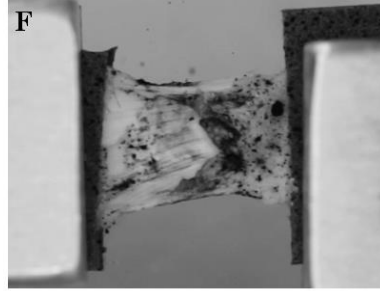
D



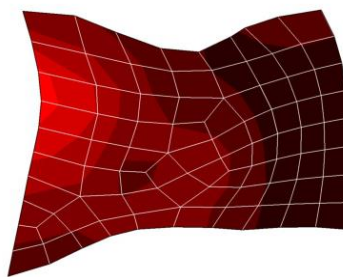
E



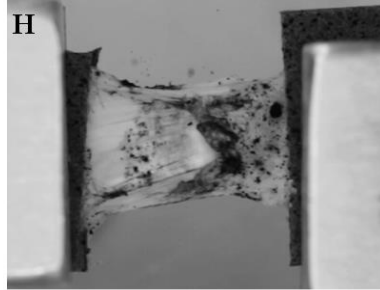
F



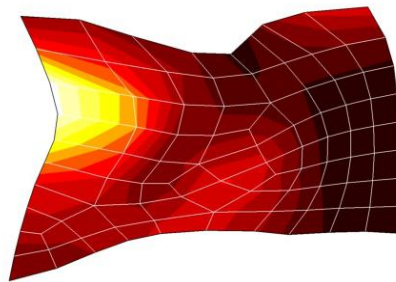
G



H



I



J

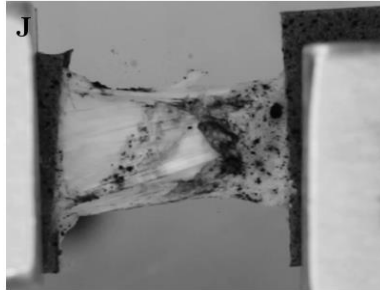


Figure 5.4. Representative Shear Lap Surface During Experiment. The letters shown correspond to force/displacement locations identified in Figure 5.3. Contour maps of strain in the direction of pull with the mesh shown in white are on the left. Frames of the sample surface are shown on the right.

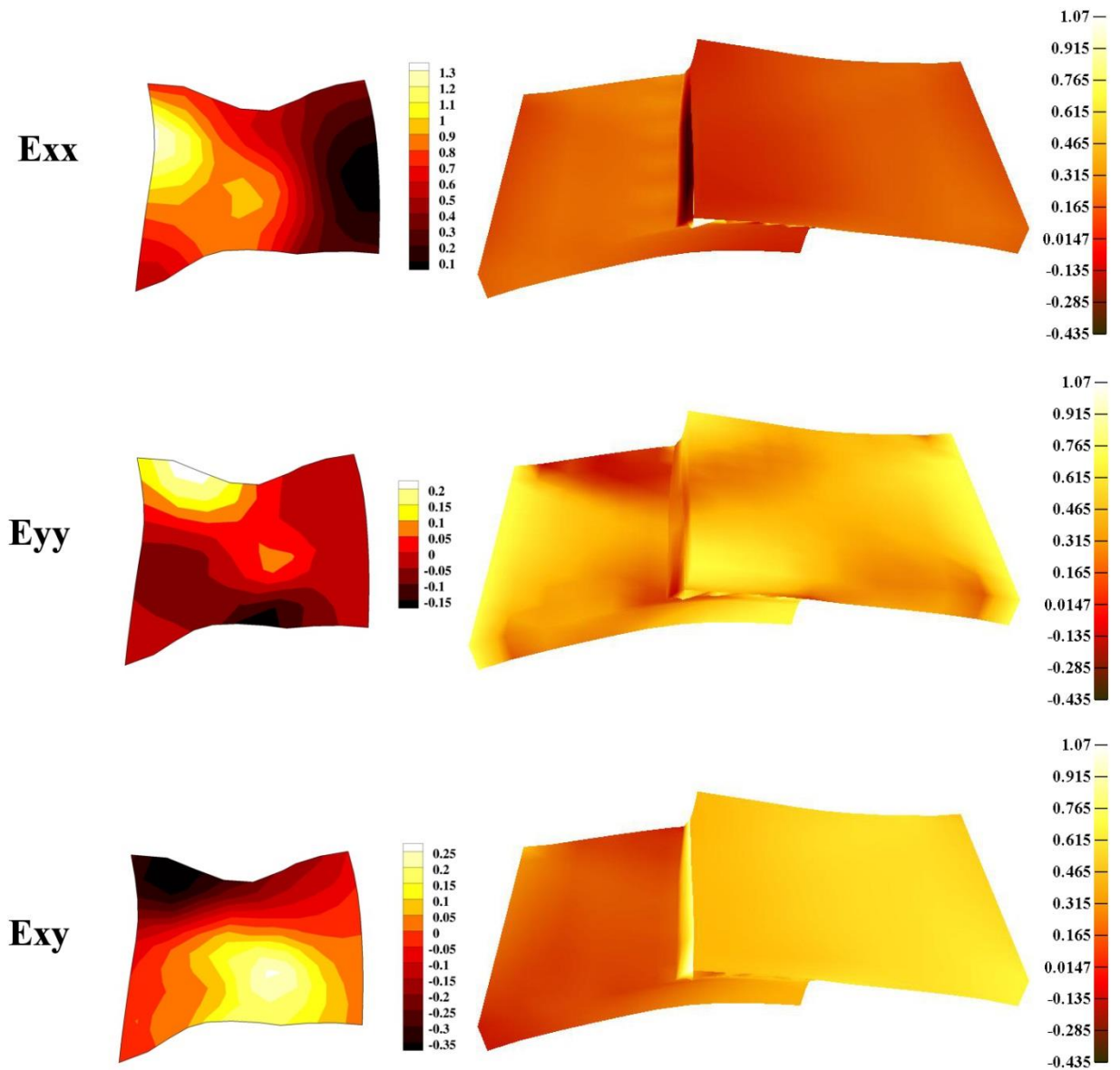


Figure 5.5. Shear Lap Surface Displacements at Maximum Strain Prior to Failure. Experimental data shown at left and FEBio data ($E_{\text{interlamellar region}} = 1\text{MPa}$) at right. A. Surface strain data, E_{xx} . B. Surface strain data, E_{yy} . C. Surface strain data, E_{xy} .

Chapter 6 – Conclusions and Future Work

The purpose of this dissertation was to assess the interlamellar connection through the pre-failure and failure mechanics of discrete AF lamellae by creating a physiologically relevant test method to deform single and multiple AF lamellae and evaluate the kinetic response using a validated structural model.

Vertebral kinematics were quantified to define a planar biaxial tensile test configuration mimicking forward-bending flexion. Intervertebral strains were found to be symmetric during the flexion movement, but intervertebral angles were not. This result suggests these two aspects are physiologically decoupled and that non-symmetric test protocols should be considered when characterizing motion segments. 20% of the maximum intervertebral strain was utilized to define the protocol, to approximate the physiologic strain due to the inability to visualize the curvature of the IVD surface and as porcine spines were used, a reduced strain was used due to differences between porcine and human cadaveric spinal tissue.

The structural model was validated using multiple fibrous tissue types. In doing so, it was found that a more robust fit of the data was accomplished by comparing the finite element model to both grip force and surface displacement data. This model could

be further assessed by fitting repeated experiments of a single tissue or testing a tissue in multiple different loading configurations.

Single and multiple lamellae mechanics were elucidated using multi-axial load cells, a physiologic protocol, as well as a validated structural model. Single lamella samples were found to produce significant in-plane shear force and moments, while multiple lamellae samples did not, after accounting for the number of lamellae. The differences suggest that single lamellae experience complex loading in biaxial tension, but this complex loading is attenuated in the context of multiple lamellae. In addition, fitted parameters of the single lamella samples had a slight trend towards difference from the multiple lamellae samples

Interlamellar mechanics were assessed in pre-failure and failure modes, showing the interlamellar connection was more influential in shear than biaxial tension. AF lamellae were found to withstand significant displacement prior to failure as well as to carry a non-zero load during the sliding phase. This non-zero response in sliding suggests a preventative feature within the AF region to resist and mitigate damage due to axial rotation, which produces shear loading. Also, although the model used was unable to characterize the shear stress of the experimental data in its present form, further improvements to the model such as a more accurate depiction of the interlamellar connection such as vertical fibers may improve the capabilities of the model.

The work accomplished in this dissertation forms a base for further assessment of discrete AF lamella(e). Using porcine tissue, experiments described within Chapters 4 and 5 should be continued to increase the sample size and strengthen possible trends seen within this work. With these tools, these experiments should also be performed with a

larger sample size using healthy human cadaver tissue, since the test protocol is based on human kinematics and mechanical properties obtained from human cadaveric spinal tissue would be more useful in applications such as multi-scale finite element modeling of the spine, as opposed to porcine tissue. It would also be interesting to use these tools to assess human cadaveric tissue from the degenerative spectrum, although it would be challenging to dissect AF from more degenerated tissue.

Bibliography

“3D Spine, Primal Interactive Human, Anatomy.tv.”
<http://www.anatomy.tv/realApps.aspx#>.

Abumi, K, M M Panjabi, K M Kramer, J Duranceau, T Oxland, and J J Crisco. 1990.
“Biomechanical Evaluation of Lumbar Spinal Stability after Graded Facetectomies.”
Spine 15 (11): 1142–47. <http://www.ncbi.nlm.nih.gov/pubmed/2267608>.

Acaroglu, E. R., J. C. Iatridis, L. A. Setton, R. J. Foster, V. C. Mow, and M. Weidenbaum. 1995. “Degeneration and Aging Affect the Tensile Behavior of Human Lumbar Anulus Fibrosus.” *Spine* 20 (24): 2690–2701.
<http://www.scopus.com/inward/record.url?eid=2-s2.0-0029564343&partnerID=tZOtx3y1>.

Adams, M. A. 2004. “Biomechanics of Back Pain.” *Acupuncture in Medicine* 22 (4): 178–88. doi:10.1136/aim.22.4.178.

Adams, M.A., and P. Dolan. 1991. “A Technique for Quantifying the Bending Moment Acting on the Lumbar Spine in Vivo.” *Journal of Biomechanics* 24 (2): 117–26. doi:10.1016/0021-9290(91)90356-R.

Adams, M.A., and W.C. Hutton. 1986. “Has the Lumbar Spine a Margin of Safety in Forward Bending?” *Clinical Biomechanics* 1 (1): 3–6.
<http://www.sciencedirect.com/science/article/pii/0268003386900288>.

Adams, Michael A, and Peter J Roughley. 2006. “What Is Intervertebral Disc Degeneration, and What Causes It?” *Spine* 31 (18): 2151–61. doi:10.1097/01.brs.0000231761.73859.2c.

Adams, P, and H Muir. 1976. “Qualitative Changes with Age of Proteoglycans of Human Lumbar Discs.” *Annals of the Rheumatic Diseases* 35 (4): 289–96. doi:10.1136/ard.35.4.289.

- Andersson, G B. 1999. "Epidemiological Features of Chronic Low-Back Pain." *Lancet* 354 (9178): 581–85. doi:10.1016/S0140-6736(99)01312-4.
- Andersson, G B, R Ortengren, and A Nachemson. 2014. "Intradiskal Pressure, Intra-Abdominal Pressure and Myoelectric Back Muscle Activity Related to Posture and Loading." *Clinical Orthopaedics and Related Research*, no. 129: 156–64. Accessed July 24. <http://www.ncbi.nlm.nih.gov/pubmed/608269>.
- Antoniou, J, T Steffen, F Nelson, N Winterbottom, A P Hollander, R A Poole, M Aebi, and M Alini. 1996. "The Human Lumbar Intervertebral Disc: Evidence for Changes in the Biosynthesis and Denaturation of the Extracellular Matrix with Growth, Maturation, Ageing, and Degeneration." *The Journal of Clinical Investigation* 98 (4): 996–1003. doi:10.1172/JCI118884.
- Auerbach, Joshua D, Wade Johannessen, Arijitt Borthakur, Andrew J Wheaton, Carol A Dolinskas, Richard A Balderston, Ravinder Reddy, and Dawn M Elliott. 2006. "In Vivo Quantification of Human Lumbar Disc Degeneration Using T(1rho)-Weighted Magnetic Resonance Imaging." *European Spine Journal : Official Publication of the European Spine Society, the European Spinal Deformity Society, and the European Section of the Cervical Spine Research Society* 15 Suppl 3 (August): S338–44. doi:10.1007/s00586-006-0083-2.
- Avril, Stéphane, Pierre Badel, Mohamed Gabr, Michael A Sutton, and Susan M Lessner. 2013. "Biomechanics of Porcine Renal Arteries and Role of Axial Stretch." *Journal of Biomechanical Engineering* 135 (8): 81007. doi:10.1115/1.4024685.
- Barbone, Paul E, and Assad A Oberai. 2007. "Elastic Modulus Imaging: Some Exact Solutions of the Compressible Elastography Inverse Problem." *Physics in Medicine and Biology* 52 (6): 1577–93. doi:10.1088/0031-9155/52/6/003.
- Bass, E. C., F. A. Ashford, M. R. Segal, and J. C. Lotz. 2004. "Biaxial Testing of Human Annulus Fibrosus and Its Implications for a Constitutive Formulation." *Annals of Biomedical Engineering* 32 (9): 1231–42. doi:10.1114/B:ABME.0000039357.70905.94.
- Beckstein, Jesse C, A Espinoza Orias, and J. M. Cloyd. 2007. "Axial and Torsion Disc Mechanics for Several Animals Compared to the Human Disc." *Trans Orthop Res Soc* 32: 1141.
- Beckstein, Jesse C, Sounok Sen, Thomas P Schaer, Edward J Vresilovic, and Dawn M Elliott. 2008. "Comparison of Animal Discs Used in Disc Research to Human Lumbar Disc: Axial Compression Mechanics and Glycosaminoglycan Content." *Spine* 33 (6): E166–73. doi:10.1097/BRS.0b013e318166e001.
- Benneker, Lorin M, Paul F Heini, Suzanne E Anderson, Mauro Alini, and Keita Ito. 2005. "Correlation of Radiographic and MRI Parameters to Morphological and

- Biochemical Assessment of Intervertebral Disc Degeneration.” *European Spine Journal : Official Publication of the European Spine Society, the European Spinal Deformity Society, and the European Section of the Cervical Spine Research Society* 14 (1): 27–35. doi:10.1007/s00586-004-0759-4.
- Bittersohl, B, F R Miese, H S Hosalkar, M Herten, G Antoch, R Krauspe, and C Zilkens. 2012. “T2* Mapping of Hip Joint Cartilage in Various Histological Grades of Degeneration.” *Osteoarthritis and Cartilage / OARS, Osteoarthritis Research Society* 20 (7): 653–60. doi:10.1016/j.joca.2012.03.011.
- Blumenkrantz, G, and S Majumdar. 2007. “Quantitative Magnetic Resonance Imaging of Articular Cartilage in Osteoarthritis.” *European Cells & Materials* 13 (January): 76–86. <http://www.ncbi.nlm.nih.gov/pubmed/17506024>.
- Boos, Norbert, Sabine Weissbach, Helmut Rohrbach, Christoph Weiler, Kevin F Spratt, and Andreas G Nerlich. 2002. “Classification of Age-Related Changes in Lumbar Intervertebral Discs: 2002 Volvo Award in Basic Science.” *Spine* 27 (23): 2631–44. doi:10.1097/01.BRS.0000035304.27153.5B.
- Boriek, Aladin M., Joseph R. Rodarte, and Michael B. Reid. 2001. “Shape and Tension Distribution of the Passive Rat Diaphragm.” *Am J Physiol Regulatory Integrative Comp Physiol* 280 (1): R33–41. <http://ajpregu.physiology.org/content/280/1/R33>.
- Brickley-Parsons, D, and M J Glimcher. 1984. “Is the Chemistry of Collagen in Intervertebral Discs an Expression of Wolff’s Law? A Study of the Human Lumbar Spine.” *Spine* 9 (2): 148–63. <http://www.ncbi.nlm.nih.gov/pubmed/6729579>.
- Buckwalter, J A. 1995. “Aging and Degeneration of the Human Intervertebral Disc.” *Spine* 20 (11): 1307–14. <http://www.ncbi.nlm.nih.gov/pubmed/7660243>.
- Busscher, Iris, Joris J W Ploegmakers, Gijsbertus J Verkerke, and Albert G Veldhuizen. 2010. “Comparative Anatomical Dimensions of the Complete Human and Porcine Spine.” *European Spine Journal : Official Publication of the European Spine Society, the European Spinal Deformity Society, and the European Section of the Cervical Spine Research Society* 19 (7): 1104–14. doi:10.1007/s00586-010-1326-9.
- Busscher, Iris, Albert J van der Veen, Jaap H van Dieën, Idsart Kingma, Gijsbertus J Verkerke, and Albert G Veldhuizen. 2010. “In Vitro Biomechanical Characteristics of the Spine: A Comparison between Human and Porcine Spinal Segments.” *Spine* 35 (2): E35–42. doi:10.1097/BRS.0b013e3181b21885.
- Chavhan, Govind B, Paul S Babyn, Bejoy Thomas, Manohar M Shroff, and E Mark Haacke. 2009. “Principles, Techniques, and Applications of T2*-Based MR Imaging and Its Special Applications.” *Radiographics : A Review Publication of the Radiological Society of North America, Inc* 29 (5). Radiological Society of North America: 1433–49. doi:10.1148/rg.295095034.

- Doehring, Todd C, Michael Kahelin, and Ivan Vesely. 2009. "Direct Measurement of Nonuniform Large Deformations in Soft Tissues during Uniaxial Extension." *Journal of Biomechanical Engineering* 131 (6): 061001. doi:10.1115/1.3116155.
- Draper, Norman Richard, and Harry Smith. 1981. "Applied Regression Analysis." In *Applied Regression Analysis*, 2nd ed., 709. Wiley.
<http://books.google.com/books?id=7mtHAAAAMAAJ&pgis=1>.
- Driscoll, Tristan P, Ryan H Nakasone, Spencer E Szczesny, Dawn M Elliott, and Robert L Mauck. 2013. "Biaxial Mechanics and Inter-Lamellar Shearing of Stem-Cell Seeded Electrospun Angle-Ply Laminates for Annulus Fibrosus Tissue Engineering." *Journal of Orthopaedic Research : Official Publication of the Orthopaedic Research Society* 31 (6): 864–70. doi:10.1002/jor.22312.
- Ebara, Sohei, James C Iatridis, Lori A Setton, Robert J Foster, Van C Mow, and Mark Weidenbaum. 1996. "Tensile Properties of Nondegenerate Human Lumbar Anulus Fibrosus." *Spine* 21 (4).
http://journals.lww.com/spinejournal/Fulltext/1996/02150/Tensile_Properties_of_Nondegenerate_Human_Lumbar.9.aspx.
- Eilaghi, Armin, John G Flanagan, G Wayne Brodland, and C Ross Ethier. 2009. "Strain Uniformity in Biaxial Specimens Is Highly Sensitive to Attachment Details." *Journal of Biomechanical Engineering* 131 (9). American Society of Mechanical Engineers: 091003. doi:10.1115/1.3148467.
- Ellingson, Arin M, and David J Nuckley. 2012. "Intervertebral Disc Viscoelastic Parameters and Residual Mechanics Spatially Quantified Using a Hybrid Confined/in Situ Indentation Method." *Journal of Biomechanics* 45 (3): 491–96. doi:10.1016/j.jbiomech.2011.11.050.
- Elliott, Dawn M, and Joseph J Sarver. 2004. "Young Investigator Award Winner: Validation of the Mouse and Rat Disc as Mechanical Models of the Human Lumbar Disc." *Spine* 29 (7): 713–22. <http://www.ncbi.nlm.nih.gov/pubmed/15087791>.
- Elliott, Dawn M., and Lori A. Setton. 2001. "Anisotropic and Inhomogeneous Tensile Behavior of the Human Anulus Fibrosus: Experimental Measurement and Material Model Predictions." *Journal of Biomechanical Engineering* 123 (3): 256. doi:10.1115/1.1374202.
- FARNDALE, R, D BUTTLE, and A BARRETT. 1986. "Improved Quantitation and Discrimination of Sulphated Glycosaminoglycans by Use of Dimethylmethylene Blue." *Biochimica et Biophysica Acta (BBA) - General Subjects* 883 (2): 173–77. doi:10.1016/0304-4165(86)90306-5.

- Flynn, Cormac, and M.B. Rubin. 2014. "An Anisotropic Discrete Fiber Model with Dissipation for Soft Biological Tissues." *Mechanics of Materials* 68: 217–27. <http://www.sciencedirect.com/science/article/pii/S0167663613001385>.
- Fujita, Y, N A Duncan, and J C Lotz. 1997. "Radial Tensile Properties of the Lumbar Annulus Fibrosus Are Site and Degeneration Dependent." *Journal of Orthopaedic Research : Official Publication of the Orthopaedic Research Society* 15 (6): 814–19. doi:10.1002/jor.1100150605.
- Fujita, Y., D.R. Wagner, A.A. Biviji, N.A. Duncan, and J.C. Lotz. 2000. "Anisotropic Shear Behavior of the Annulus Fibrosus: Effect of Harvest Site and Tissue Prestrain." *Medical Engineering & Physics* 22 (5): 349–57. doi:10.1016/S1350-4533(00)00053-9.
- Fung, Y C. 1973. "Biorheology of Soft Tissues." *Biorheology* 10 (2): 139–55. <http://europepmc.org/abstract/MED/4728631/reload=0>.
- Gatton, M L, and M J Pearcy. 1999. "Kinematics and Movement Sequencing during Flexion of the Lumbar Spine." *Clinical Biomechanics (Bristol, Avon)* 14 (6): 376–83. <http://www.ncbi.nlm.nih.gov/pubmed/10521618>.
- Gaudette, Glenn R., Joseph Todaro, Irvin B. Krukenkamp, and Fu-Pen Chiang. 2001. "Computer Aided Speckle Interferometry: A Technique for Measuring Deformation of the Surface of the Heart." *Annals of Biomedical Engineering* 29 (9): 775–80. doi:10.1114/1.1397785.
- Gore, Mugdha, Alesia Sadosky, Brett R Stacey, Kei-Sing Tai, and Douglas Leslie. 2012. "The Burden of Chronic Low Back Pain: Clinical Comorbidities, Treatment Patterns, and Health Care Costs in Usual Care Settings." *Spine* 37 (11): E668–77. doi:10.1097/BRS.0b013e318241e5de.
- Gregory, Diane E, and Jack P Callaghan. 2011. "A Comparison of Uniaxial and Biaxial Mechanical Properties of the Annulus Fibrosus: A Porcine Model." *Journal of Biomechanical Engineering* 133 (2). American Society of Mechanical Engineers: 024503. doi:10.1115/1.4003327.
- Gregory, Diane E, Jim H Veldhuis, Caleb Horst, G Wayne Brodland, and Jack P Callaghan. 2011. "Novel Lap Test Determines the Mechanics of Delamination between Annular Lamellae of the Intervertebral Disc." *Journal of Biomechanics* 44 (1): 97–102. doi:10.1016/j.jbiomech.2010.08.031.
- Guerin, Heather Anne L, and Dawn M Elliott. 2006. "Degeneration Affects the Fiber Reorientation of Human Annulus Fibrosus under Tensile Load." *Journal of Biomechanics* 39 (8): 1410–18. doi:10.1016/j.jbiomech.2005.04.007.

- Haughton, Victor M., Timothy A. Schmidt, Kevin Keele, Howard S. An, and Tae-Hong Lim. 2000. "Flexibility of Lumbar Spinal Motion Segments Correlated to Type of Tears in the Annulus Fibrosus." *Journal of Neurosurgery: Spine* 92 (1). Journal of Neurosurgery Publishing Group: 81–86. doi:10.3171/spi.2000.92.1.0081.
- Hayes, Mark A, Thomas C Howard, Curtis R Gruel, and Joseph A Kopta. 1989. "Roentgenographic Evaluation of Lumbar Spine Flexion-Extension in Asymptomatic Individuals." *Spine* 14 (3). http://journals.lww.com/spinejournal/Fulltext/1989/03000/Roentgenographic_Evaluation_of_Lumbar_Spine.14.aspx.
- Holzappel, G A, C A J Schulze-Bauer, G Feigl, and P Regitnig. 2005. "Single Lamellar Mechanics of the Human Lumbar Anulus Fibrosus." *Biomechanics and Modeling in Mechanobiology* 3 (3): 125–40. doi:10.1007/s10237-004-0053-8.
- Hoppe, Sven, Sebastian Quirbach, Tallal C Mamisch, Fabian G Krause, Stefan Werlen, and Lorin M Benneker. 2012. "Axial T2 Mapping in Intervertebral Discs: A New Technique for Assessment of Intervertebral Disc Degeneration." *European Radiology* 22 (9): 2013–19. doi:10.1007/s00330-012-2448-8.
- Huyghe, J M, and M R Drost. 2004. "Uniaxial Tensile Testing of Canine Annulus Fibrosus Tissue under Changing Salt Concentrations." *Biorheology* 41 (3-4): 255–61. <http://www.ncbi.nlm.nih.gov/pubmed/15299258>.
- Iatridis, James C, Lori A Setton, Mark Weidenbaum, and Van C Mow. 1997. "Alterations in the Mechanical Behavior of the Human Lumbar Nucleus Pulposus with Degeneration and Aging." *Journal of Orthopaedic Research* 15 (2). Wiley Subscription Services, Inc., A Wiley Company: 318–22. doi:10.1002/jor.1100150224.
- Jacobs, Nathan T, Daniel H Cortes, Edward J Vresilovic, and Dawn M Elliott. 2013. "Biaxial Tension of Fibrous Tissue: Using Finite Element Methods to Address Experimental Challenges Arising from Boundary Conditions and Anisotropy." *Journal of Biomechanical Engineering* 135 (2). American Society of Mechanical Engineers: 021004. doi:10.1115/1.4023503.
- Johannessen, Wade, Joshua D Auerbach, Andrew J Wheaton, Alykhan Kurji, Arijitt Borthakur, Ravinder Reddy, and Dawn M Elliott. 2006. "Assessment of Human Disc Degeneration and Proteoglycan Content Using T1rho-Weighted Magnetic Resonance Imaging." *Spine* 31 (11): 1253–57. doi:10.1097/01.brs.0000217708.54880.51.
- Johannessen, Wade, and Dawn M Elliott. 2005. "Effects of Degeneration on the Biphasic Material Properties of Human Nucleus Pulposus in Confined Compression." *Spine* 30 (24): E724–9. <http://www.ncbi.nlm.nih.gov/pubmed/16371889>.

- JP, Urban, and Roberts S. 2003. "Degeneration of the Intervertebral Disc." *Arthritis Research & Therapy*. doi:10.1186/ar629.
- Kaigle, A M, P Wessberg, and T H Hansson. 1998. "Muscular and Kinematic Behavior of the Lumbar Spine during Flexion-Extension." *Journal of Spinal Disorders* 11 (2): 163–74. <http://www.ncbi.nlm.nih.gov/pubmed/9588475>.
- Kaigle, Allison M., Sten H. Holm, and Tommy H. Hansson. 1997. "1997 Volvo Award Winner in Biomechanical Studies." *Spine* 22 (24): 2796–2806. doi:10.1097/00007632-199712150-00002.
- Kanayama, Masahiro, Kuniyoshi Abumi, Kiyoshi Kaneda, Shigeru Tadano, and Takayoshi Ukai. 1996. "Phase Lag of the Intersegmental Motion in Flexion-Extension of the Lumbar and Lumbosacral Spine." *Spine* 21 (12): 1416–22. doi:10.1097/00007632-199606150-00004.
- Keyes, Joseph T, Darren G Haskett, Urs Utzinger, Mohamad Azhar, and Jonathan P Vande Geest. 2011. "Adaptation of a Planar Microbiaxial Optomechanical Device for the Tubular Biaxial Microstructural and Macroscopic Characterization of Small Vascular Tissues." *Journal of Biomechanical Engineering* 133 (7): 075001. doi:10.1115/1.4004495.
- Kim, Jung, and Mandayam A. Srinivasan. 2005. "Characterization of Viscoelastic Soft Tissue Properties from In Vivo Animal Experiments and Inverse FE Parameter Estimation." In *Medical Image Computing and Computer-Assisted Intervention – MICCAI 2005 Lecture Notes in Computer Science*, edited by James S. Duncan and Guido Gerig, 3750:595–606. Lecture Notes in Computer Science. Berlin, Heidelberg: Springer Berlin Heidelberg. doi:10.1007/11566489.
- Knapp, David M., Victor H. Barocas, Alice G. Moon, Kyeonga Yoo, Linda R. Petzold, and Robert T Tranquillo. 1997. "Rheology of Reconstituted Type I Collagen Gel in Confined Compression." *Journal of Rheology* 41 (5). American Institute of Physics: 971. doi:10.1122/1.550817.
- Krause, Fabian G, Georg Klammer, Lorin M Benneker, Stefan Werlen, Tallal C Mamisch, and Martin Weber. 2010. "Biochemical T2* MR Quantification of Ankle Arthrosis in Pes Cavovarus." *Journal of Orthopaedic Research : Official Publication of the Orthopaedic Research Society* 28 (12): 1562–68. doi:10.1002/jor.21192.
- Li, W G, X Y Luo, N A Hill, R W Ogden, A Smythe, A W Majeed, and N Bird. 2012. "A Quasi-Nonlinear Analysis of the Anisotropic Behaviour of Human Gallbladder Wall." *Journal of Biomechanical Engineering* 134 (10). American Society of Mechanical Engineers: 101009. doi:10.1115/1.4007633.

- Lin, H S, Y K Liu, and K H Adams. 1978. "Mechanical Response of the Lumbar Intervertebral Joint under Physiological (complex) Loading." *The Journal of Bone and Joint Surgery. American Volume* 60 (1): 41–55.
<http://www.ncbi.nlm.nih.gov/pubmed/624758>.
- Luoma, K, T Vehmas, H Riihimäki, and R Raininko. 2001. "Disc Height and Signal Intensity of the Nucleus Pulposus on Magnetic Resonance Imaging as Indicators of Lumbar Disc Degeneration." *Spine* 26 (6): 680–86.
<http://www.ncbi.nlm.nih.gov/pubmed/11246386>.
- Maas, Steve A, Benjamin J Ellis, Gerard A Ateshian, and Jeffrey A Weiss. 2012. "FEBio: Finite Elements for Biomechanics." *Journal of Biomechanical Engineering* 134 (1). American Society of Mechanical Engineers: 011005. doi:10.1115/1.4005694.
- Malgorzata, Zak, and Celina Pezowicz. 2013. "Spinal Sections and Regional Variations in the Mechanical Properties of the Annulus Fibrosus Subjected to Tensile Loading." *Acta of Bioengineering and Biomechanics* 15 (1).
- Mamisch, Tallal Charles, Timothy Hughes, Timothy J Mosher, Christoph Mueller, Siegfried Trattnig, Chris Boesch, and Goetz Hannes Welsch. 2012. "T2 Star Relaxation Times for Assessment of Articular Cartilage at 3 T: A Feasibility Study." *Skeletal Radiology* 41 (3): 287–92. doi:10.1007/s00256-011-1171-x.
- Marchand, F, and A M Ahmed. 1990. "Investigation of the Laminate Structure of Lumbar Disc Anulus Fibrosus." *Spine* 15 (5): 402–10.
<http://www.ncbi.nlm.nih.gov/pubmed/2363068>.
- Marik, W, S Apprich, G H Welsch, T C Mamisch, and S Trattnig. 2012. "Biochemical Evaluation of Articular Cartilage in Patients with Osteochondrosis Dissecans by Means of Quantitative T2- and T2-Mapping at 3T MRI: A Feasibility Study." *European Journal of Radiology* 81 (5): 923–27. doi:10.1016/j.ejrad.2011.01.124.
- Marinelli, Nicholas L, Victor M Haughton, Alejandro Muñoz, and Paul A Anderson. 2009. "T2 Relaxation Times of Intervertebral Disc Tissue Correlated with Water Content and Proteoglycan Content." *Spine* 34 (5): 520–24.
 doi:10.1097/BRS.0b013e318195dd44.
- Martufi, Giampaolo, and T Christian Gasser. 2013. "Review: The Role of Biomechanical Modeling in the Rupture Risk Assessment for Abdominal Aortic Aneurysms." *Journal of Biomechanical Engineering* 135 (2). American Society of Mechanical Engineers: 021010. doi:10.1115/1.4023254.
- Michalek, A.J., M.G. Gardner-Morse, and J.C. Iatridis. 2012. "Large Residual Strains Are Present in the Intervertebral Disc Annulus Fibrosus in the Unloaded State." *Journal of Biomechanics* 45 (7): 1227–31.
<http://www.sciencedirect.com/science/article/pii/S0021929012000851>.

- Miese, Falk Roland, Christoph Zilkens, Arne Holstein, Bernd Bittersohl, Patric Kröpil, Tallal Charles Mamisch, Rotem Shlomo Lanzman, et al. 2011. "Assessment of Early Cartilage Degeneration after Slipped Capital Femoral Epiphysis Using T2 and T2* Mapping." *Acta Radiologica (Stockholm, Sweden : 1987)* 52 (1). SAGE Publications: 106–10. doi:10.3109/02841851.2010.516015.
- Miller, Kristin S, Brianne K Connizzo, Elizabeth Feeney, Jennica J Tucker, and Louis J Soslowsky. 2012. "Examining Differences in Local Collagen Fiber Crimp Frequency throughout Mechanical Testing in a Developmental Mouse Supraspinatus Tendon Model." *Journal of Biomechanical Engineering* 134 (4): 041004. doi:10.1115/1.4006538.
- Miller, Kristin S, Lena Edelstein, Brianne K Connizzo, and Louis J Soslowsky. 2012. "Effect of Preconditioning and Stress Relaxation on Local Collagen Fiber Re-Alignment: Inhomogeneous Properties of Rat Supraspinatus Tendon." *Journal of Biomechanical Engineering* 134 (3): 031007. doi:10.1115/1.4006340.
- Nachemson, A L F L, Albert B Schultz, and Michael H Berkson. 1979. "Mechanical Properties of Human Lumbar Spine Motion Segments: Influences of Age, Sex, Disc Level, and Degeneration." *Spine* 4 (1). http://journals.lww.com/spinejournal/Fulltext/1979/01000/Mechanical_Properties_of_Human_Lumbar_Spine_Motion.1.aspx.
- Nagel, Tina M, Jared L Zitnay, Victor H Barocas, and David J Nuckley. 2014. "Quantification of Continuous in Vivo Flexion-Extension Kinematics and Intervertebral Strains." *European Spine Journal : Official Publication of the European Spine Society, the European Spinal Deformity Society, and the European Section of the Cervical Spine Research Society* 23 (4): 754–61. doi:10.1007/s00586-014-3195-0.
- Nagel, Tina M., Mohammad F. Hadi, Amy A. Claeson, David J. Nuckley, and Victor H. Barocas. 2014. "Combining Displacement Field and Grip Force Information to Determine Mechanical Properties of Planar Tissue with Complicated Geometry." *Journal of Biomechanical Engineering*.
- Nagel, Tina M., Ramesh Raghupathy, Arin M. Ellingson, David J. Nuckley, and Victor H. Barocas. 2011. "A Non-Linear Model to Describe the Material Properties of Single Lamellae in the Human Annulus Fibrosus." In *ASME 2011 Summer Bioengineering Conference, Parts A and B*, 497–98. Farmington, PA: ASME. doi:10.1115/SBC2011-53848.
- Nerurkar, Nandan L, Dawn M Elliott, and Robert L Mauck. 2010. "Mechanical Design Criteria for Intervertebral Disc Tissue Engineering." *Journal of Biomechanics* 43 (6): 1017–30. doi:10.1016/j.jbiomech.2009.12.001.

- Nguyen, An M, Wade Johannessen, Jonathon H Yoder, Andrew J Wheaton, Edward J Vresilovic, Arijitt Borthakur, and Dawn M Elliott. 2008. "Noninvasive Quantification of Human Nucleus Pulposus Pressure with Use of T1rho-Weighted Magnetic Resonance Imaging." *The Journal of Bone and Joint Surgery. American Volume* 90 (4). The Journal of Bone and Joint Surgery, Inc. 796–802. doi:10.2106/JBJS.G.00667.
- O'Connell, Grace D, Wade Johannessen, Edward J Vresilovic, and Dawn M Elliott. 2007. "Human Internal Disc Strains in Axial Compression Measured Noninvasively Using Magnetic Resonance Imaging." *Spine* 32 (25). http://journals.lww.com/spinejournal/Fulltext/2007/12010/Human_Internal_Disc_Strains_in_Axial_Compression.13.aspx.
- O'Connell, Grace D, S. Sen, Daniel H Cortes, and Dawn M. Elliott. 2010. "Biaxial Mechanics Are Inhomogeneous and Altered with Degeneration in the Human Annulus Fibrosus." *Transactions of the 56th Annual Meeting of the Orthopaedic Research Society, New Orleans, LA*.
- O'Connell, Grace D, Sounok Sen, and Dawn M Elliott. 2012. "Human Annulus Fibrosus Material Properties from Biaxial Testing and Constitutive Modeling Are Altered with Degeneration." *Biomechanics and Modeling in Mechanobiology* 11 (3-4): 493–503. doi:10.1007/s10237-011-0328-9.
- O'Connell, Grace D, Edward J Vresilovic, and Dawn M Elliott. 2011. "Human Intervertebral Disc Internal Strain in Compression: The Effect of Disc Region, Loading Position, and Degeneration." *Journal of Orthopaedic Research : Official Publication of the Orthopaedic Research Society* 29 (4): 547–55. doi:10.1002/jor.21232.
- Okawa, A, K Shinomiya, H Komori, T Muneta, Y Arai, and O Nakai. 1998. "Dynamic Motion Study of the Whole Lumbar Spine by Videofluoroscopy." *Spine* 23 (16): 1743–49. <http://www.ncbi.nlm.nih.gov/pubmed/9728375>.
- Pearce, R H, B J Grimmer, and M E Adams. 1987. "Degeneration and the Chemical Composition of the Human Lumbar Intervertebral Disc." *Journal of Orthopaedic Research : Official Publication of the Orthopaedic Research Society* 5 (2): 198–205. doi:10.1002/jor.1100050206.
- Pearcy, M J, and S B Tibrewal. 1984. "Lumbar Intervertebral Disc and Ligament Deformations Measured in Vivo." *Clinical Orthopaedics and Related Research*, no. 191 (December): 281–86. <http://www.ncbi.nlm.nih.gov/pubmed/6499321>.
- Pearcy, Mark, Ian Portek, and Janis Sheperd. 1984. "Three-Dimensional X-Ray Analysis of Normal Movement in the Lumbar Spine." *Spine* 9 (3). http://journals.lww.com/spinejournal/Fulltext/1984/04000/Three_Dimensional_X_ray_Analysis_of_Normal.13.aspx.

- Pellot-Barakat, Claire, Frédérique Frouin, Michael F Insana, and Alain Herment. 2004. "Ultrasound Elastography Based on Multiscale Estimations of Regularized Displacement Fields." *IEEE Transactions on Medical Imaging* 23 (2): 153–63. doi:10.1109/TMI.2003.822825.
- Pezowicz, C. 2010. "Analysis of Selected Mechanical Properties of Intervertebral Disc Annulus Fibrosus in Macro and Microscopic Scale." *Journal of Theoretical and Applied Mechanics* Vol. 48 nr: 917–32. <http://yadda.icm.edu.pl/yadda/element/bwmeta1.element.baztech-article-BWM7-0002-0048>.
- Pezowicz, Celina A, Peter A Robertson, and Neil D Broom. 2006. "The Structural Basis of Interlamellar Cohesion in the Intervertebral Disc Wall." *Journal of Anatomy* 208 (3): 317–30. doi:10.1111/j.1469-7580.2006.00536.x.
- Pfirrmann, C W, A Metzdorf, M Zanetti, J Hodler, and N Boos. 2001. "Magnetic Resonance Classification of Lumbar Intervertebral Disc Degeneration." *Spine* 26 (17): 1873–78. <http://www.ncbi.nlm.nih.gov/pubmed/11568697>.
- Quinn, Kyle P, and Beth A Winkelstein. 2010. "Full Field Strain Measurements of Collagenous Tissue by Tracking Fiber Alignment through Vector Correlation." *Journal of Biomechanics* 43 (13): 2637–40. doi:10.1016/j.jbiomech.2010.05.008.
- Raghupathy, Ramesh, and Victor H Barocas. 2009. "A Closed-Form Structural Model of Planar Fibrous Tissue Mechanics." *Journal of Biomechanics* 42 (10): 1424–28. doi:10.1016/j.jbiomech.2009.04.005.
- Raghupathy, Ramesh, Colleen Witzenburg, Spencer P Lake, Edward A Sander, and Victor H Barocas. 2010. "Generalized Anisotropic Inverse Mechanics for Soft Tissues." *Journal of Biomechanical Engineering* 132 (8). American Society of Mechanical Engineers: 081006. doi:10.1115/1.4001257.
- Raghupathy, Ramesh, Colleen Witzenburg, Spencer P Lake, Edward A Sander, and Victor H Barocas. 2011. "Identification of Regional Mechanical Anisotropy in Soft Tissue Analogs." *Journal of Biomechanical Engineering* 133 (9): 091011. doi:10.1115/1.4005170.
- Roughley, Peter J. 2004. "Biology of Intervertebral Disc Aging and Degeneration: Involvement of the Extracellular Matrix." *Spine* 29 (23): 2691–99. <http://www.ncbi.nlm.nih.gov/pubmed/15564918>.
- Sacks, M S, and D C Gloeckner. 1999. "Quantification of the Fiber Architecture and Biaxial Mechanical Behavior of Porcine Intestinal Submucosa." *Journal of Biomedical Materials Research* 46 (1): 1–10. <http://www.ncbi.nlm.nih.gov/pubmed/10357130>.

- Sacks, Michael S. 2000. "Biaxial Mechanical Evaluation of Planar Biological Materials." *Journal of Elasticity and the Physical Science of Solids* 61 (1-3). Kluwer Academic Publishers: 199–246. doi:10.1023/A:1010917028671.
- Shea, M, T Y Takeuchi, R H Wittenberg, A A White, and W C Hayes. 1994. "A Comparison of the Effects of Automated Percutaneous Diskectomy and Conventional Diskectomy on Intradiscal Pressure, Disk Geometry, and Stiffness." *Journal of Spinal Disorders* 7 (4): 317–25.
<http://www.ncbi.nlm.nih.gov/pubmed/7949699>.
- Skaggs, D L, M Weidenbaum, J C Latridis, A Ratcliffe, and V C Mow. 1994. "Regional Variation in Tensile Properties and Biochemical Composition of the Human Lumbar Anulus Fibrosus." *Spine* 19 (12).
http://journals.lww.com/spinejournal/Fulltext/1994/06000/Regional_Variation_in_Tensile_Properties_and.2.aspx.
- Starcher, B. 2001. "A Ninhydrin-Based Assay to Quantitate the Total Protein Content of Tissue Samples." *Analytical Biochemistry* 292 (1): 125–29.
doi:10.1006/abio.2001.5050.
- Stegemann, Hermann, and Karlheinz Stalder. 1967. "Determination of Hydroxyproline." *Clinica Chimica Acta* 18 (2): 267–73. doi:10.1016/0009-8981(67)90167-2.
- Stokes, I A. 1987. "Surface Strain on Human Intervertebral Discs." *Journal of Orthopaedic Research : Official Publication of the Orthopaedic Research Society* 5 (3): 348–55. doi:10.1002/jor.1100050306.
- Sun, Wei, and Michael S Sacks. 2005. "Finite Element Implementation of a Generalized Fung-Elastic Constitutive Model for Planar Soft Tissues." *Biomechanics and Modeling in Mechanobiology* 4 (2-3): 190–99. doi:10.1007/s10237-005-0075-x.
- Sun, Wei, Michael S. Sacks, and Michael J. Scott. 2005. "Effects of Boundary Conditions on the Estimation of the Planar Biaxial Mechanical Properties of Soft Tissues." *Journal of Biomechanical Engineering* 127 (4). American Society of Mechanical Engineers: 709. doi:10.1115/1.1933931.
- Takayanagi, Kenji, Kazuhisa Takahashi, Masatsune Yamagata, Hideshige Moriya, Hiroshi Kitahara, and Tamotsu Tamaki. 2001. "Using Cineradiography for Continuous Dynamic-Motion Analysis of the Lumbar Spine." *Spine* 26 (17).
http://journals.lww.com/spinejournal/Fulltext/2001/09010/Using_Cineradiography_for_Continuous.8.aspx.
- Tertti, M, H Paajanen, M Laato, H Aho, M Komu, and M Kormano. 1991. "Disc Degeneration in Magnetic Resonance Imaging. A Comparative Biochemical, Histologic, and Radiologic Study in Cadaver Spines." *Spine* 16 (6): 629–34.
<http://www.ncbi.nlm.nih.gov/pubmed/1862401>.

- Teyhen, Deydre S, Timothy W Flynn, John D Childs, Timothy R Kuklo, Michael K Rosner, David W Polly, and Lawrence D Abraham. 2007. "Fluoroscopic Video to Identify Aberrant Lumbar Motion." *Spine* 32 (7): E220–9. doi:10.1097/01.brs.0000259206.38946.cb.
- Wagner, Diane R, and Jeffrey C Lotz. 2004. "Theoretical Model and Experimental Results for the Nonlinear Elastic Behavior of Human Annulus Fibrosus." *Journal of Orthopaedic Research : Official Publication of the Orthopaedic Research Society* 22 (4): 901–9. doi:10.1016/j.orthres.2003.12.012.
- Waldman, S, and J Lee. 2002. "Boundary Conditions during Biaxial Testing of Planar Connective Tissues Part II Fiber Orientation." *Journal of Materials Science Letters* 21 (15). Kluwer Academic Publishers: 1215–21. doi:10.1023/A:1016576603938.
- Waldman, S, M Sacks, and J Lee. 2002. "Boundary Conditions during Biaxial Testing of Planar Connective Tissues. Part 1: Dynamic Behavior." *Journal of Materials Science: Materials in Medicine* 13 (10). Kluwer Academic Publishers: 933–38. doi:10.1023/A:1019896210320.
- Wan, Chao, Zhixiu Hao, and Shizhu Wen. 2013. "The Effect of the Variation in ACL Constitutive Model on Joint Kinematics and Biomechanics Under Different Loads: A Finite Element Study." *Journal of Biomechanical Engineering* 135 (4). American Society of Mechanical Engineers: 41002. doi:10.1115/1.4023696.
- Weidenbaum, M, R J Foster, B A Best, F Saed-Nejad, E Nickoloff, J Newhouse, A Ratcliffe, and V C Mow. 1992. "Correlating Magnetic Resonance Imaging with the Biochemical Content of the Normal Human Intervertebral Disc." *Journal of Orthopaedic Research : Official Publication of the Orthopaedic Research Society* 10 (4): 552–61. doi:10.1002/jor.1100100410.
- Welsch, Goetz H, Siegfried Trattinig, Timothy Hughes, Sebastian Quirbach, Alexander Olk, Matthias Blanke, Stefan Marlovits, and Tallal C Mamisch. 2010. "T2 and T2* Mapping in Patients after Matrix-Associated Autologous Chondrocyte Transplantation: Initial Results on Clinical Use with 3.0-Tesla MRI." *European Radiology* 20 (6): 1515–23. doi:10.1007/s00330-009-1669-y.
- Welsch, Goetz Hannes, Siegfried Trattinig, Tatjana Paternostro-Sluga, Klaus Bohndorf, Sabine Goed, David Stelzeneder, and Tallal Charles Mamisch. 2011. "Parametric T2 and T2* Mapping Techniques to Visualize Intervertebral Disc Degeneration in Patients with Low Back Pain: Initial Results on the Clinical Use of 3.0 Tesla MRI." *Skeletal Radiology* 40 (5): 543–51. doi:10.1007/s00256-010-1036-8.
- Wheaton, Andrew J, George R Dodge, Arijitt Borthakur, J Bruce Kneeland, H Ralph Schumacher, and Ravinder Reddy. 2005. "Detection of Changes in Articular Cartilage Proteoglycan by T(1rho) Magnetic Resonance Imaging." *Journal of*

Orthopaedic Research : Official Publication of the Orthopaedic Research Society 23 (1): 102–8. doi:10.1016/j.orthres.2004.06.015.

Wilke, Hans-Joachim, Peter Neef, Barbara Hinz, Helmut Seidel, and Lutz Claes. 2001. “Intradiscal Pressure Together with Anthropometric Data – a Data Set for the Validation of Models.” *Clinical Biomechanics* 16 (January): S111–S126. doi:10.1016/S0268-0033(00)00103-0.

Williams, A, Y Qian, D Bear, and C R Chu. 2010. “Assessing Degeneration of Human Articular Cartilage with Ultra-Short Echo Time (UTE) T2* Mapping.” *Osteoarthritis and Cartilage / OARS, Osteoarthritis Research Society* 18 (4): 539–46. doi:10.1016/j.joca.2010.02.001.

Williams, A, Y Qian, and C R Chu. 2011. “UTE-T2* Mapping of Human Articular Cartilage in Vivo: A Repeatability Assessment.” *Osteoarthritis and Cartilage / OARS, Osteoarthritis Research Society* 19 (1): 84–88. doi:10.1016/j.joca.2010.10.018.

Witzenburg, Colleen, Ramesh Raghupathy, Stefan M Kren, Doris A Taylor, and Victor H Barocas. 2012. “Mechanical Changes in the Rat Right Ventricle with Decellularization.” *Journal of Biomechanics* 45 (5): 842–49. doi:10.1016/j.jbiomech.2011.11.025.

Yamamoto, Isao, Manohar M Panjabi, Trey Crisco, and Tom Oxland. 1989. “Three-Dimensional Movements of the Whole Lumbar Spine and Lumbosacral Joint.” *Spine* 14 (11). http://journals.lww.com/spinejournal/Fulltext/1989/11000/Three_Dimensional_Movements_of_the_Whole_Lumbar.20.aspx.

Appendices

Appendix A – Directions for structural model use

This Appendix details how to set up and run the regression code with a four-parameter structural model (Nagel, Hadi, et al. 2014). The regression code is executed in Matlab and calls the structural model in C. The structural model code defaults to displacement control boundary conditions on the arms of the sample rather than force control. Sample files are provided as an example and a flow chart to describe the parameter finding scheme.

Set Up

The structural model code needs to be compiled to generate the executable. Place Makefile, elmt01.cc, meshLin2Quad.h, myFEM.cc, pformpar.cc, pmain.cc, and tmpMakefile in a directory. Type the following commands:

```
mkdir bin
mkdir obj
module load intel mkl
make
```

The bin and obj directories should populate, and the bin directory will contain the executable.

The following input files are necessary to run the regression code: mesh.dat, boundaries.dat, bc.dat, expForceData.csv, and dispXX.dat.

mesh.dat

```
line 1: numberOfNodes
line 2: numberOfElements
line 3 – (number of nodes + 3): NodeXCoordinate NodeYCoordinate
(number of nodes + 4) – (number of nodes + 4 + number of elements):
globalNode#ForLocalNode1 globalNode#ForLocalNode2 globalNode#ForLocalNode3
globalNode#ForLocalNode4
```

boundaries.dat

```
line 1: number of nodes in bottom arm
line 2: [list of nodes in bottom arm delimited by spaces]
line 3: number of nodes in right arm
line 4: [list of nodes in right arm delimited by spaces]
```

line 5: number of nodes in top arm
line 6: [list of nodes in top arm delimited by spaces]
line 7: number of nodes in left arm
line 8: [list of nodes in left arm delimited by spaces]

bc.dat

The following are possible boundary condition definitions:

- ID1 node# freeInX freeInY (0 = free, 1 = fixed)
- ID2 startNode# endNode# freeInX freeInY (0 = free, 1 = fixed)
- ID3 startNode# endNode# inStepsOf freeInX freeInY
- ID4 startNode# endNode# inStepsOf xDisplacement yDisplacement
- ID5 startNode# endNode# inStepsOf xDisplacement
- ID6 startNode# endNode# inStepsOf yDisplacement
- ID7 node# xDisplacement
- ID8 node# yDisplacement

The initial guesses for each parameter are defined on the last line.

lines 1-(number of boundary condition lines): ID# ...
line (number of boundary condition lines + 1): NUMMAT 1
line (number of boundary condition lines + 2): DTYPE 1
line (number of boundary condition lines + 3): DPARAM kappaVal muVal aVal bVal

expForceData.csv

The code is set up to read in data from a comma delimited file where column 3 is the top arm, column 5 is the bottom arm, column 7 is the right arm, and column 9 is the left arm.

dispXX.dat

The code is set up to read in multiple steps of nodal displacements; one file for each step. The nodal displacements are determined from digital image correlation. Each file contains the x displacement and y displacement for each node at the current step.

forward_min.m

The regression code is executed in Matlab (forward_min.m). The following lines need to be customized for the problem:

(line 18) Enter the initial guess for μ in degrees.

(line 20) Enter the initial guess for κ .

(line 22) Enter the initial guess for A in Newtons/(mesh length units).

(line 24) Enter the initial guess for B.

(line 74) This is the system call the structural model executable. It includes a path to the executable, the number of steps to generate to fit the data, and a path to a temporary output file. Edit the path to the directory with the executable and simple structural model files, and change the number of steps to match the number of displacement files you will use.

(line 80) Add paths to all of the displacement files that will be used.

(line 102) Make sure the number of calls to the experiment displacement paths matches the number of displacement files that will be used.

(line 117) This is the system call to the structural model executable. It includes a path to the executable, the number of steps to generate to fit the data, and a path to a temporary output file. Edit the path to the directory with the executable and simple structural model files, and change the number of steps to match the number of displacement files you will use.

(line 123) Add paths to all of the displacement files that will be used.

(line 144) Make sure the number of calls to the experiment displacement paths match the number of displacement files that will be used.

(line 157) Make sure the number of calls to the experiment displacement paths match the number of displacement files that will be used.

(line 171) Make sure the number of calls to the experiment displacement paths match the number of displacement files that will be used.

(line 185) Make sure the number of calls to the experiment displacement paths match the number of displacement files that will be used.

(line 199) Make sure the number of calls to the experiment displacement paths match the number of displacement files that will be used.

(line 216) Enter the number of lines in bc.dat minus 1.

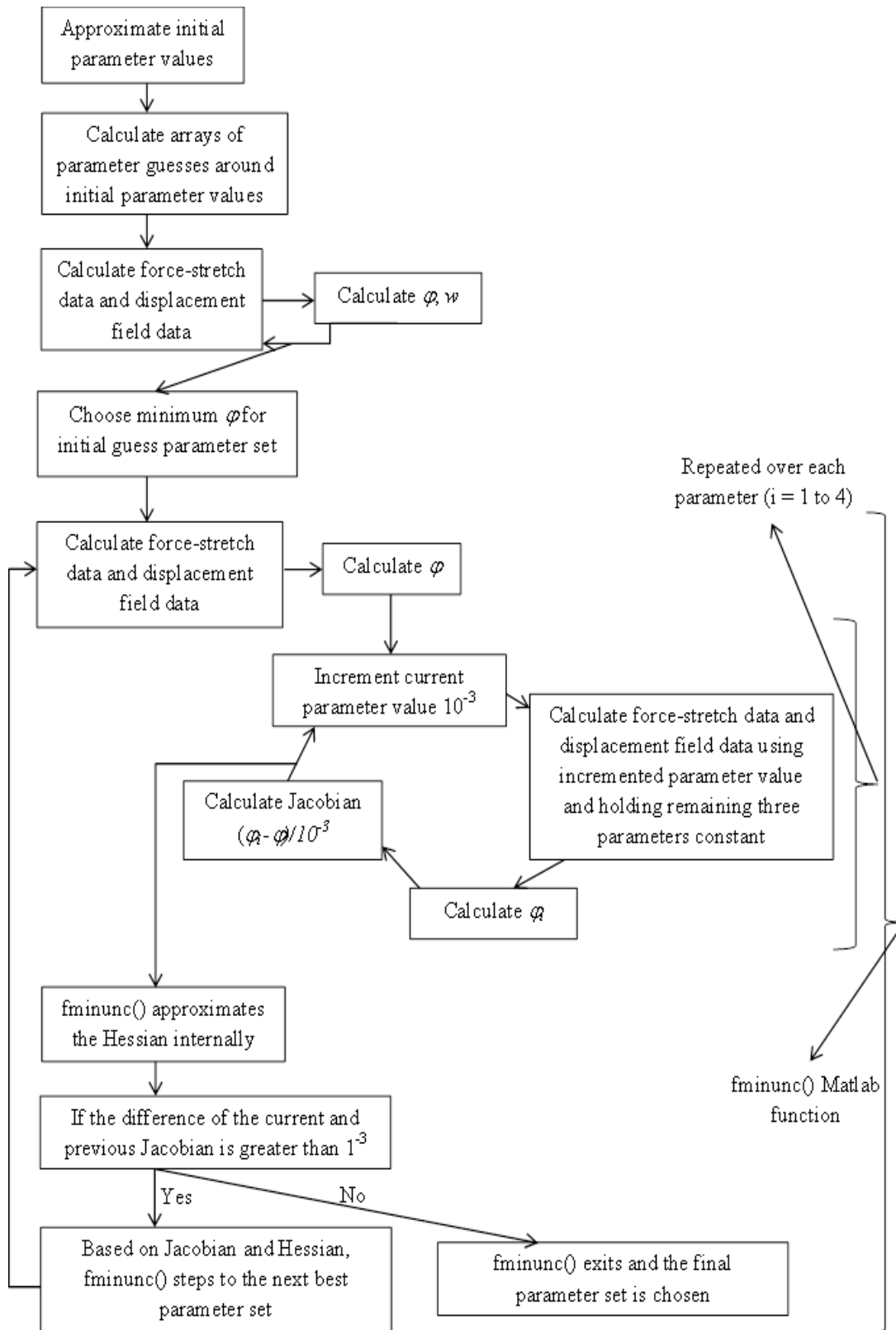
(line 232) Make sure the number of calls to the experiment displacement paths match the number of displacement files that will be used.

(line 242) Enter the line where you want to start reading in expForceData.csv.

(line 248) Make sure the loop goes to the number of steps used in the call to the executable.

(line 254) Enter the number of lines in expForceData.csv to read divided by the number of steps used in the call to the executable.

- (line 270) Enter the total number of nodes in the mesh.
- (line 273) Enter the nodes at the grips. These nodes will be excluded from the sum of squared error calculation.
- (line 290) Enter the sum of the total number of nodes, elements, and one.
- (line 292) Make sure the loop goes to the number of steps used in the call to the executable.
- (line 319) Make sure the loop goes to the number of steps used in the call to the executable.
- (line 322) Make sure the correct number of displacement paths are read in.
- (line 413) Make sure the loop goes to the number of steps used in the call to the executable.
- (line 434) Make sure the correct number of displacement paths are read in.
- (line 443) Enter the line where you want to start reading in expForceData.csv.
- (line 450) Make sure the loop goes to the number of steps used in the call to the executable.
- (line 454) Enter the number of lines in expForceData.csv to read divided by the number of steps used in the call to the executable.
- (line 470) Enter the total number of nodes in the mesh.
- (line 473) Enter the nodes at the grips. These nodes will be excluded from the sum of squared error calculation.
- (line 489) Enter the sum of the total number of nodes, elements, and one.
- (line 491) Make sure the loop goes to the number of steps used in the call to the executable.
- (line 517) Make sure the loop goes to the number of steps used in the call to the executable.
- (line 521) Make sure the correct number of displacement paths are read in.
- (line 615) Make sure the correct number of displacement paths are read in.



forward_min.m

```
% vvDESCRIPTION
% =====
% FORWARD_MIN() successively calls the executable runNLcoarse
% in order to minimize the sum of squared error between a set
% of experimental and a set of model force data and displacement data.
% Relies on minimizers in the MATLAB minimization toolbox.
%
% HISTORY
% =====
% May 21 2011 -- Created -- MFH
% Sept 16, 2011 -- Updated to minimize forces and displacements -- TMN
% Aug 5, 2013 -- Updated to minimize using fminunc using gradients -- TMN

function forward_min()

    fprintf(1,'=====
\nMinimizing forward problem...
\n');

    mu = 30.;% in degrees

    kappa =4.;

    A = 0.013;

    B = 13.;

    X0 = [kappa mu A B]; % initial guesses [kappa mu A B]

    kspace = linspace(X0(1)*0.75,X0(1)*1.05,5);
    mspace = linspace(X0(2)*0.75,X0(2)*1.05,5);
    aspace = linspace(X0(3)*0.75,X0(3)*1.05,5);
    bspace = linspace(X0(4)*0.75,X0(4)*1.05,5);

    error_tens = zeros(5,5,5,5);

    %loop through all parameter values to find best initial guess
    global w
    for i=1:5
        fprintf(1,'We are at kappa # %d\n',i);
        for j= 1:5
            for k = 1:5
                for m = 1:5
                    X_current = [kspace(i),mspace(j),aspace(k),bspace(m)];
                    [error_tens(i,j,k,m),w] = test_function2(X_current);
                end
            end
        end
    end
```

```

        end
    end
end

[val,indices] = min(error_tens);

X_initial =
[kspace(indices(1)),mspace(indices(2)),aspace(indices(3)),bspace(indices(4))]

[val,w]=test_function2(X_initial);

fprintf(1,'The SSE for the initial guess is %f\n',val);

% passes initial guesses to determine sse
[X, fval, exitflag, output] = fminunc( @test_function, X_initial,
optimset('DiffMinChange',1e-3,'GradObj','on','Display','iter','PlotFcns',@optimplotfval))

fprintf(1,'All done folks...\n=====');

fprintf(1,'kappa = %f\n', X(1));
fprintf(1,'mu = %f\n',X(2));
fprintf(1,'A = %f\n',X(3));
fprintf(1,'B = %f\n', X(4));

end

function [sse,w] = test_function2( X )
% this function determines the sse of the current guess without
% calculating each of the Jacobians

parameter_file_path    = './bc.dat';
forward_problem_bin    = '~/forward_search/bin/runNLcoarse 15 > ./temp_output';
armforce_experiment_path = './expForceData.csv';
armforce_model_path    = './armForce.dat';
disp_model_path        = './plot.tec';

% make sure has correct # of paths
disp_experiment_path1  = './disp01.dat';
disp_experiment_path2  = './disp02.dat';
disp_experiment_path3  = './disp03.dat';
disp_experiment_path4  = './disp04.dat';
disp_experiment_path5  = './disp05.dat';
disp_experiment_path6  = './disp06.dat';
disp_experiment_path7  = './disp07.dat';
disp_experiment_path8  = './disp08.dat';
disp_experiment_path9  = './disp09.dat';

```

```

disp_experiment_path10    = './disp10.dat';
disp_experiment_path11    = './disp11.dat';
disp_experiment_path12    = './disp12.dat';
disp_experiment_path13    = './disp13.dat';
disp_experiment_path14    = './disp14.dat';
disp_experiment_path15    = './disp15.dat';

write_test_bc( X, parameter_file_path );

system( forward_problem_bin );

% make sure it passes all displacement paths
[sse,w] = calc_sse1( armforce_experiment_path, armforce_model_path, ...
disp_experiment_path1, disp_experiment_path2, disp_experiment_path3, ...
disp_experiment_path4, disp_experiment_path5, disp_experiment_path6, ...
disp_experiment_path7, disp_experiment_path8, disp_experiment_path9, ...
disp_experiment_path10, disp_experiment_path11, disp_experiment_path12, ...
disp_experiment_path13, disp_experiment_path14, disp_experiment_path15, ...
disp_model_path );

end

function [sse,g] = test_function( X )
% this function determines the sse of the current guess and calculates
% the Jacobians

parameter_file_path      = './bc.dat';
forward_problem_bin      = '~/forward_search/bin/runNLcoarse 15 > ./temp_output';
armforce_experiment_path = './expForceData.csv';
armforce_model_path      = './armForce.dat';
disp_model_path          = './plot.tec';

% make sure has correct # of paths
disp_experiment_path1     = './disp01.dat';
disp_experiment_path2     = './disp02.dat';
disp_experiment_path3     = './disp03.dat';
disp_experiment_path4     = './disp04.dat';
disp_experiment_path5     = './disp05.dat';
disp_experiment_path6     = './disp06.dat';
disp_experiment_path7     = './disp07.dat';
disp_experiment_path8     = './disp08.dat';
disp_experiment_path9     = './disp09.dat';
disp_experiment_path10    = './disp10.dat';
disp_experiment_path11    = './disp11.dat';
disp_experiment_path12    = './disp12.dat';

```

```

disp_experiment_path13    = './disp13.dat';
disp_experiment_path14    = './disp14.dat';
disp_experiment_path15    = './disp15.dat';

write_test_bc( X, parameter_file_path );

system( forward_problem_bin );

% make sure it passes all displacement paths
sse = calc_sse( armforce_experiment_path, armforce_model_path, ...
disp_experiment_path1, disp_experiment_path2, disp_experiment_path3, ...
disp_experiment_path4, disp_experiment_path5, disp_experiment_path6, ...
disp_experiment_path7, disp_experiment_path8, disp_experiment_path9, ...
disp_experiment_path10, disp_experiment_path11, disp_experiment_path12, ...
disp_experiment_path13, disp_experiment_path14, disp_experiment_path15, ...
disp_model_path );

%% find kappa derivative
X_k = [X(1)+10e-3, X(2), X(3), X(4)];
write_test_bc( X_k, parameter_file_path );
system( forward_problem_bin );

sse_k = calc_sse( armforce_experiment_path, armforce_model_path, ...
disp_experiment_path1, disp_experiment_path2, disp_experiment_path3, ...
disp_experiment_path4, disp_experiment_path5, disp_experiment_path6, ...
disp_experiment_path7, disp_experiment_path8, disp_experiment_path9, ...
disp_experiment_path10, disp_experiment_path11, disp_experiment_path12, ...
disp_experiment_path13, disp_experiment_path14, disp_experiment_path15, ...
disp_model_path );
g(1) = (sse_k - sse)/10e-3;

%% find mu derivative
X_mu = [X(1), X(2)+10e-3, X(3), X(4)];
write_test_bc( X_mu, parameter_file_path );
system( forward_problem_bin );

sse_mu = calc_sse(armforce_experiment_path, armforce_model_path, ...
disp_experiment_path1, disp_experiment_path2, disp_experiment_path3, ...
disp_experiment_path4, disp_experiment_path5, disp_experiment_path6, ...
disp_experiment_path7, disp_experiment_path8, disp_experiment_path9, ...
disp_experiment_path10, disp_experiment_path11, disp_experiment_path12, ...
disp_experiment_path13, disp_experiment_path14, disp_experiment_path15, ...
disp_model_path );
g(2) = (sse_mu - sse)/10e-3;

%% find A derivative

```

```

X_a = [X(1), X(2), X(3)+10e-3, X(4)];
write_test_bc( X_a, parameter_file_path );
system( forward_problem_bin );

sse_a = calc_sse( armforce_experiment_path, armforce_model_path, ...
disp_experiment_path1, disp_experiment_path2, disp_experiment_path3, ...
disp_experiment_path4, disp_experiment_path5, disp_experiment_path6, ...
disp_experiment_path7, disp_experiment_path8, disp_experiment_path9, ...
disp_experiment_path10, disp_experiment_path11, disp_experiment_path12, ...
disp_experiment_path13, disp_experiment_path14, disp_experiment_path15, ...
disp_model_path );
g(3) = (sse_a - sse)/10e-3;

% find B derivative
X_b = [X(1), X(2), X(3), X(4)+10e-3];
write_test_bc( X_b, parameter_file_path );
system( forward_problem_bin );

sse_b = calc_sse( armforce_experiment_path, armforce_model_path, ...
disp_experiment_path1, disp_experiment_path2, disp_experiment_path3, ...
disp_experiment_path4, disp_experiment_path5, disp_experiment_path6, ...
disp_experiment_path7, disp_experiment_path8, disp_experiment_path9, ...
disp_experiment_path10, disp_experiment_path11, disp_experiment_path12, ...
disp_experiment_path13, disp_experiment_path14, disp_experiment_path15, ...
disp_model_path );
g(4) = (sse_b - sse)/10e-3;

end

function write_test_bc( X, parameter_file_path )
% this function writes the new bc.dat file

fid = fopen( parameter_file_path, 'r+' );

nbc = 116; % number of boundary condition lines in bc.dat file - 1

for n = 1 : nbc % loop over boundary conditions in bc.dat and do not write over

    line_val = fgetl( fid );

end

% write over parameter line, 5 digits of precision for each parameter
fprintf(fid,'%s %.5f %.5f %.5f %.5f\n', 'DPARAM', X(1), X(2), X(3), X(4));

```

```

fclose( fid );

end

function sse = calc_sse( armforce_experiment_path, armforce_model_path, ...
    disp_experiment_path1, disp_experiment_path2, disp_experiment_path3, ...
    disp_experiment_path4, disp_experiment_path5, disp_experiment_path6, ...
    disp_experiment_path7, disp_experiment_path8, disp_experiment_path9, ...
    disp_experiment_path10, disp_experiment_path11, disp_experiment_path12, ...
    disp_experiment_path13, disp_experiment_path14, disp_experiment_path15, ...
    disp_model_path )

% this function calculates the sse for arm forces and nodal displacements
global w
startread = 3151; %line in file where force data you want starts
exp_data = dlmread( armforce_experiment_path, ',', startread, 0);
model_data = load( armforce_model_path );

Ff = 0; %residual for forces
Fn = 0;

for n=1:15 % number of steps

    % Subtract the first data point from each to make sure that it starts
    % from zero

    frac = 150/15;%total number of experimental force data lines / number of steps

    top_error = (exp_data(round(n*frac),3) - exp_data(1,3)) - model_data(n,7);
    bot_error = (exp_data(round(n*frac),5) - exp_data(1,5)) - (-1*model_data(n,3));
    rgt_error = (exp_data(round(n*frac),7) - exp_data(1,7)) - model_data(n,4);
    lft_error = (exp_data(round(n*frac),9) - exp_data(1,9)) - (-1*model_data(n,8));

    Ff = Ff + bot_error^2 + rgt_error^2 + top_error^2 + lft_error^2;

    Fn = Fn + (exp_data(round(n*frac),5)-exp_data(1,5))^2 +
(exp_data(round(n*frac),7)-exp_data(1,7))^2 + (exp_data(round(n*frac),3)-
exp_data(1,3))^2 + (exp_data(round(n*frac),9)-exp_data(1,9))^2;

end

Rf = (Ff/Fn);%normalized residual for forces

total_nodes=414;

```

```

nodes = linspace(1,total_nodes,total_nodes);

edge_nodes = [15,16,17,59,60,12,61,62,63,45,8,44,43,3,4,5]; % listing of grip nodes to
exclude
edge_nodes=sort(edge_nodes);
nodes(edge_nodes)=[];

Ex = 0; %residual for strains
En = 0;

i=1;% counter for number of nodes to read the displacements
l = length(nodes);

% read model displacements

start = 3; % data starts on line 3

m=1; % counter for strain steps in plot.tec file

skip = 791; % # nodes + # elements + 1

for m=1:15 %# of steps

    if m==1
        s = (start + ((m-1)*skip)) - 1;
    else
        s = (start + ((1*(m-1))*skip)) - 1;
    end

    e = s + nodes(l) - 1;

    % read the file only in the area you want
    disp_model = dlmread(disp_model_path,'',[s,2,e,3]);

    for i=1:l
        % store x and y displacements at the current node

        disp_x(m,i)=disp_model(nodes(i),1);
        disp_y(m,i)=disp_model(nodes(i),2);

    end

end

% read experiment displacements

```

```
m=1;% counter for number of nodes to read the displacements from each file
```

```
for m=1:15
```

```
    e = nodes(length(nodes))-1; %last node in list - 1
```

```
    if m==1
```

```
        disp_exp = dlmread(disp_experiment_path1,'',[0,0,e,1]);
```

```
    end
```

```
    if m==2
```

```
        disp_exp = dlmread(disp_experiment_path2,'',[0,0,e,1]);
```

```
    end
```

```
    if m==3
```

```
        disp_exp = dlmread(disp_experiment_path3,'',[0,0,e,1]);
```

```
    end
```

```
    if m==4
```

```
        disp_exp = dlmread(disp_experiment_path4,'',[0,0,e,1]);
```

```
    end
```

```
    if m==5
```

```
        disp_exp = dlmread(disp_experiment_path5,'',[0,0,e,1]);
```

```
    end
```

```
    if m==6
```

```
        disp_exp = dlmread(disp_experiment_path6,'',[0,0,e,1]);
```

```
    end
```

```
    if m==7
```

```
        disp_exp = dlmread(disp_experiment_path7,'',[0,0,e,1]);
```

```
    end
```

```
    if m==8
```

```
        disp_exp = dlmread(disp_experiment_path8,'',[0,0,e,1]);
```

```
    end
```

```
    if m==9
```

```
        disp_exp = dlmread(disp_experiment_path9,'',[0,0,e,1]);
```

```
    end
```

```
    if m==10
```

```
        disp_exp = dlmread(disp_experiment_path10,'',[0,0,e,1]);
```

```
    end
```

```

if m==11
    disp_exp = dlmread(disp_experiment_path11, '[0,0,e,1]');
end

if m==12
    disp_exp = dlmread(disp_experiment_path12, '[0,0,e,1]');
end

if m==13
    disp_exp = dlmread(disp_experiment_path13, '[0,0,e,1]');
end

if m==14
    disp_exp = dlmread(disp_experiment_path14, '[0,0,e,1]');
end

if m==15
    disp_exp = dlmread(disp_experiment_path15, '[0,0,e,1]');
end

t=1; % counter for displacement files

dispx_exp(1,1:length(nodes))=0;% set first value in array to zero
dispy_exp(1,1:length(nodes))=0;

%store displacements

if m==1

    for t=1:length(nodes) % for each tracked node

        k=m;

        dispx_exp(k,t)=disp_exp(nodes(t),1);
        dispy_exp(k,t)=disp_exp(nodes(t),2);
    end
else
    for t=1:length(nodes) % for each tracked node

        k=m;

        dispx_exp(k,t)=disp_exp(nodes(t),1) + dispx_exp(m-1,t);
        dispy_exp(k,t)=disp_exp(nodes(t),2) + dispy_exp(m-1,t);
    end
end
end
end

```

```

% compute sse for each node displacement

i=1;

for i=1:15

    j = 1;

    for j = 1:length(nodes)

        ux = disp_x_exp(i,j)-disp_x(i,j);
        uy = disp_y_exp(i,j)-disp_y(i,j);
        En = En + (disp_x_exp(i,j))^2 + (disp_y_exp(i,j))^2;

        Ex = Ex + ux^2 + uy^2;

    end
end

Rx = Ex/En; %normalized residual for displacements

sse = Rf + w*Rx; % total residual

end

function [sse,w] = calc_sse1( armforce_experiment_path, armforce_model_path, ...
    disp_experiment_path1, disp_experiment_path2, disp_experiment_path3, ...
    disp_experiment_path4, disp_experiment_path5, disp_experiment_path6, ...
    disp_experiment_path7, disp_experiment_path8, disp_experiment_path9, ...
    disp_experiment_path10, disp_experiment_path11, disp_experiment_path12, ...
    disp_experiment_path13, disp_experiment_path14, disp_experiment_path15, ...
    disp_model_path )
% this function calculates the sse for arm forces and nodal displacements and the
weighting factor

startread = 3151; %line in file where force data you want starts
exp_data = dlmread( armforce_experiment_path, ',',startread,0);
model_data = load( armforce_model_path );

Ff = 0; %residual for forces
Fn = 0;

for n=1:15

    % Subtracting the first data point from each to make sure that it

```

```

% starts from zero.
frac = 150/15;

top_error = (exp_data(round(n*frac),3) - exp_data(1,3)) - model_data(n,7);
bot_error = (exp_data(round(n*frac),5) - exp_data(1,5)) - (-1*model_data(n,3));
rgt_error = (exp_data(round(n*frac),7) - exp_data(1,7)) - model_data(n,4);
lft_error = (exp_data(round(n*frac),9) - exp_data(1,9)) - (-1*model_data(n,8));

Ff = Ff + bot_error^2 + rgt_error^2 + top_error^2 + lft_error^2;
% I'm subtracting the first data point from each to make sure that it
% starts from zero. I didn't zero out after the preload.
Fn = Fn + (exp_data(round(n*frac),5)-exp_data(1,5))^2 +
(exp_data(round(n*frac),7)-exp_data(1,7))^2 + (exp_data(round(n*frac),3)-
exp_data(1,3))^2 + (exp_data(round(n*frac),9)-exp_data(1,9))^2;

end

Rf = (Ff/Fn);%normalized residual for forces

total_nodes=414;
nodes = linspace(1,total_nodes,total_nodes);

edge_nodes = [15,16,17,59,60,12,61,62,63,45,8,44,43,3,4,5]; % listing of grip nodes to
exclude
edge_nodes=sort(edge_nodes);% listing of grip nodes in mesh
nodes(edge_nodes)=[];

Ex = 0; %residual for strains
En = 0;

i=1;% counter for number of nodes to read the displacements
l = length(nodes);
% read model displacements

start = 3; % data starts on line 3

m=1; % counter for strain steps in plot.tec file

skip = 791; % # nodes + # elements + 1

for m=1:15 %# of steps

    if m==1
        s = (start + ((m-1)*skip)) - 1;
    else

```

```

        s = (start + ((1*(m-1))*skip)) - 1;
    end

    e = s + nodes(1) - 1;

    % read the file only in the area you want
    disp_model = dlmread(disp_model_path, '[s,2,e,3]');

    for i=1:l
        % store x and y displacements at the current node

        disp_x(m,i)=disp_model(nodes(i),1);
        disp_y(m,i)=disp_model(nodes(i),2);

    end
end

% read experiment displacements

m=1;% counter for number of nodes to read the displacements from each file

for m=1:15

    e = nodes(length(nodes))-1; % last node in list - 1

    if m==1
        disp_exp = dlmread(disp_experiment_path1, '[0,0,e,1]');
    end

    if m==2
        disp_exp = dlmread(disp_experiment_path2, '[0,0,e,1]');
    end

    if m==3
        disp_exp = dlmread(disp_experiment_path3, '[0,0,e,1]');
    end

    if m==4
        disp_exp = dlmread(disp_experiment_path4, '[0,0,e,1]');
    end

    if m==5
        disp_exp = dlmread(disp_experiment_path5, '[0,0,e,1]');
    end

    if m==6

```

```

    disp_exp = dlmread(dis_experiment_path6,'',[0,0,e,1]);
end

if m==7
    disp_exp = dlmread(dis_experiment_path7,'',[0,0,e,1]);
end

if m==8
    disp_exp = dlmread(dis_experiment_path8,'',[0,0,e,1]);
end

if m==9
    disp_exp = dlmread(dis_experiment_path9,'',[0,0,e,1]);
end

if m==10
    disp_exp = dlmread(dis_experiment_path10,'',[0,0,e,1]);
end

if m==11
    disp_exp = dlmread(dis_experiment_path11,'',[0,0,e,1]);
end

if m==12
    disp_exp = dlmread(dis_experiment_path12,'',[0,0,e,1]);
end

if m==13
    disp_exp = dlmread(dis_experiment_path13,'',[0,0,e,1]);
end

if m==14
    disp_exp = dlmread(dis_experiment_path14,'',[0,0,e,1]);
end

if m==15
    disp_exp = dlmread(dis_experiment_path15,'',[0,0,e,1]);
end

t=1; % counter for displacement files

disp_x_exp(1,1:length(nodes))=0;% set first value in array to zero
disp_y_exp(1,1:length(nodes))=0;

%store displacements

```

```

if m==1

    for t=1:length(nodes) % for each tracked node

        k=m;

        disp_x_exp(k,t)=disp_exp(nodes(t),1);
        disp_y_exp(k,t)=disp_exp(nodes(t),2);

    end

else
    for t=1:length(nodes) % for each tracked node

        k=m;

        disp_x_exp(k,t)=disp_exp(nodes(t),1) + disp_x_exp(m-1,t);
        disp_y_exp(k,t)=disp_exp(nodes(t),2) + disp_y_exp(m-1,t);

    end
end

% compute sse for each node displacement

i=1;

for i=1:15

    j = 1;
    for j = 1:length(nodes)

        ux = disp_x_exp(i,j)-disp(i,j);
        uy = disp_y_exp(i,j)-disp(i,j);
        En = En + (disp_x_exp(i,j))^2 + (disp_y_exp(i,j))^2;

        Ex = Ex + ux^2 + uy^2;

    end
end

Rx = Ex/En; %normalized residual for displacements

% you will need to determine what weighting factor you need
% use one that roughly makes the residuals from the forces equal to
% the residuals of the displacements

```

$w = R_f/R_x$; % weighting factor for the strains

$sse = R_f + w \cdot R_x$; % total residual

end

dc.dat

```
ID7 6 -1.733973
ID7 33 0.892991
ID7 34 2.677917
ID7 35 3.799754
ID7 36 4.492055
ID7 37 4.920443
ID7 38 5.238386
ID7 39 5.570272
ID7 40 6.014214
ID7 41 6.676855
ID7 42 7.645051
ID7 7 8.967751
ID8 6 -2.883153
ID8 33 -3.984370
ID8 34 -4.916021
ID8 35 -5.661165
ID8 36 -6.223242
ID8 37 -6.632371
ID8 38 -6.906060
ID8 39 -7.052223
ID8 40 -7.083636
ID8 41 -7.047569
ID8 42 -7.011608
ID8 7 -7.000334
ID7 11 12.305037
ID7 46 13.141642
ID7 47 13.899331
ID7 48 14.614521
ID7 49 15.254178
ID7 50 15.789190
ID7 51 16.207906
ID7 52 16.524063
ID7 53 16.788988
ID7 54 17.046324
ID7 55 17.334567
ID7 56 17.699417
ID7 57 18.104066
ID7 58 18.475889
ID7 10 18.780928
ID8 11 -1.843249
ID8 46 -1.553954
ID8 47 -1.298759
```

ID8 48 -1.119973
ID8 49 -1.064100
ID8 50 -1.148545
ID8 51 -1.364303
ID8 52 -1.677662
ID8 53 -2.028608
ID8 54 -2.382093
ID8 55 -2.745108
ID8 56 -3.159179
ID8 57 -3.638621
ID8 58 -4.179620
ID8 10 -4.779392
ID7 14 -6.386165
ID7 64 -5.570261
ID7 65 -4.974575
ID7 66 -4.571780
ID7 67 -4.322333
ID7 68 -4.151414
ID7 69 -3.975719
ID7 70 -3.730976
ID7 71 -3.441708
ID7 72 -3.155624
ID7 73 -2.840952
ID7 74 -2.433993
ID7 13 -1.873331
ID8 14 3.855633
ID8 64 3.839984
ID8 65 3.230117
ID8 66 2.235147
ID8 67 1.038766
ID8 68 -0.196595
ID8 69 -1.331991
ID8 70 -2.262606
ID8 71 -2.944900
ID8 72 -3.368961
ID8 73 -3.563055
ID8 74 -3.626776
ID8 13 -3.644665
ID7 1 -10.023709
ID7 18 -10.625626
ID7 19 -11.270620
ID7 20 -11.977173
ID7 21 -12.703211
ID7 22 -13.372359
ID7 23 -1.3957440e+01
ID7 24 -1.4456293e+01
ID7 25 -1.4878938e+01
ID7 26 -15.234530
ID7 27 -15.509862
ID7 28 -15.674797
ID7 29 -15.702346
ID7 30 -15.558355

```
ID7 31 -15.214935
ID7 32 -14.671188
ID7 2 -13.925438
ID8 1 1.562892
ID8 18 1.151153
ID8 19 0.984469
ID8 20 1.003100
ID8 21 1.134172
ID8 22 1.336240
ID8 23 1.563443
ID8 24 1.779071
ID8 25 1.955800
ID8 26 2.066806
ID8 27 2.108547
ID8 28 2.095076
ID8 29 2.034911
ID8 30 1.921487
ID8 31 1.738035
ID8 32 1.464855
ID8 2 1.095942
NUMMAT 1
DTYPE 1
DPARAM 3.00000 22.50000 0.00975 10.72500
```

boundaries.dat

```
12
6 33 34 35 36 37 38 39 40 41 42 7
14
11 46 47 48 49 50 51 52 53 54 55 56 57 10
13
14 64 65 66 67 68 69 70 71 72 73 74 13
17
1 18 19 20 21 22 23 24 25 26 27 28 29 30 31 32 2
```

disp01.dat

```
-0.891516 0.050138
-1.280682 -0.057682
-0.680838 -0.287744
-0.872744 -0.204967
-1.097182 -0.119354
-0.559534 -0.347645
0.469191 -0.703674
1.177733 -0.633373
0.690026 -0.713851
1.700617 -0.308396
1.044492 0.100472
0.102057 0.248362
-0.138786 0.255042
```

-0.447965 0.255940
-0.767026 0.101921
-0.639507 0.158373
-0.537227 0.209393
-0.936861 0.047978
-0.984564 0.056284
-1.037958 0.068379
-1.095555 0.077836
-1.152902 0.083171
-1.207993 0.083001
-1.258574 0.078040
-1.301923 0.070078
-1.337144 0.058887
-1.362558 0.046034
-1.376098 0.033595
-1.376802 0.021159
-1.365482 0.007226
-1.344203 -0.009904
-1.315437 -0.031366
-0.385700 -0.410392
-0.253068 -0.448569
-0.157735 -0.465453
-0.091068 -0.470954
-0.047507 -0.477353
-0.017415 -0.492834
0.010234 -0.521381
0.048635 -0.562765
0.122645 -0.612626
0.258952 -0.663453
1.546770 -0.420007
1.379308 -0.535113
0.939504 -0.695294
1.130327 0.091611
1.224356 0.082082
1.328678 0.064293
1.433411 0.034421
1.529630 -0.007439
1.612745 -0.057405
1.682546 -0.108501
1.737382 -0.154163
1.777357 -0.191526
1.802292 -0.221281
1.804856 -0.244635
1.783946 -0.264170
1.745843 -0.283867
-0.110389 0.259967
-0.033007 0.258624
0.290667 0.225480
0.522853 0.190603
0.781178 0.147078
-0.341779 0.298503
-0.261741 0.314424

-0.205560 0.306562
-0.172545 0.280806
-0.157788 0.246947
-0.155074 0.214139
-0.158359 0.188674
-0.160737 0.175441
-0.160209 0.178151
-0.160120 0.198047
-0.156074 0.227168
-0.657860 0.148018
-0.797605 0.095541
-0.452038 -0.369393
-0.714687 -0.249096
-0.909726 -0.172552
0.950071 -0.684647
1.217629 -0.624341
1.432866 -0.520288
1.600204 -0.397992
-0.226140 0.122076
-0.237684 0.089023
-0.248467 0.070564
-0.262171 0.091938
-0.247539 0.250510
-0.219816 0.165937
-0.445187 0.238468
-0.292393 0.270759
-0.225034 0.212088
-0.256498 0.070409
-1.209366 0.032338
-1.220959 0.008837
-1.194407 -0.039049
-1.183996 0.056315
-1.163539 -0.065578
-1.131478 -0.092894
-1.216083 -0.014381
1.425679 -0.077103
1.509492 -0.151167
1.626325 -0.271361
1.665563 -0.350823
0.842187 0.139621
1.575532 -0.216601
-0.684999 0.149134
0.172214 -0.608972
-0.043420 -0.495326
-0.154543 -0.417910
-0.119743 -0.416237
-0.096955 -0.426973
-0.076223 -0.453591
0.029362 -0.549532
0.659868 -0.690884
-0.317300 -0.405274
-0.094641 0.205338

0.067881 0.214808
-0.193758 0.185433
0.287989 0.208177
0.552853 0.182063
-0.260113 0.125183
-0.832862 0.102040
-0.786917 -0.197023
-0.360088 0.266152
-0.319412 -0.004548
-0.339018 -0.026643
-0.297075 0.192693
-0.355369 -0.028384
-0.283525 0.143141
-0.286083 0.086842
-0.299889 0.034616
-0.364893 -0.006725
-1.067758 -0.019081
-1.099636 0.097265
-1.020479 -0.090180
-1.146815 0.078525
-0.932255 0.120906
-0.989165 0.120370
-1.046306 0.111884
-1.058925 0.014956
-1.056811 -0.053069
1.659309 -0.315832
1.320328 -0.001262
1.386975 -0.265748
0.929130 0.131320
1.190030 0.064056
1.050339 0.108819
1.311424 -0.179787
1.444965 -0.341704
1.246284 -0.596836
0.955282 -0.648650
-0.212829 -0.421416
-0.180439 -0.368751
-0.227796 -0.371806
-0.162493 -0.390469
-0.046759 -0.483762
-0.127064 -0.429280
-0.199443 -0.363324
-0.725138 0.157352
0.620945 0.174212
-0.462634 0.220414
0.321420 0.193111
0.057810 0.183991
-0.137276 0.155075
1.473740 -0.497402
-0.594970 0.191645
-0.640042 -0.254531
-0.330803 0.225033

-0.371973 -0.043929
-0.398289 -0.086736
-0.342279 0.079396
-0.351455 0.014355
-0.424761 -0.110124
-0.446575 -0.111878
-0.349120 0.139973
-0.966339 -0.130972
-0.997439 0.083671
-0.947783 0.113691
-0.832966 0.154226
-0.891454 0.137914
-0.911362 -0.017421
-0.920155 -0.058847
-0.907290 -0.098465
-1.035725 0.049733
1.492947 -0.459864
1.221272 -0.087059
1.102079 0.009204
0.937515 0.093760
1.147209 -0.284122
1.073143 -0.182332
1.482752 -0.407048
0.105545 -0.545802
-0.272107 -0.382446
-0.305997 -0.335218
-0.280051 -0.323529
-0.259889 -0.325564
-0.247327 -0.338020
-0.204023 -0.371110
1.255318 -0.545422
-0.261456 0.115836
0.749878 0.149985
-0.442003 -0.350559
0.944566 -0.583112
-0.386503 0.233761
-0.337883 -0.378121
0.066123 0.150940
-0.161190 0.109132
-0.545414 -0.292406
-0.495053 0.209918
1.239871 -0.471412
-0.778001 0.160300
-0.499030 -0.181265
-0.468834 -0.157163
-0.398564 0.022514
-0.412624 -0.049300
-0.437985 -0.111741
-0.374984 0.185111
-0.864028 0.078144
-0.814008 0.119079
-0.788369 -0.114864

-0.697906 0.175493
-0.756261 0.152012
-0.859648 -0.144628
-0.764951 -0.078919
-0.897848 0.030910
-0.401204 0.092062
-0.446304 -0.050830
1.201813 -0.381425
0.872369 0.020516
0.798219 -0.160478
0.702706 0.106288
0.987237 -0.080024
0.605989 -0.569774
-0.110595 -0.421631
1.643139 -0.377347
-0.340424 -0.349437
-0.355048 -0.301356
-0.323370 -0.303213
-0.345088 -0.301554
-0.277834 -0.329928
-0.311570 0.055727
-0.389180 -0.351135
0.414516 0.164001
-0.422993 0.208693
-0.724053 -0.196939
0.061355 0.102746
0.343844 -0.604049
-0.644202 0.188112
0.331124 0.114675
-0.422053 -0.349034
-0.581641 -0.241069
-0.526769 -0.214590
-0.494871 -0.168272
-0.467068 -0.103088
-0.754920 0.058527
-0.878773 0.113716
-0.423405 0.147705
-0.593901 0.176013
-0.707346 0.106973
-0.650818 0.146161
-0.780306 -0.148172
-0.657684 -0.178159
-0.781178 -0.000834
0.917255 -0.489739
-0.450549 -0.026954
-0.359887 0.029897
0.862448 -0.268579
0.625661 0.033485
0.553064 0.094283
0.718850 -0.057437
-0.532217 -0.160968
0.899344 -0.379529

-0.170986 -0.370300
-0.409980 -0.328050
-0.449257 -0.306874
-0.414505 -0.295128
-0.342149 -0.310263
-0.446710 -0.330460
0.050238 -0.479200
-0.170227 0.060486
-0.468773 0.183382
-0.402236 -0.000131
-0.498732 -0.310622
-0.599159 -0.281392
-0.541412 -0.214062
-0.513650 -0.147807
-0.622137 -0.240490
-0.692410 -0.034406
-0.452179 0.047745
-0.574582 0.118379
-0.670812 0.025191
-0.541446 0.196581
0.528578 -0.456866
-0.676458 -0.104258
-0.670893 -0.189347
-0.627634 0.075292
-0.497335 -0.070181
0.294399 -0.532382
0.432404 -0.036495
-0.588117 -0.219302
0.570726 -0.237282
-0.514658 -0.118562
0.510272 -0.133271
0.591357 -0.345082
-0.238943 -0.331817
-0.473942 -0.318706
-0.010131 -0.415040
-0.508276 -0.310971
-0.413330 -0.302406
-0.474393 0.109995
-0.499885 -0.317808
-0.343097 0.001701
0.216810 -0.451301
-0.604424 -0.292469
-0.578039 -0.250729
-0.551208 -0.183791
0.637024 -0.643629
-0.501255 0.004708
-0.639918 -0.065240
-0.574428 0.022882
-0.622309 -0.286115
-0.620569 -0.136224
-0.633823 -0.178198
-0.613341 -0.027491

0.221798 -0.119059
0.147417 -0.035055
0.286410 -0.207266
-0.562081 -0.174650
-0.567260 -0.257678
-0.327244 -0.305515
-0.091673 -0.356714
-0.530685 -0.319549
-0.497513 -0.309186
0.089431 0.040133
-0.557575 -0.319706
-0.525995 0.069391
-0.545871 -0.313292
0.313570 -0.293513
0.259302 -0.360185
-0.603121 -0.280871
-0.577214 -0.207417
-0.520504 0.153881
-0.579576 -0.247097
-0.620439 -0.304952
-0.536922 -0.108680
-0.054220 -0.129726
-0.553144 -0.272388
0.088015 -0.373136
-0.585751 -0.109505
0.017700 -0.198248
-0.623209 -0.264728
-0.614965 -0.186067
-0.487958 -0.115964
-0.534280 -0.294960
-0.503891 -0.305732
-0.194565 -0.309923
-0.578701 -0.325928
0.074152 -0.262877
-0.583124 -0.313487
0.095169 -0.310375
-0.598674 -0.274797
-0.547051 -0.042011
-0.627937 -0.317722
-0.564241 -0.142181
-0.589249 -0.237089
-0.643154 -0.319223
-0.134913 -0.263426
-0.225014 -0.216990
-0.589652 -0.207475
-0.587107 -0.220493
-0.595741 -0.217997
-0.038563 -0.312633
-0.456336 -0.328396
-0.592877 -0.322665
-0.435394 -0.293637
-0.614264 -0.331768

-0.607703 -0.314799
-0.414831 -0.254176
-0.619032 -0.314940
-0.594530 -0.253529
-0.353859 -0.052547
-0.341178 -0.110690
-0.586932 -0.277594
-0.536426 -0.294921
-0.633580 -0.331106
-0.307734 -0.277048
-0.330045 0.072400
-0.508404 -0.232116
-0.637323 -0.328036
-0.500214 -0.169992
-0.603893 -0.297402
-0.540372 0.197702
0.392416 -0.660755
-0.241506 0.158639
-0.541131 -0.316351
-0.560863 0.190737
-0.457404 -0.090682
-0.689273 -0.192767
-0.382244 -0.313523
-0.523069 -0.183035
-0.455820 -0.061641
-0.156359 0.003712
-0.557770 -0.239076
-0.564759 -0.285005
-0.411228 -0.297476
-0.468728 -0.299437
-0.451534 -0.300549
0.364012 0.048136
-0.116518 -0.060925
-0.304989 -0.168866
-0.570574 -0.258370
-0.507595 -0.306753
-0.633390 -0.293751

disp02.dat

-0.828805 0.106927
-1.221684 -0.054444
-0.560897 -0.275090
-0.773234 -0.192096
-1.019716 -0.110101
-0.425656 -0.338867
0.609460 -0.669240
1.254969 -0.653474
0.808142 -0.689013
1.714785 -0.400161

0.939567 0.196678
0.092187 0.301405
-0.109802 0.241476
-0.417871 0.268189
-0.715487 0.146501
-0.597955 0.191120
-0.502234 0.232354
-0.869987 0.096332
-0.911807 0.096255
-0.956842 0.102094
-1.003057 0.107280
-1.046542 0.108052
-1.088642 0.103019
-1.129910 0.093862
-1.168812 0.083958
-1.204430 0.075096
-1.235003 0.067649
-1.258231 0.060391
-1.272120 0.049848
-1.275424 0.033004
-1.267701 0.008945
-1.249368 -0.020539
-0.225166 -0.399311
-0.071102 -0.435624
0.038352 -0.450415
0.112269 -0.452586
0.157200 -0.454686
0.183912 -0.465325
0.204952 -0.488419
0.234548 -0.523489
0.295581 -0.568032
0.415649 -0.618980
1.583788 -0.490919
1.436998 -0.582070
1.036043 -0.689006
1.009632 0.175706
1.086232 0.154385
1.171232 0.123213
1.255900 0.081048
1.334428 0.030280
1.405938 -0.024874
1.472974 -0.079104
1.534797 -0.126947
1.591297 -0.166401
1.641936 -0.201001
1.680713 -0.240584
1.703587 -0.287913
1.712147 -0.341201
-0.092213 0.269185
-0.027543 0.290224
0.260818 0.295563
0.468786 0.272025

0.701384 0.236009
-0.319064 0.288348
-0.245167 0.280810
-0.192345 0.252288
-0.159259 0.211893
-0.141652 0.168414
-0.134114 0.129622
-0.131097 0.102097
-0.126458 0.091410
-0.120193 0.102685
-0.119103 0.138755
-0.119161 0.189680
-0.615128 0.172614
-0.743269 0.132192
-0.297781 -0.351162
-0.590981 -0.227523
-0.807154 -0.153412
1.004483 -0.645384
1.250054 -0.612595
1.443761 -0.535378
1.589397 -0.436168
-0.197236 0.046927
-0.201728 0.009697
-0.205294 -0.008952
-0.214462 0.031260
-0.232539 0.201252
-0.197338 0.097262
-0.418234 0.239316
-0.276163 0.237463
-0.207580 0.151601
-0.208063 -0.003399
-1.077730 0.051782
-1.096132 0.035155
-1.093192 -0.010653
-1.050336 0.069505
-1.073976 -0.043108
-1.050265 -0.077728
-1.102140 0.015573
1.218838 -0.034156
1.298637 -0.107489
1.441741 -0.225041
1.552502 -0.322256
0.746161 0.216296
1.372701 -0.172149
-0.639792 0.165008
0.306337 -0.538436
0.133586 -0.442391
0.046861 -0.392263
0.081366 -0.386119
0.099411 -0.391242
0.112347 -0.410583
0.188153 -0.485955

0.739819 -0.631709
-0.139143 -0.383167
-0.092778 0.226630
0.050292 0.255988
-0.176439 0.185526
0.246004 0.265008
0.483610 0.250274
-0.219100 0.083253
-0.773958 0.129937
-0.662589 -0.170434
-0.339326 0.250926
-0.272170 -0.072778
-0.285705 -0.097327
-0.277969 0.152972
-0.298848 -0.095989
-0.258729 0.095387
-0.253786 0.031816
-0.259813 -0.027579
-0.311052 -0.064709
-0.937131 0.005133
-0.976285 0.107992
-0.905959 -0.061371
-1.015844 0.088701
-0.853512 0.139202
-0.894515 0.136023
-0.935554 0.124879
-0.925214 0.032553
-0.933430 -0.024435
1.503300 -0.270288
1.130315 0.040967
1.190052 -0.204691
0.813656 0.195727
1.025409 0.109144
0.912322 0.161739
1.107262 -0.121354
1.266190 -0.275407
1.224486 -0.549510
0.959186 -0.577336
-0.017818 -0.398779
0.010948 -0.327049
-0.030584 -0.341509
0.021285 -0.340035
0.102514 -0.408109
0.044060 -0.367065
-0.003284 -0.328212
-0.674076 0.167383
0.532706 0.228296
-0.438467 0.213840
0.264599 0.235132
0.032616 0.212523
-0.137254 0.166895
1.430492 -0.475575

-0.558949 0.191565
-0.500760 -0.227267
-0.313902 0.195580
-0.317456 -0.092203
-0.337337 -0.141851
-0.306018 0.045536
-0.305497 -0.026380
-0.359951 -0.168886
-0.381373 -0.169334
-0.321836 0.112238
-0.859097 -0.105910
-0.872062 0.091764
-0.833604 0.120456
-0.753029 0.161039
-0.792975 0.144538
-0.777639 -0.000794
-0.785908 -0.036383
-0.776615 -0.071590
-0.903829 0.061481
1.393891 -0.406654
1.022869 -0.032257
0.925454 0.056170
0.793415 0.135868
0.973073 -0.213022
0.893614 -0.115564
1.335688 -0.338181
0.222630 -0.458921
-0.079968 -0.355189
-0.115907 -0.304112
-0.090791 -0.286547
-0.074251 -0.280910
-0.068462 -0.283867
-0.037238 -0.304846
1.177559 -0.470431
-0.242717 0.108994
0.638598 0.194361
-0.281225 -0.324342
0.898813 -0.491593
-0.367813 0.215826
-0.157259 -0.351640
0.037356 0.171906
-0.159897 0.115828
-0.395980 -0.264968
-0.469618 0.201699
1.114941 -0.386135
-0.714892 0.167953
-0.421146 -0.228415
-0.392746 -0.200399
-0.347123 0.000585
-0.350345 -0.078095
-0.367146 -0.148132
-0.353577 0.163508

-0.745699 0.085243
-0.710079 0.123407
-0.651431 -0.093587
-0.632865 0.175598
-0.670719 0.154189
-0.733378 -0.116286
-0.631583 -0.064362
-0.769555 0.042141
-0.360508 0.075473
-0.394476 -0.090166
1.045028 -0.302432
0.721851 0.069334
0.665462 -0.095697
0.584688 0.144911
0.814686 -0.019063
0.607725 -0.471129
0.033277 -0.341950
1.581132 -0.379708
-0.154235 -0.322129
-0.173977 -0.263763
-0.142886 -0.258470
-0.172142 -0.249568
-0.116031 -0.264279
-0.288800 0.046445
-0.212005 -0.325642
0.340590 0.197261
-0.402515 0.193537
-0.587970 -0.169473
0.035748 0.122225
0.421993 -0.512869
-0.596813 0.187093
0.266851 0.144337
-0.255947 -0.322149
-0.492837 -0.277557
-0.435285 -0.248863
-0.407255 -0.196436
-0.387358 -0.124121
-0.643078 0.064647
-0.812071 0.135348
-0.390237 0.134901
-0.539719 0.172895
-0.611911 0.110222
-0.575323 0.146516
-0.644110 -0.122732
-0.518077 -0.162812
-0.656968 0.008880
0.832519 -0.396603
-0.381580 -0.041177
-0.314271 -0.013238
0.732999 -0.197257
0.514435 0.078806
0.454953 0.131243

0.592592 -0.000074
-0.461799 -0.202597
0.785634 -0.297620
-0.030840 -0.292822
-0.232198 -0.303440
-0.277501 -0.278169
-0.241728 -0.256177
-0.187923 -0.248596
-0.275962 -0.309029
0.157123 -0.387526
-0.164232 0.067661
-0.437566 0.173582
-0.363131 -0.025279
-0.343372 -0.283813
-0.494311 -0.311291
-0.437834 -0.237463
-0.416961 -0.165173
-0.478134 -0.214136
-0.571906 -0.028206
-0.393970 0.038888
-0.504227 0.118046
-0.563101 0.029491
-0.505218 0.190161
0.509357 -0.365576
-0.546983 -0.096692
-0.529518 -0.167987
-0.536853 0.077614
-0.410368 -0.081154
0.351844 -0.433926
0.361387 0.011354
-0.505964 -0.250968
0.498538 -0.172165
-0.454103 -0.151042
0.435597 -0.076511
0.533612 -0.268389
-0.102537 -0.261127
-0.304896 -0.297749
0.093771 -0.328053
-0.345763 -0.284323
-0.267141 -0.249550
-0.423513 0.104224
-0.336329 -0.301964
-0.313785 -0.004916
0.269564 -0.359297
-0.486333 -0.315210
-0.460566 -0.270366
-0.440023 -0.198869
0.675501 -0.557290
-0.423631 -0.000585
-0.521216 -0.062520
-0.482961 0.023083
-0.520174 -0.312940

-0.493439 -0.135093
-0.496655 -0.169367
-0.505170 -0.026225
0.205726 -0.072981
0.129001 0.000760
0.273750 -0.151228
-0.490604 -0.197740
-0.418259 -0.240383
-0.195311 -0.246112
0.014984 -0.279696
-0.369959 -0.302720
-0.337028 -0.289809
0.067576 0.065685
-0.405657 -0.296754
-0.454587 0.067659
-0.389129 -0.303585
0.311017 -0.226530
0.282454 -0.283325
-0.473565 -0.295383
-0.454955 -0.219362
-0.471287 0.149518
-0.433578 -0.236652
-0.505896 -0.328992
-0.434245 -0.118260
-0.021517 -0.094083
-0.402716 -0.248636
0.154873 -0.293587
-0.470006 -0.113142
0.056284 -0.150502
-0.528382 -0.285704
-0.479389 -0.181995
-0.430210 -0.127783
-0.378865 -0.282278
-0.362795 -0.267605
-0.085181 -0.245636
-0.426918 -0.314942
0.118014 -0.203867
-0.433434 -0.310680
0.145960 -0.242943
-0.461344 -0.282622
-0.450395 -0.045982
-0.501423 -0.334265
-0.450257 -0.150776
-0.447402 -0.233147
-0.526224 -0.335470
-0.053636 -0.209484
-0.147822 -0.176944
-0.460661 -0.214670
-0.503187 -0.232732
-0.460127 -0.219919
0.041314 -0.245886
-0.292011 -0.303899

-0.455303 -0.305556
-0.308127 -0.250008
-0.471804 -0.328827
-0.465227 -0.318951
-0.312366 -0.221785
-0.482717 -0.324593
-0.499206 -0.256725
-0.314434 -0.051807
-0.287697 -0.098977
-0.443133 -0.278954
-0.414723 -0.269750
-0.499731 -0.338449
-0.199756 -0.227742
-0.296532 0.046859
-0.415650 -0.219367
-0.510685 -0.328818
-0.427884 -0.170417
-0.489870 -0.290290
-0.506728 0.210520
0.499562 -0.591438
-0.211192 0.137690
-0.394843 -0.292184
-0.527848 0.195054
-0.396559 -0.141342
-0.548711 -0.168124
-0.201283 -0.283428
-0.446857 -0.229671
-0.408800 -0.081997
-0.142628 0.017254
-0.466010 -0.276548
-0.414945 -0.279397
-0.248452 -0.246745
-0.304986 -0.261047
-0.297085 -0.253296
0.297708 0.084867
-0.092917 -0.037149
-0.236385 -0.143856
-0.464681 -0.286493
-0.354339 -0.270033
-0.526721 -0.302397

disp03.dat

-0.844667 0.110586
-1.244965 -0.007450
-0.507889 -0.229277
-0.752573 -0.145411
-1.026964 -0.063160
-0.343953 -0.293078
0.648123 -0.586825

1.145630 -0.588215
0.793905 -0.597090
1.552467 -0.418925
0.991069 0.195495
0.169265 0.199040
-0.048097 0.066128
-0.427853 0.241124
-0.734119 0.144666
-0.617172 0.183186
-0.518271 0.216609
-0.895020 0.095831
-0.945449 0.089898
-0.998730 0.090799
-1.052658 0.094820
-1.102812 0.099753
-1.149272 0.103031
-1.191972 0.104360
-1.229645 0.104676
-1.262389 0.102129
-1.289640 0.096103
-1.310139 0.087466
-1.322304 0.077423
-1.323606 0.064573
-1.311633 0.046616
-1.285289 0.022478
-0.120567 -0.356197
0.047486 -0.396897
0.163804 -0.417764
0.239287 -0.426840
0.282567 -0.435657
0.306893 -0.450733
0.325830 -0.472568
0.351750 -0.497340
0.401706 -0.523983
0.496638 -0.553906
1.428390 -0.486889
1.297845 -0.548003
0.969050 -0.601673
1.035767 0.157368
1.084969 0.121586
1.140085 0.084435
1.194403 0.046461
1.243262 0.006674
1.286172 -0.035207
1.326293 -0.076640
1.366121 -0.114306
1.406999 -0.147643
1.448505 -0.180882
1.487678 -0.223902
1.518317 -0.280248
1.537643 -0.347142
-0.025206 0.113031

0.045013 0.159052
0.338536 0.221083
0.539153 0.222571
0.761355 0.210460
-0.326213 0.239516
-0.247528 0.204954
-0.187882 0.147874
-0.146410 0.081626
-0.119385 0.014755
-0.101770 -0.045175
-0.088607 -0.089241
-0.076644 -0.111039
-0.066834 -0.104000
-0.063508 -0.063065
-0.061086 -0.000981
-0.646137 0.162160
-0.771790 0.127114
-0.220270 -0.309763
-0.560128 -0.183454
-0.801466 -0.108171
0.904543 -0.543340
1.107905 -0.533805
1.277343 -0.489219
1.415051 -0.420352
-0.164103 -0.116474
-0.156162 -0.172529
-0.150807 -0.205558
-0.153599 -0.173299
-0.238266 0.104822
-0.177503 -0.044516
-0.446843 0.209680
-0.292464 0.166152
-0.200956 0.032050
-0.148989 -0.208092
-1.123506 0.078797
-1.137672 0.062585
-1.127834 0.023142
-1.101586 0.093019
-1.102576 -0.003172
-1.069308 -0.033220
-1.140498 0.044649
1.090387 -0.047837
1.140230 -0.103482
1.241531 -0.195554
1.345868 -0.284222
0.781377 0.172155
1.190241 -0.153984
-0.683496 0.149681
0.362941 -0.465461
0.227336 -0.411677
0.141796 -0.368845
0.176119 -0.367374

0.194302 -0.374875
0.207964 -0.391256
0.271481 -0.436167
0.695081 -0.526164
-0.057457 -0.348980
-0.024339 0.080475
0.116828 0.136270
-0.109107 0.016568
0.305558 0.171008
0.531018 0.181121
-0.156772 -0.114505
-0.812625 0.119176
-0.651874 -0.129294
-0.363227 0.203256
-0.225469 -0.240857
-0.229460 -0.282014
-0.293733 0.067673
-0.237407 -0.291462
-0.257973 -0.009825
-0.236275 -0.094225
-0.226622 -0.175239
-0.247681 -0.263718
-0.969200 0.031270
-1.037016 0.113622
-0.924938 -0.025134
-1.072587 0.104715
-0.908950 0.121647
-0.954815 0.122426
-0.997603 0.119810
-0.963501 0.054362
-0.959731 0.006136
1.292752 -0.233148
1.034445 0.006278
1.004203 -0.181598
0.820362 0.136175
0.964283 0.055100
0.886269 0.097804
0.948036 -0.117267
1.059991 -0.235115
1.050664 -0.463045
0.827600 -0.471967
0.074396 -0.370049
0.078709 -0.305564
0.031271 -0.320502
0.091583 -0.313012
0.161640 -0.352230
0.113426 -0.328604
0.061333 -0.308051
-0.729096 0.147629
0.551669 0.142072
-0.485408 0.181479
0.300620 0.123840

0.086344 0.079372
-0.073660 0.012722
1.238055 -0.417404
-0.620173 0.166778
-0.476330 -0.190252
-0.344457 0.130259
-0.286940 -0.222165
-0.293863 -0.291998
-0.310751 -0.043972
-0.291427 -0.135384
-0.307838 -0.335716
-0.324604 -0.347199
-0.346055 0.040081
-0.867769 -0.064099
-0.925575 0.099633
-0.893433 0.119127
-0.818249 0.142918
-0.856909 0.133848
-0.810459 0.012364
-0.810344 -0.014638
-0.792551 -0.042238
-0.949679 0.077252
1.182120 -0.344845
0.895017 -0.050669
0.832237 0.009987
0.739385 0.062630
0.801698 -0.186584
0.749721 -0.113669
1.118254 -0.283461
0.254611 -0.382192
-0.022097 -0.332337
-0.085447 -0.284485
-0.053808 -0.263508
-0.031150 -0.252813
-0.023914 -0.247093
0.007020 -0.256517
0.981285 -0.387000
-0.175834 -0.063394
0.624161 0.104885
-0.230447 -0.291341
0.744696 -0.395070
-0.409212 0.168833
-0.107982 -0.327201
0.077296 0.037615
-0.103271 -0.034129
-0.368703 -0.234419
-0.531591 0.169447
0.912384 -0.316740
-0.777299 0.146638
-0.378722 -0.372307
-0.356914 -0.330036
-0.356690 -0.075232

-0.340985 -0.171397
-0.342349 -0.260124
-0.395740 0.107062
-0.796789 0.083139
-0.768983 0.113814
-0.669582 -0.077775
-0.702052 0.152893
-0.735908 0.137315
-0.738071 -0.080258
-0.660843 -0.062736
-0.811637 0.047522
-0.390304 0.014543
-0.333290 -0.270279
0.852833 -0.253328
0.642016 0.012343
0.552756 -0.099473
0.543499 0.057808
0.701384 -0.044760
0.511111 -0.372682
0.068536 -0.279503
1.388769 -0.349573
-0.129493 -0.304766
-0.160037 -0.236273
-0.118826 -0.225360
-0.155991 -0.204710
-0.096334 -0.206149
-0.225828 -0.116386
-0.193485 -0.309879
0.346817 0.083997
-0.458053 0.150652
-0.582257 -0.137263
0.062476 0.001984
0.406146 -0.417008
-0.665289 0.161708
0.263925 0.038485
-0.221519 -0.297904
-0.463777 -0.399342
-0.410586 -0.356604
-0.390901 -0.290908
-0.384082 -0.203838
-0.692296 0.052306
-0.860050 0.119413
-0.438514 0.086396
-0.608266 0.144952
-0.668925 0.092118
-0.639022 0.123070
-0.652093 -0.097337
-0.538936 -0.161938
-0.697244 0.002859
0.670901 -0.318795
-0.395467 -0.106482
-0.249608 -0.208793

0.594583 -0.171532
0.459511 0.011475
0.422470 0.041788
0.508592 -0.035944
-0.414316 -0.357992
0.629310 -0.244658
-0.018179 -0.223694
-0.234365 -0.289894
-0.290940 -0.255573
-0.243820 -0.221928
-0.189766 -0.184352
-0.282890 -0.300873
0.166889 -0.309442
-0.118647 -0.063055
-0.499619 0.135129
-0.299780 -0.198354
-0.320747 -0.259860
-0.481291 -0.402041
-0.432185 -0.314845
-0.421175 -0.232911
-0.468812 -0.188583
-0.612002 -0.045920
-0.426613 -0.014035
-0.562271 0.087367
-0.609657 0.007034
-0.574119 0.159337
0.406262 -0.285268
-0.581017 -0.110930
-0.539674 -0.154866
-0.589417 0.050826
-0.428506 -0.138453
0.314993 -0.342150
0.312892 -0.034075
-0.476715 -0.371817
0.398082 -0.148142
-0.404175 -0.303666
0.359315 -0.085800
0.419257 -0.215065
-0.109871 -0.188337
-0.325963 -0.286042
0.085384 -0.249428
-0.371928 -0.259454
-0.286580 -0.187786
-0.472989 0.061463
-0.361197 -0.299595
-0.260578 -0.143959
0.222609 -0.274647
-0.489386 -0.379697
-0.467570 -0.331042
-0.453003 -0.255655
0.601127 -0.450097
-0.457308 -0.048058

-0.560296 -0.088960
-0.527353 -0.012401
-0.510868 -0.400128
-0.529059 -0.162137
-0.525722 -0.180636
-0.546429 -0.057895
0.162134 -0.085020
0.112263 -0.050715
0.207481 -0.128533
-0.459451 -0.313554
-0.432672 -0.238161
-0.218946 -0.177225
-0.006860 -0.202153
-0.402527 -0.292495
-0.347594 -0.285537
0.075501 -0.024082
-0.440037 -0.271763
-0.502161 0.028924
-0.424166 -0.306480
0.232687 -0.176378
0.211044 -0.213657
-0.494711 -0.338731
-0.477400 -0.265758
-0.533282 0.115054
-0.460081 -0.245347
-0.506130 -0.398148
-0.456781 -0.169017
-0.043295 -0.105687
-0.399414 -0.233290
0.109512 -0.216101
-0.503625 -0.151424
0.013570 -0.126638
-0.520943 -0.367985
-0.512493 -0.201798
-0.395718 -0.236190
-0.404747 -0.286857
-0.394464 -0.219922
-0.116869 -0.174016
-0.465009 -0.308811
0.063600 -0.154528
-0.471722 -0.320761
0.089798 -0.178971
-0.493355 -0.313941
-0.484369 -0.089149
-0.518081 -0.378910
-0.476315 -0.196422
-0.480564 -0.251529
-0.538482 -0.385248
-0.095456 -0.156220
-0.180687 -0.149924
-0.491230 -0.251911
-0.494516 -0.308160

-0.494482 -0.247902
-0.002342 -0.176655
-0.281243 -0.289474
-0.493167 -0.285632
-0.342214 -0.196205
-0.509401 -0.332364
-0.500786 -0.338315
-0.346278 -0.192952
-0.512033 -0.353447
-0.508649 -0.300032
-0.279130 -0.153424
-0.276853 -0.154979
-0.479352 -0.300693
-0.451582 -0.241738
-0.529305 -0.360882
-0.236445 -0.171805
-0.230009 -0.139514
-0.434477 -0.233214
-0.541387 -0.341180
-0.418618 -0.233266
-0.519203 -0.296386
-0.538084 0.192140
0.510595 -0.497806
-0.146358 -0.048331
-0.345307 -0.252443
-0.575412 0.172861
-0.337424 -0.323494
-0.551461 -0.146468
-0.196504 -0.263226
-0.401382 -0.382259
-0.355693 -0.228438
-0.115024 -0.078847
-0.437393 -0.394124
-0.449312 -0.292166
-0.253194 -0.193957
-0.320881 -0.221457
-0.314452 -0.199343
0.274989 0.005159
-0.089295 -0.090991
-0.250640 -0.154367
-0.453214 -0.372255
-0.380538 -0.227279
-0.540578 -0.345470

disp04.dat

-0.829164 0.180632
-1.264023 0.017255
-0.435156 -0.197356
-0.705156 -0.111525

-1.014528 -0.032487
-0.257887 -0.269112
0.742318 -0.553828
1.206256 -0.516676
0.861609 -0.542724
1.711490 -0.353690
0.992381 0.132568
0.241547 0.077070
0.035530 -0.042919
-0.425841 0.309052
-0.721655 0.213170
-0.608211 0.252477
-0.513025 0.287055
-0.876634 0.150884
-0.923804 0.130986
-0.973203 0.119956
-1.022305 0.115120
-1.066705 0.115731
-1.107159 0.120234
-1.144668 0.125951
-1.179370 0.129446
-1.213056 0.127998
-1.245496 0.122074
-1.274450 0.114079
-1.296861 0.104976
-1.309566 0.092905
-1.309689 0.075148
-1.294946 0.049914
-0.008255 -0.340351
0.175172 -0.393345
0.295625 -0.429197
0.367740 -0.453758
0.405543 -0.475514
0.426108 -0.497015
0.444703 -0.516521
0.473092 -0.530765
0.523731 -0.539830
0.610396 -0.546657
1.561495 -0.416115
1.393277 -0.475254
1.021102 -0.534235
1.040938 0.110884
1.091448 0.093881
1.144245 0.074802
1.193724 0.049938
1.236440 0.017073
1.272183 -0.023462
1.303669 -0.067976
1.335526 -0.111312
1.372256 -0.150629
1.418446 -0.186887
1.479900 -0.224656

1.553466 -0.264826
1.632203 -0.307184
0.060987 -0.002743
0.127184 0.037690
0.396494 0.105720
0.579244 0.120781
0.782061 0.127141
-0.326338 0.290341
-0.248649 0.232899
-0.188284 0.153012
-0.142073 0.064979
-0.106513 -0.021827
-0.077504 -0.099681
-0.050696 -0.160217
-0.025292 -0.196200
-0.003846 -0.199631
0.009621 -0.164589
0.019442 -0.106074
-0.633942 0.218821
-0.756137 0.182076
-0.112400 -0.281147
-0.479356 -0.144953
-0.748594 -0.070980
0.909025 -0.476657
1.111792 -0.469232
1.309144 -0.431605
1.481210 -0.371647
-0.127661 -0.165300
-0.104359 -0.238503
-0.083542 -0.287049
-0.058992 -0.275395
-0.233254 0.110042
-0.154349 -0.076118
-0.442958 0.265070
-0.290641 0.190813
-0.188559 0.018342
-0.067381 -0.301819
-1.064436 0.106516
-1.084056 0.091832
-1.090651 0.055889
-1.040413 0.120388
-1.075310 0.030675
-1.051456 -0.000226
-1.094447 0.075760
1.070337 -0.036519
1.104541 -0.090845
1.179404 -0.192378
1.301754 -0.277760
0.806536 0.100187
1.139281 -0.144816
-0.667716 0.192141
0.453588 -0.446690

0.330344 -0.432865
0.253390 -0.387026
0.280893 -0.399702
0.295134 -0.413098
0.308680 -0.425248
0.374151 -0.438942
0.723861 -0.468280
0.060677 -0.329371
0.079041 -0.044192
0.205966 0.012016
0.001369 -0.103288
0.374920 0.055756
0.577899 0.084154
-0.051991 -0.222548
-0.793308 0.160108
-0.569854 -0.089751
-0.361452 0.246403
-0.162166 -0.297025
-0.150323 -0.353809
-0.281630 0.074849
-0.142759 -0.376145
-0.236244 -0.017756
-0.202405 -0.117538
-0.178803 -0.214550
-0.138484 -0.358377
-0.900183 0.061204
-0.983682 0.134929
-0.863089 0.010360
-1.013447 0.130350
-0.879066 0.140641
-0.917616 0.137054
-0.952233 0.135961
-0.893405 0.082663
-0.893874 0.038732
1.229515 -0.233751
1.027524 0.009814
0.940075 -0.161367
0.844719 0.080675
0.969668 0.043057
0.903045 0.064201
0.904619 -0.098022
0.980440 -0.218586
1.007869 -0.409379
0.797095 -0.408743
0.192376 -0.370073
0.162501 -0.330780
0.122462 -0.329362
0.175495 -0.330999
0.244931 -0.336238
0.198827 -0.331503
0.147666 -0.329659
-0.708779 0.177145

0.598331 0.056915
-0.479698 0.223353
0.375259 0.017090
0.188478 -0.038098
0.047062 -0.105799
1.209805 -0.378659
-0.605969 0.197394
-0.379520 -0.151231
-0.338428 0.151859
-0.230811 -0.249137
-0.223884 -0.333706
-0.280245 -0.044676
-0.248632 -0.148591
-0.223663 -0.391184
-0.225984 -0.414014
-0.325956 0.050502
-0.810235 -0.026408
-0.861845 0.125335
-0.837678 0.140277
-0.782304 0.157992
-0.811122 0.150253
-0.735344 0.040510
-0.731867 0.015119
-0.712671 -0.009330
-0.881163 0.105135
1.113361 -0.323096
0.872931 -0.039363
0.828921 0.005329
0.755543 0.032514
0.737795 -0.150259
0.708761 -0.085428
1.034125 -0.269937
0.323848 -0.347251
0.074238 -0.325214
-0.016311 -0.281260
0.014824 -0.269850
0.037551 -0.260003
0.043901 -0.242651
0.075071 -0.235347
0.908434 -0.344705
-0.047028 -0.177825
0.659805 0.043799
-0.123190 -0.258327
0.692973 -0.334653
-0.405159 0.202736
-0.009939 -0.305794
0.182862 -0.059006
0.024369 -0.132309
-0.269735 -0.197698
-0.521934 0.199394
0.828374 -0.280718
-0.749938 0.166115

-0.296329 -0.406316
-0.285691 -0.354294
-0.319142 -0.068613
-0.292301 -0.174232
-0.282202 -0.273472
-0.383191 0.126601
-0.733028 0.108323
-0.714295 0.135146
-0.589084 -0.047968
-0.669862 0.169477
-0.692383 0.154981
-0.657210 -0.043422
-0.590478 -0.034698
-0.741350 0.074990
-0.362323 0.028854
-0.207978 -0.353089
0.773357 -0.215866
0.648953 0.001731
0.526346 -0.062640
0.575394 0.017011
0.685297 -0.032548
0.492904 -0.303423
0.132620 -0.240493
1.389444 -0.324821
-0.059001 -0.289897
-0.107212 -0.222230
-0.061493 -0.214263
-0.104472 -0.170532
-0.043757 -0.155979
-0.090275 -0.210485
-0.121737 -0.285220
0.413423 0.004028
-0.449073 0.176803
-0.491189 -0.100516
0.161855 -0.061010
0.444362 -0.365679
-0.643208 0.182423
0.332977 -0.015190
-0.126778 -0.267216
-0.381424 -0.410180
-0.343641 -0.362087
-0.331836 -0.290382
-0.333671 -0.196938
-0.632661 0.076706
-0.836196 0.147886
-0.417582 0.105697
-0.579362 0.163641
-0.617665 0.113907
-0.598527 0.142551
-0.566036 -0.064440
-0.475143 -0.131287
-0.631737 0.029380

0.609842 -0.258129
-0.353737 -0.093497
-0.128527 -0.311052
0.545637 -0.119289
0.484798 -0.002604
0.465111 0.003629
0.509080 -0.022677
-0.308340 -0.404404
0.568128 -0.185079
0.029127 -0.158711
-0.188915 -0.263924
-0.257970 -0.215441
-0.202324 -0.183324
-0.149468 -0.104562
-0.237383 -0.270295
0.215753 -0.254406
0.001495 -0.125979
-0.482185 0.156762
-0.166123 -0.286893
-0.228435 -0.225498
-0.418168 -0.387818
-0.379459 -0.300573
-0.373655 -0.217084
-0.377455 -0.153173
-0.556777 -0.019747
-0.392062 0.003785
-0.524269 0.108385
-0.557135 0.031114
-0.556057 0.181148
0.378057 -0.203526
-0.527548 -0.082528
-0.461485 -0.123388
-0.542758 0.073190
-0.386079 -0.120316
0.333847 -0.275559
0.336605 -0.018243
-0.386043 -0.381683
0.369960 -0.081367
-0.287028 -0.353649
0.353855 -0.040098
0.381175 -0.136361
-0.075345 -0.097305
-0.300100 -0.245500
0.117824 -0.172366
-0.349021 -0.195720
-0.255278 -0.084907
-0.443260 0.081698
-0.336961 -0.260486
-0.132968 -0.202215
0.229343 -0.190294
-0.443193 -0.347852
-0.425333 -0.302966

-0.412130 -0.231413
0.601898 -0.388135
-0.418503 -0.027645
-0.514252 -0.062517
-0.484846 0.010328
-0.444851 -0.378462
-0.491039 -0.132584
-0.477966 -0.149582
-0.501751 -0.033330
0.178114 -0.028342
0.159258 -0.028961
0.200632 -0.048137
-0.360323 -0.321850
-0.376085 -0.205478
-0.192399 -0.064258
0.015191 -0.103546
-0.388099 -0.234852
-0.298178 -0.252742
0.153268 -0.044364
-0.421318 -0.184602
-0.464807 0.050338
-0.412603 -0.257242
0.215450 -0.082867
0.198341 -0.114796
-0.465950 -0.296475
-0.444988 -0.234320
-0.505487 0.135358
-0.421866 -0.211479
-0.454424 -0.365337
-0.416802 -0.146272
-0.009846 -0.035717
-0.320779 -0.199885
0.114114 -0.114926
-0.466851 -0.124473
0.024706 -0.031709
-0.450008 -0.339328
-0.476203 -0.169752
-0.291148 -0.243953
-0.375594 -0.250255
-0.368791 -0.107408
-0.099293 -0.057122
-0.453525 -0.235528
0.062953 -0.048116
-0.462680 -0.263172
0.086784 -0.070358
-0.475013 -0.268452
-0.444304 -0.066230
-0.483088 -0.328313
-0.440270 -0.169703
-0.454038 -0.215823
-0.492885 -0.331067
-0.084344 -0.037480

-0.157894 -0.040274
-0.464727 -0.217456
-0.417934 -0.273729
-0.470388 -0.212089
0.004071 -0.062247
-0.208000 -0.258497
-0.471798 -0.181300
-0.318167 -0.072212
-0.494197 -0.252602
-0.487159 -0.277981
-0.318787 -0.073557
-0.491126 -0.295702
-0.450647 -0.234193
-0.174316 -0.164146
-0.203387 -0.114998
-0.465389 -0.255625
-0.424935 -0.122716
-0.505289 -0.290881
-0.217301 -0.045901
-0.101685 -0.248093
-0.387959 -0.143108
-0.511673 -0.254882
-0.342437 -0.191071
-0.482760 -0.199288
-0.530409 0.250203
0.572897 -0.457535
-0.035918 -0.161908
-0.242615 -0.215639
-0.565128 0.216572
-0.224543 -0.399249
-0.465022 -0.113313
-0.148018 -0.243586
-0.307465 -0.423444
-0.230407 -0.281873
-0.018409 -0.095208
-0.362704 -0.403896
-0.432571 -0.250638
-0.213490 -0.125054
-0.288422 -0.155080
-0.281668 -0.109059
0.325853 -0.013714
-0.024946 -0.060019
-0.206837 -0.071116
-0.395243 -0.359099
-0.353606 -0.135148
-0.489484 -0.280161

disp05.dat

-0.847624 0.185896

-1.213800 0.066655
-0.353002 -0.139136
-0.641894 -0.056527
-0.964425 0.018025
-0.154794 -0.211554
0.733593 -0.522360
1.073181 -0.479758
0.816631 -0.503251
1.487907 -0.358362
0.964636 0.104502
0.213100 -0.033492
-0.010156 -0.183420
-0.442466 0.325713
-0.742434 0.220056
-0.628807 0.263704
-0.531353 0.302305
-0.902489 0.149788
-0.954986 0.124326
-1.007536 0.108471
-1.057743 0.100250
-1.100969 0.099204
-1.137541 0.102572
-1.169345 0.109157
-1.198143 0.118608
-1.225552 0.126323
-1.251410 0.130068
-1.274026 0.130209
-1.290817 0.127343
-1.297645 0.120601
-1.289566 0.108788
-1.262098 0.091318
0.098625 -0.287799
0.275845 -0.351744
0.384524 -0.402509
0.443437 -0.441727
0.469307 -0.473554
0.481010 -0.498506
0.494139 -0.515257
0.519007 -0.522885
0.563207 -0.524225
0.633389 -0.523130
1.357307 -0.407615
1.219257 -0.451926
0.933162 -0.492134
1.010843 0.077716
1.056521 0.054115
1.103167 0.032167
1.146304 0.009507
1.182604 -0.018048
1.211053 -0.052841
1.233270 -0.092330
1.254259 -0.130335

1.277419 -0.163952
1.305427 -0.194904
1.344225 -0.227332
1.391544 -0.264301
1.440855 -0.307699
0.027452 -0.140794
0.099721 -0.090291
0.362783 0.017054
0.544456 0.053595
0.750553 0.080643
-0.347016 0.297167
-0.276467 0.222288
-0.225104 0.122417
-0.188357 0.013520
-0.160754 -0.092361
-0.136782 -0.185518
-0.112202 -0.257644
-0.088024 -0.303151
-0.067224 -0.315849
-0.051434 -0.290738
-0.035060 -0.241161
-0.663212 0.221777
-0.784881 0.182305
-0.030433 -0.224402
-0.421385 -0.089241
-0.701038 -0.019767
0.832519 -0.426568
0.992829 -0.425446
1.155501 -0.403078
1.304286 -0.358405
-0.179455 -0.239975
-0.154755 -0.321511
-0.131146 -0.377261
-0.094547 -0.383057
-0.271101 0.076307
-0.204360 -0.139991
-0.468858 0.268950
-0.321926 0.172914
-0.233425 -0.031498
-0.110827 -0.399744
-1.070037 0.114696
-1.081691 0.109246
-1.075187 0.087652
-1.054446 0.117340
-1.051461 0.069111
-1.015255 0.044952
-1.085372 0.100714
1.011441 -0.056970
1.036877 -0.100767
1.090726 -0.187684
1.178042 -0.265462
0.776432 0.049987

1.062100 -0.146073
-0.705862 0.184521
0.477928 -0.409844
0.366088 -0.412487
0.300910 -0.370673
0.320869 -0.391699
0.330782 -0.406216
0.343405 -0.413348
0.408795 -0.409891
0.689266 -0.419132
0.124248 -0.281742
0.077171 -0.161966
0.197707 -0.092730
-0.002158 -0.227853
0.355525 -0.031740
0.550478 0.015093
-0.076153 -0.340004
-0.829090 0.152842
-0.531563 -0.040692
-0.388387 0.242366
-0.203251 -0.361461
-0.184388 -0.423061
-0.323217 0.037796
-0.167463 -0.451159
-0.281762 -0.064068
-0.249835 -0.171402
-0.224764 -0.274105
-0.150006 -0.441314
-0.898064 0.079269
-1.013391 0.114587
-0.842381 0.046859
-1.035523 0.116922
-0.922180 0.120342
-0.959535 0.114233
-0.989221 0.113083
-0.901354 0.089873
-0.882552 0.066306
1.125751 -0.225446
0.976417 -0.022199
0.866565 -0.142796
0.812927 0.026755
0.925942 -0.000265
0.866175 0.012631
0.839981 -0.091639
0.897808 -0.193816
0.905624 -0.363923
0.730876 -0.353815
0.248694 -0.339187
0.181200 -0.311085
0.142931 -0.304878
0.196328 -0.304333
0.270033 -0.290288

0.222816 -0.294964
0.166228 -0.311022
-0.754136 0.159092
0.575277 -0.011542
-0.516584 0.210556
0.367355 -0.063813
0.196879 -0.129345
0.066594 -0.204131
1.080036 -0.349055
-0.653557 0.174954
-0.343562 -0.100930
-0.376398 0.124336
-0.274332 -0.289988
-0.259364 -0.375590
-0.329902 -0.084370
-0.296889 -0.189085
-0.248458 -0.435179
-0.237371 -0.461325
-0.374726 0.012735
-0.777817 0.018261
-0.889730 0.109114
-0.874170 0.116070
-0.831269 0.128251
-0.855205 0.121483
-0.750879 0.048193
-0.734047 0.034694
-0.702321 0.020723
-0.899428 0.100029
1.004537 -0.294913
0.817043 -0.049137
0.782283 -0.020706
0.719246 -0.010103
0.669705 -0.111688
0.649052 -0.062593
0.940779 -0.243430
0.342343 -0.294314
0.097276 -0.289767
-0.017996 -0.241632
0.016865 -0.234757
0.043524 -0.223299
0.052794 -0.196386
0.087529 -0.178268
0.820530 -0.299072
-0.025054 -0.278594
0.633311 -0.014561
-0.080521 -0.204980
0.632813 -0.274844
-0.441544 0.183700
0.012847 -0.259593
0.200374 -0.125431
0.056896 -0.200890
-0.244671 -0.147616

-0.569855 0.172475
0.749344 -0.234045
-0.799324 0.139975
-0.317567 -0.419879
-0.319784 -0.369246
-0.375447 -0.097617
-0.344360 -0.197631
-0.326647 -0.291820
-0.430739 0.091722
-0.770086 0.090387
-0.759495 0.107711
-0.598627 -0.023290
-0.724745 0.133843
-0.743883 0.121321
-0.634242 -0.003430
-0.621223 -0.019596
-0.768481 0.069339
-0.419795 -0.004967
-0.186184 -0.410935
0.699229 -0.169632
0.609967 -0.014908
0.474901 -0.023998
0.549837 -0.019388
0.635166 -0.030019
0.460831 -0.233709
0.146138 -0.174398
1.240946 -0.310079
-0.063882 -0.242973
-0.114804 -0.164047
-0.063012 -0.159719
-0.104844 -0.096350
-0.039440 -0.074268
-0.052109 -0.277625
-0.129914 -0.232189
0.406804 -0.054993
-0.496402 0.145564
-0.471706 -0.058671
0.180819 -0.092701
0.443542 -0.308392
-0.696869 0.150564
0.331652 -0.045470
-0.110578 -0.215838
-0.387228 -0.386110
-0.379474 -0.347256
-0.379511 -0.283240
-0.391113 -0.200054
-0.681614 0.060736
-0.876947 0.133249
-0.474795 0.068751
-0.638769 0.125118
-0.672637 0.086959
-0.657222 0.107694

-0.560155 -0.031428
-0.509042 -0.096955
-0.672689 0.027226
0.550109 -0.192661
-0.417435 -0.107970
-0.125198 -0.402498
0.486322 -0.062986
0.457691 -0.008710
0.447290 -0.021671
0.469180 -0.006723
-0.296567 -0.419497
0.506346 -0.119480
0.032909 -0.071108
-0.211415 -0.197906
-0.277808 -0.126514
-0.211982 -0.098771
-0.148794 0.002783
-0.266841 -0.203901
0.223699 -0.182723
0.036494 -0.155251
-0.538832 0.118978
-0.132097 -0.350031
-0.217349 -0.175143
-0.441824 -0.334984
-0.431004 -0.266581
-0.436347 -0.198193
-0.367808 -0.109474
-0.613048 -0.015438
-0.457782 -0.021184
-0.589406 0.076714
-0.618125 0.021219
-0.611957 0.145162
0.339184 -0.119435
-0.580948 -0.061906
-0.475210 -0.088014
-0.607116 0.051272
-0.456037 -0.117803
0.325917 -0.202156
0.311899 0.011027
-0.374639 -0.355421
0.321350 -0.009160
-0.258174 -0.371185
0.314616 0.013799
0.331307 -0.053899
-0.076975 0.012086
-0.331692 -0.156696
0.115072 -0.081904
-0.369234 -0.081331
-0.255547 0.044433
-0.508260 0.048674
-0.379695 -0.177438
-0.090051 -0.227403

0.212538 -0.100245
-0.482120 -0.274745
-0.479356 -0.243111
-0.478384 -0.191884
0.571797 -0.329721
-0.490437 -0.039900
-0.580690 -0.050310
-0.556463 -0.001361
-0.452957 -0.315564
-0.559339 -0.100374
-0.530088 -0.111478
-0.572105 -0.031189
0.154427 0.041515
0.152365 0.013816
0.165096 0.039410
-0.333026 -0.295311
-0.410761 -0.155277
-0.194572 0.065693
0.005935 0.004931
-0.422844 -0.124635
-0.332167 -0.191455
0.162479 -0.036429
-0.437481 -0.050088
-0.534696 0.026312
-0.461967 -0.158672
0.176257 0.013776
0.165031 -0.014263
-0.520069 -0.212828
-0.513441 -0.179369
-0.568214 0.097664
-0.474198 -0.155227
-0.480366 -0.288677
-0.490261 -0.127005
-0.016715 0.051143
-0.330320 -0.152530
0.093230 -0.009916
-0.541553 -0.099353
0.004663 0.072178
-0.441940 -0.271664
-0.539052 -0.125166
-0.254832 -0.218169
-0.425717 -0.178484
-0.369815 0.035975
-0.108856 0.068279
-0.485832 -0.110074
0.035849 0.061948
-0.512567 -0.155094
0.058943 0.040036
-0.536206 -0.181950
-0.519343 -0.063028
-0.516983 -0.230188
-0.514303 -0.136459

-0.517335 -0.153985
-0.506046 -0.231169
-0.099137 0.087057
-0.163531 0.081315
-0.535667 -0.159125
-0.396523 -0.204919
-0.539507 -0.151482
-0.015663 0.055401
-0.219112 -0.204409
-0.479072 -0.037127
-0.317504 0.071970
-0.522079 -0.123060
-0.534284 -0.168090
-0.315430 0.063304
-0.534895 -0.189287
-0.435354 -0.134823
-0.138383 -0.141735
-0.181422 -0.046859
-0.527853 -0.169466
-0.421309 0.022969
-0.533359 -0.171555
-0.221825 0.091258
-0.085837 -0.346255
-0.374259 -0.026875
-0.520491 -0.124933
-0.316567 -0.118366
-0.477087 -0.068103
-0.558031 0.254832
0.572959 -0.413706
-0.048123 -0.286118
-0.185046 -0.159320
-0.603259 0.207027
-0.219391 -0.451354
-0.464094 -0.076257
-0.162927 -0.181159
-0.313381 -0.436989
-0.189950 -0.302781
0.007401 -0.079341
-0.384485 -0.383792
-0.491830 -0.169141
-0.215582 -0.019462
-0.297627 -0.043904
-0.283819 0.015454
0.315618 -0.012861
-0.015040 -0.003412
-0.199624 0.032577
-0.433861 -0.314439
-0.359968 -0.002968
-0.484238 -0.175527

disp06.dat

-0.829263 0.200827
-1.139197 0.042112
-0.255423 -0.142346
-0.549724 -0.064891
-0.882869 0.001453
-0.055840 -0.215642
0.756175 -0.529920
1.047123 -0.470327
0.823589 -0.502850
1.440849 -0.359540
0.936391 -0.005015
0.192175 -0.203886
-0.076414 -0.334695
-0.500961 0.323274
-0.739539 0.226568
-0.644835 0.264015
-0.567789 0.299880
-0.870842 0.161419
-0.913805 0.134745
-0.960800 0.117795
-1.008898 0.107461
-1.052150 0.103866
-1.089443 0.106239
-1.121727 0.112967
-1.150506 0.121427
-1.177388 0.127532
-1.201549 0.127984
-1.220610 0.122054
-1.232956 0.112759
-1.235215 0.101675
-1.222916 0.087879
-1.191685 0.068455
0.188782 -0.292194
0.352116 -0.361245
0.446586 -0.420471
0.494380 -0.468706
0.514616 -0.506855
0.525392 -0.534137
0.540066 -0.549273
0.566577 -0.552295
0.609679 -0.547264
0.672129 -0.538667
1.315066 -0.403905
1.183222 -0.444151
0.922465 -0.485617
0.997303 -0.002628
1.053823 -0.001403
1.106482 -0.004087
1.152400 -0.014064
1.189205 -0.032972

1.215836 -0.059993
1.233501 -0.091676
1.248098 -0.123031
1.263866 -0.152093
1.284358 -0.180939
1.316835 -0.214316
1.358709 -0.255298
1.401979 -0.304283
-0.013099 -0.304016
0.074586 -0.260386
0.338971 -0.145847
0.517860 -0.093957
0.722973 -0.047215
-0.421724 0.293224
-0.363558 0.216758
-0.324543 0.112183
-0.300590 -0.005480
-0.284474 -0.123304
-0.267582 -0.230137
-0.242565 -0.316590
-0.212684 -0.377355
-0.182931 -0.407109
-0.153476 -0.401345
-0.119553 -0.372326
-0.661794 0.218203
-0.767347 0.185918
0.057393 -0.221359
-0.332752 -0.091903
-0.615240 -0.028801
0.832259 -0.413008
0.974500 -0.407253
1.126541 -0.386420
1.269538 -0.347531
-0.271412 -0.274273
-0.242298 -0.364027
-0.208768 -0.429110
-0.139457 -0.462329
-0.338942 0.062346
-0.292821 -0.166364
-0.499294 0.257727
-0.377655 0.161464
-0.312850 -0.050753
-0.174609 -0.463444
-1.026454 0.112022
-1.031485 0.101555
-1.009420 0.072775
-1.015457 0.118029
-0.979404 0.053253
-0.938057 0.028633
-1.027323 0.088497
1.026627 -0.061046
1.047711 -0.096188

1.087651 -0.169245
1.157417 -0.243571
0.768953 -0.046364
1.066855 -0.133661
-0.689117 0.177817
0.532464 -0.419316
0.425280 -0.435387
0.353655 -0.385696
0.371270 -0.415581
0.382587 -0.434267
0.398713 -0.440641
0.469056 -0.426513
0.710470 -0.413178
0.195253 -0.275444
0.099859 -0.294592
0.218271 -0.226602
0.011889 -0.353164
0.366027 -0.159342
0.550465 -0.099118
-0.099587 -0.436645
-0.799969 0.154805
-0.452468 -0.046404
-0.432189 0.231093
-0.249312 -0.385896
-0.215765 -0.451174
-0.364059 0.017291
-0.179562 -0.486350
-0.332377 -0.085023
-0.305883 -0.193064
-0.279696 -0.296832
-0.138855 -0.487896
-0.852018 0.070273
-0.979370 0.114510
-0.773938 0.034526
-0.999799 0.118280
-0.883732 0.119178
-0.922403 0.111705
-0.954387 0.110983
-0.865209 0.084988
-0.825193 0.054492
1.113685 -0.203856
0.993696 -0.035913
0.886524 -0.127530
0.820264 -0.040482
0.943191 -0.025863
0.880797 -0.030260
0.864577 -0.083818
0.909845 -0.172221
0.897043 -0.339049
0.742734 -0.335059
0.308330 -0.342624
0.242364 -0.328829

0.200346 -0.304887
0.261823 -0.322251
0.341624 -0.299343
0.292810 -0.309371
0.224547 -0.322557
-0.727899 0.149945
0.596219 -0.091726
-0.522191 0.191487
0.407253 -0.152387
0.253538 -0.222783
0.131502 -0.295995
1.059055 -0.324606
-0.635865 0.156447
-0.269565 -0.099603
-0.405298 0.103908
-0.298190 -0.297663
-0.269694 -0.379455
-0.359181 -0.103756
-0.327146 -0.202295
-0.239319 -0.438485
-0.204114 -0.468217
-0.396995 -0.012030
-0.700213 0.007271
-0.866708 0.107038
-0.853862 0.110616
-0.805180 0.117325
-0.833440 0.112459
-0.722525 0.043057
-0.692905 0.026300
-0.647255 0.010479
-0.870741 0.098370
0.993182 -0.267118
0.844547 -0.049495
0.812058 -0.031679
0.750780 -0.036582
0.708945 -0.095650
0.691328 -0.052123
0.941204 -0.217440
0.409243 -0.297442
0.155046 -0.277254
0.046850 -0.223664
0.085042 -0.230647
0.115061 -0.227223
0.129463 -0.200002
0.168106 -0.179983
0.823936 -0.271532
0.038131 -0.363429
0.664229 -0.064245
-0.010703 -0.192810
0.658063 -0.252799
-0.458384 0.163212
0.071377 -0.238555

0.283937 -0.180949
0.155604 -0.254289
-0.180296 -0.137501
-0.560917 0.147275
0.766932 -0.208368
-0.770297 0.129284
-0.277564 -0.396440
-0.302993 -0.349568
-0.391250 -0.109244
-0.356460 -0.197088
-0.327585 -0.280336
-0.442661 0.063849
-0.758017 0.084046
-0.750567 0.096159
-0.561046 -0.025152
-0.708615 0.113939
-0.733288 0.104627
-0.565887 -0.012435
-0.598819 -0.015638
-0.749545 0.065566
-0.432457 -0.027501
-0.103229 -0.436378
0.730753 -0.148543
0.656166 -0.022088
0.535872 -0.009679
0.599968 -0.042624
0.678956 -0.026831
0.508702 -0.218004
0.227259 -0.173209
1.213045 -0.292024
-0.003725 -0.212015
-0.035304 -0.140793
0.017457 -0.148020
-0.014538 -0.075006
0.053069 -0.057238
0.051916 -0.324023
-0.075184 -0.194275
0.465624 -0.103829
-0.497328 0.117334
-0.407836 -0.061140
0.285122 -0.115961
0.497563 -0.305312
-0.676491 0.130154
0.413639 -0.066889
-0.053280 -0.192743
-0.297261 -0.336035
-0.344078 -0.303791
-0.364470 -0.250626
-0.390898 -0.182293
-0.676684 0.053552
-0.840795 0.133837
-0.480215 0.039377

-0.630830 0.098454
-0.670861 0.072091
-0.654207 0.085729
-0.508758 -0.035882
-0.479845 -0.077130
-0.660855 0.026454
0.589311 -0.169270
-0.425111 -0.106862
-0.091021 -0.462818
0.543747 -0.044351
0.523911 -0.012096
0.513225 -0.037693
0.532736 0.000450
-0.201079 -0.402845
0.557057 -0.097767
0.123888 -0.055499
-0.144206 -0.147823
-0.191537 -0.068160
-0.120282 -0.056249
-0.043571 0.041637
-0.209545 -0.149536
0.300061 -0.177574
0.160422 -0.174858
-0.535501 0.087801
-0.033459 -0.386509
-0.161592 -0.155991
-0.367966 -0.264631
-0.403945 -0.213949
-0.426574 -0.162977
-0.312023 -0.102065
-0.605195 -0.008098
-0.466353 -0.035264
-0.591308 0.054606
-0.616474 0.018549
-0.599987 0.117327
0.402101 -0.096988
-0.565615 -0.043452
-0.435887 -0.078043
-0.608978 0.038533
-0.457360 -0.102248
0.391088 -0.192198
0.398652 0.023171
-0.255549 -0.309523
0.396079 0.014268
-0.138331 -0.363410
0.395647 0.033674
0.399640 -0.029235
0.025623 0.045735
-0.255557 -0.088620
0.200214 -0.065369
-0.271736 -0.004267
-0.137918 0.105164

-0.513185 0.024145
-0.317229 -0.108477
0.045113 -0.239481
0.288241 -0.081174
-0.421377 -0.194191
-0.441005 -0.174076
-0.459785 -0.142128
0.606708 -0.319251
-0.495887 -0.041987
-0.573104 -0.033829
-0.559118 -0.004661
-0.349775 -0.241861
-0.543630 -0.066820
-0.506060 -0.079738
-0.569636 -0.022299
0.257929 0.069470
0.264658 0.032772
0.258430 0.070106
-0.189503 -0.257905
-0.373182 -0.119271
-0.077935 0.119840
0.101811 0.035392
-0.337974 -0.041221
-0.285180 -0.142283
0.276654 -0.034502
-0.328262 0.041294
-0.539729 0.011104
-0.394333 -0.078001
0.261525 0.044306
0.247151 0.014787
-0.469074 -0.131687
-0.487444 -0.120746
-0.567205 0.068873
-0.439287 -0.107653
-0.400590 -0.205463
-0.484835 -0.098075
0.111028 0.090420
-0.284428 -0.129828
0.180858 0.019109
-0.531956 -0.069070
0.118535 0.113690
-0.310083 -0.201601
-0.515135 -0.083698
-0.099158 -0.190690
-0.377806 -0.117229
-0.243214 0.117234
0.001270 0.114901
-0.393147 -0.015440
0.137593 0.101272
-0.441551 -0.066735
0.153562 0.076175
-0.487190 -0.103483

-0.519674 -0.051230
-0.439791 -0.138018
-0.501892 -0.096923
-0.483184 -0.098282
-0.399473 -0.139318
0.017182 0.137344
-0.030479 0.137431
-0.508118 -0.101141
-0.242246 -0.143891
-0.508965 -0.094187
0.085600 0.095698
-0.169511 -0.168634
-0.355160 0.059953
-0.186229 0.145667
-0.424683 -0.023436
-0.462202 -0.076187
-0.171209 0.135643
-0.463120 -0.096570
-0.280755 -0.058990
0.014671 -0.124496
-0.024532 -0.006566
-0.478215 -0.093888
-0.279952 0.110098
-0.440827 -0.072594
-0.094554 0.153463
-0.033467 -0.420011
-0.216099 0.045919
-0.400025 -0.025521
-0.153115 -0.065974
-0.332694 0.023015
-0.572718 0.245876
0.613383 -0.415721
-0.051266 -0.399096
-0.102965 -0.155004
-0.597611 0.192580
-0.159838 -0.466073
-0.415312 -0.072842
-0.087958 -0.143053
-0.246076 -0.414560
-0.055908 -0.305080
0.144786 -0.071115
-0.323614 -0.334551
-0.442211 -0.098773
-0.110835 0.027622
-0.193904 0.019056
-0.169645 0.078845
0.404397 -0.014181
0.122455 0.024945
-0.050625 0.086950
-0.385869 -0.250350
-0.244525 0.075112
-0.345988 -0.089100

Appendix B – Directions For Biaxial Annulus Fibrosus Lamella(e) Sample Dissection

The following pictorial directions provide an explanation as how to obtain single or multiple-lamella samples tested in Chapter 4. During this dissection, maintain hydration by spraying the tissue with saline.

1. Harvest the lumbar motion segment such that at least 5mm (along the long axis of the spine) is maintained on each adjacent vertebra using a bone saw.
2. Using rangeurs, remove trabecular bone from each adjacent vertebra.
3. Figure AB.1 shows the set-up just prior to fine dissection with the tools necessary: a scalpel handle, a 15 blade, a hemostat, and a tweezers without texture at the tip.



Figure AB.1 Initial Set-Up. The far left shows an L3-L4 motion segment, where the trabecular bone has been removed from each vertebra. The right shows the three tools

used in dissection. From left to right the tools are a scalpel handle with a 15 blade, a hemostat, and a tweezers without any texture at the tip.

4. Remove excess tissue from the surface of the vertebrae to reveal the cortical bone.
5. Remove excess tissue from the surface of the intervertebral disc to reveal the annulus fibrosus.
6. Remove annulus fibrosus tissue until the annulus fibrosus is level with the adjacent vertebrae. This will ensure the lamella(e) are attached to the vertebrae that will be cut in Step 9.
7. Cut down medially about 1mm, and use the scalpel to find a distinct lamella to begin cutting away. Once a small section is revealed, grab the section with the hemostat and gently pull the section away from the medial surface. Small fibers will appear connecting the adjacent lamellae. Maintaining tension with the hemostat, align the scalpel blade parallel to the medial lamella surface. Slowly slide the blade against the small fibers. Continue cutting these small fibers by maintaining tension with the hemostat and keeping the blade parallel to the medial surface until the sample is at least 10mm longer than needed. The resulting continuous lamellar surface will maintain fiber alignment at $\pm 30^\circ$ from the horizontal, shown in Figure AB.2.



Figure AB.2 Single Lamellar Surface Revealed.

8. Centered around the revealed lamellar surface, mark the each adjacent vertebra where two cuts should be made to form a 10 mm tab.
9. Stabilize the motion segment with a hemostat or another tool with one hand and cut at the marked locations using a rotating saw with the other hand. The result is shown in Figure AB.3.



Figure AB.3. Adjacent Vertebral Attachments Revealed

10. Using the rotating saw remove all cortical bone that will not remain attached to the final sample (keep the section that was just cut). The result is shown in Figure AB.4.

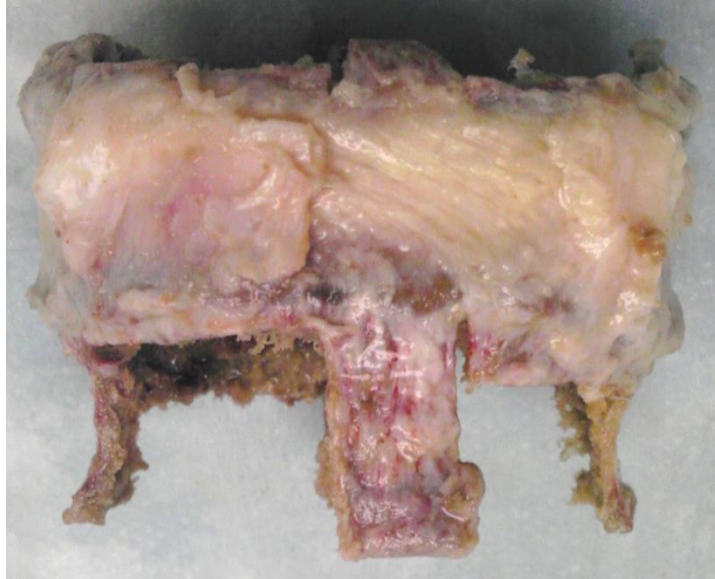


Figure AB.4. Motion Segment Following Excess Cortical Bone Removal

11. Using the rotating saw and/or the scalpel blade, cut the motion segment apart (along the long axis of the spine) maintaining the section with the single lamellar surface.

The result is shown in Figure AB.5.



Figure AB. 5. Motion Segment Following Cut Down Into Smaller Pieces

12. Separating the pieces, the sample that will be further dissected into a single or multiple-lamella sample, shown in Figure AB.6.



Figure AB.6. Sample Prior to Fine Dissection

13. The remaining cortical bone attached is the endplate and is for the axial vertebral attachments (that will become sample arms). Slide the scalpel blade along the interface of the endplate and the annulus fibrosus to remove all of the endplate except endplate in the region below the axial vertebral attachments. This will ensure the final annulus fibrosus is not cut away from the axial vertebral attachments.
14. Using the approach in step 7 and starting from the side that was nearest the nucleus pulposus (approach from the medial portion of the intervertebral disc), cut away lamellae until a single or desired number of lamellae are reached. This maintains the single lamellar surface that was obtained in Step 7 and creates the other single lamellar surface. The final single-lamella sample is shown in Figure AB.7.

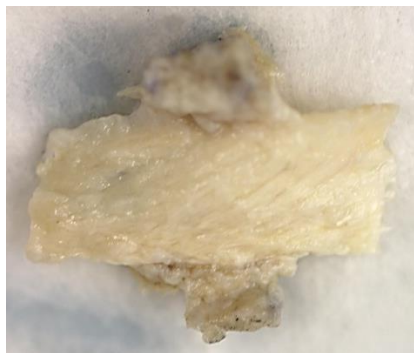


Figure AB.7. Final Single-Lamella Sample

Appendix C – Directions for use of JR3 load cells

These directions were created to describe how to set up and use the JR3 load cells due to their inherent complexity in measuring each possible force and moment. In conjunction with these directions, I collaborated with Dr. Hallie Wagner and Dr. Spencer Lake to write a LabView program to collect data from the load cells and communicate with the current actuator software.

1. General Warnings and Cautions

!! WARNING

Impact to the load cells will invalidate the calibration and may cause permanent damage.
Handle load cells with precision and care. Double-check actuator protocols to be sure load cells will not hit any object during use.

!! CAUTION

Liquid contact with the load cells and/or connected wiring may cause permanent damage.

Orient each load cell such that the connected wiring is at the top. Carefully pour saline away from the load cells. If you adjust any component in the saline bath, slowly remove your hands away from the load cells.

2. Purpose of the 6 Degree of Freedom Load Cells

The 6 degree of freedom load cells allow for data collection of three forces and three moments on each sample arm. As a result, additional care and attention needs to be paid to study design, equipment setup, and data analysis.

3. Description of the Load Cells and Associated Equipment

Equipment:

- Four 6 degree of freedom load cells and sensor and power boxes.

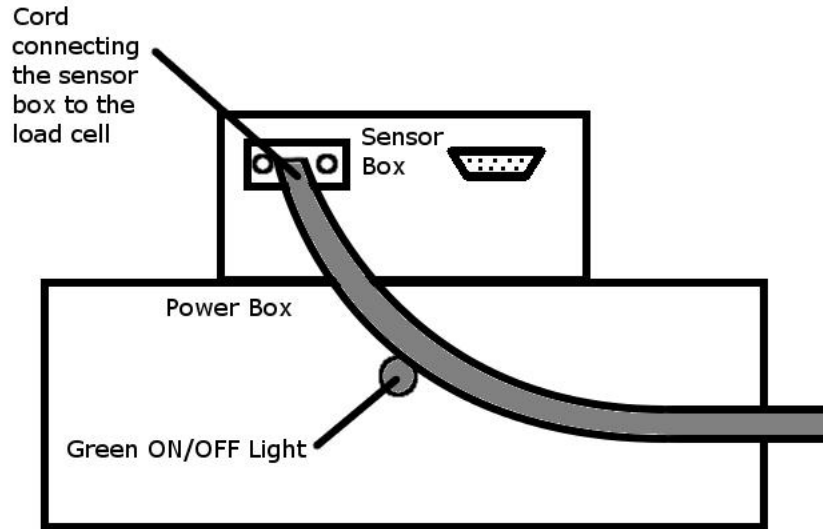


Figure AC.1. Front panels of sensor and power boxes.

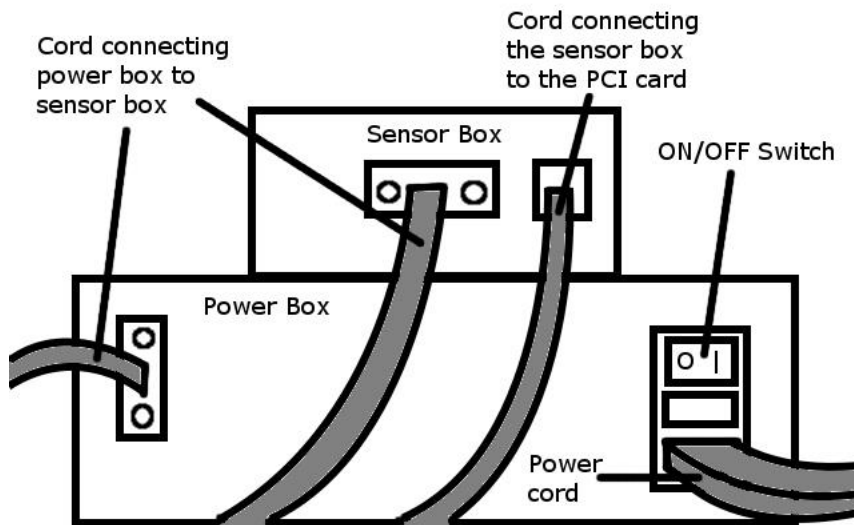


Figure AC.2. Back panels of sensor and power boxes.

Accessories:

- Four custom stainless steel grips with optional transverse sliding attachment

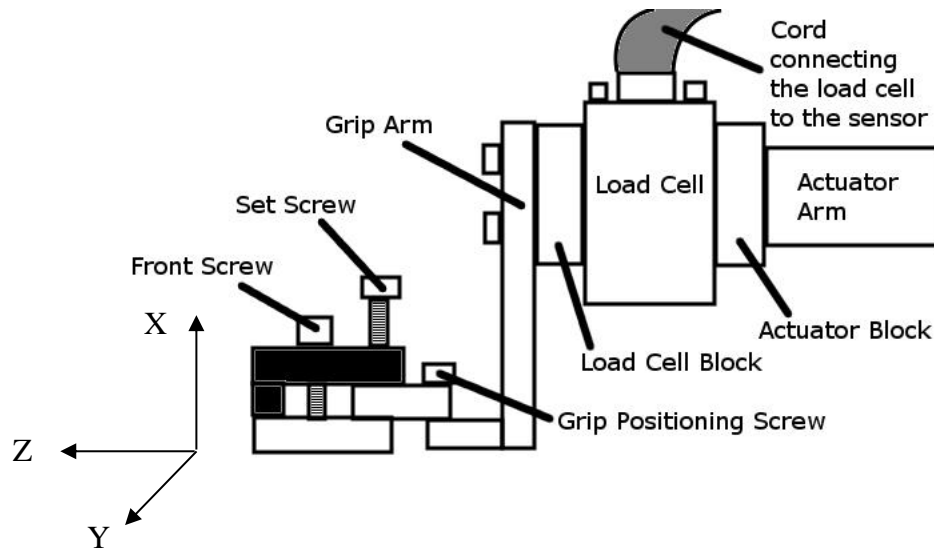


Figure AC.3. Grip and load cell setup with coordinate system.

The Z-direction is the normal direction, the Y-direction is the in-plane shear direction, and the X-direction is the out-of-plane direction. The moment directions follow placing your right thumb in the positive direction and curling your fingers around the axis.

Load Cell Specifications:

Degree of Freedom	Most Sensitive to Loads at	Upper Level of Sensitivity	Absolute Maximum Load (1.25 safety factor)	Digital Resolution
F _x	27 N	111 N	445 N	0.013 N
F _y	27 N	111 N	445 N	0.013 N
F _z	53 N	222 N	1246 N	0.025 N
M _x	1356 Nmm	5649 Nmm	19207 Nmm	1.0 Nmm
M _y	1356 Nmm	5649 Nmm	19207 Nmm	1.0 Nmm
M _z	1356 Nmm	5649 Nmm	13558 Nmm	1.0 Nmm

- Load cell accuracy: $\pm 0.25\%$ of the measuring range

4. Setup Instructions

The protocol below describes how to attach the load cells to the Instron and how to use the associated software.

The computer on the *right controls the Instron* (“Instron Control”), i.e. defines the protocol to move the actuator arms. The computer on the *left is connected to the load cells* (“6 DOF Load Cell Control”) and can read the load and moment values. From here on the computers will be referred to with these labels as they are also on the corresponding monitor of each computer.

Instron software Initialization (“Instron Control”)

1. Flip the ON/OFF switch on the Instron tower to ON.
2. Login to the “Instron computer”.
3. Double-click on the Instron Console icon on the desktop.
4. Double-click on the RS Save icon on the desktop.
5. Click “Restore” -> Select Independent or Modal Actuators -> Select all 4 channels -> Click “Select All” -> Click “Start”.
6. Click “X” to close RS Save.

Load Cell and Grip Attachment

(Pictorial steps given in Section A)

*All load cells need to be attached and on for **15 minutes** before testing starts.

NOTE: If using a saline bath, place the empty bath on the table in the correct position before continuing.

1. Remove the 5N load cells and connecting plate from each actuator.
2. Take grip #1 and remove the grip arm from the load cell block (Figure AC.3).
3. Then, remove the load cell block from the actuator block.
4. Loosely screw the actuator block into the Axis 1 Left actuator arm with the indented surface facing outwards.
5. Screw the actuator block in tightly using a square.
|!| CAUTION If the actuator block is not square with the table, the grips may not line up to attach the sample and/or unwanted forces and moments will be introduced to the test.
6. Carefully remove the Axis 1 Left load cell from its box.

7. Place the load cell against the actuator block with the cord connector and “this side up” sticker facing up and the screw tips aligned with the four holes on the actuator block.
8. Tighten the screws using the torque limiting Allen wrench (Figure AC.4).

!! CAUTION If the screws are not tightened in this order, moments are imposed on the load cell, which can damage the sensor.

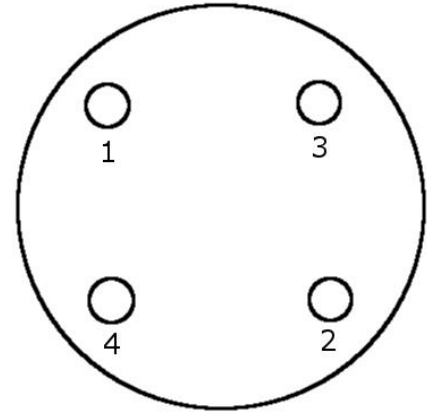


Figure 4. Screw tightening order

9. Place the load cell block against the load cell with the two screw holes oriented vertically. If they are not oriented vertically, the grip will not be attached in the correct orientation.
10. Tighten the screws using a screw driver (Figure AC.4).
11. Place the grip arm against the load cell block.
12. Tighten the screws using a screw driver.
13. Connect the cord from the Axis 1 Left sensor box to the Axis 1 left load cell #1 and tighten the screws.
14. Flip the ON/OFF switch to ON on the back panel of power box #1. This will turn on a green light on the front panel of the power box.
15. Repeat steps 2-14 with the components associated with Axis 1 right and Axis 2 rear and front associated grips and load cells.

Sample Preparation and Attachment

1. Prepare the sample as desired.
2. Load the sample into the grips one at a time.
 - a. Loosen the set screw so the tip does not touch the bottom surface.
 - b. Loosen the front screw so the grip can move up enough to bite the sample.
 - c. Place the sample into the grip.
 - d. Tighten the front screw.
 - e. Tighten the set screw $\frac{1}{4}$ turn past the bottom surface.
3. Repeat step 2 for each grip.

4. Measure the grip to grip distance along axis 1 and 2.
- 5.

Instron Initialize GPIB Signal (“Instron Control”)

NOTE: This section will ensure a start signal is sent correctly to the “6DOF Load Cell Control” computer during sample testing to save data.

1. Double-click on the Instron WaveMatrix icon on the desktop.
2. Click “Test” -> Click “Continue Project” -> Select your project -> Select the GPIB method (from WaveMatrix\Methods).
3. Click “Start”.
4. Click “Continue” in the “System Errors and Warnings” pop-up window.
5. Click “OK” in “Confirm Test Start...” pop-up window.

Instron Test Method Setup (“Instron Control”)

1. Click the “Home” button.
2. Click “Test” -> Click “Continue Project” -> Select your project -> Select your test method.
3. Click “Method” -> Click “Test” -> Click “Resources”.
4. Expand “Left” -> Click on “Digital Output 4” -> Click the right arrow (“Digital Output 4 (Left)” will appear in the right panel).
5. Click “Sequence” under “Test”.
6. Insert one step before the protocol starts.
7. Click in the Step 1, Digital Output 4 (Left) box -> Select “Set State to Low”.
8. In subsequent method steps, select “Set State to High” in the Digital Output 4 (Left) boxes.
9. Insert one step after the end of the protocol.
10. Click in the last step, Digital Output 4 (Left) box -> Select “Set State to Low”.
11. Click in the last step, Axis 1 Left box -> Click the “Hold” box -> Enter 10 seconds.
12. Click “Channels” -> “Click” Tracking”.
13. Select Axis 1 Left strain channel -> Enter the sample half-length in the gauge length.
14. Repeat Step 13 for the other actuators.

Labview Setup (“6 DOF Load Cell Control”)

1. Login to the computer (username: Tina, password: none just hit enter).
2. Double-click on the shortcut “JR3 Data Acquisition.vi”.
3. Type UNIQUE file names in Pre-Test and Test Data boxes (i.e. filename.lvm).
NOTE: It is recommended to append a reference to the load cell to the file name (i.e. 7Jan2014_1Left.lvm). File names cannot be the same as any other file in the folder.
NOTE: If you wish to record data at a different rate than 10 data points/sec, enter the new interval in the “Data Sampling Rate Box” (100 ms = 10 data points/sec).
4. Turn on “Save Axis # ___ Pre_Test Data?” and “Save Axis ___ Test Data?” for each load cell in BOTH the Pre-Test and Test data sections. Each button will shine green.
5. Turn on the “Start?” button. The button will shine green. This will show a live display of the loads and moments for each load cell in the Pre-Test area.
!! CAUTION If the display is static, loads and moments will not be recorded.
Click the stop button at the top left and close Labview. Double click on the JR3 icon on the desktop. Type 3114 into the Device ID box. Click the box with two horizontal arrows. Click “OK” in the pop-up window. Click the start button. You will see a live display of the loads and moments. Click the stop button. Close the window. Repeat instructions from step 2 of this section.

Zeroing Load Cells

1. Change the Pre-Test options to “Reset Offsets”.
2. Click the “Save Axis # ___ Pre-Test Data?” button for each load cell. Each green light will turn off.
3. Wait for each “Done Saving Pre-Test Data...” indicator to change from grey to light blue.
4. Click “Stop Pre-Test Data Saving” button (when “Done Saving..” indicators are ALL ON).
5. Wait one second.
6. Unclick “Stop Pre-Test Data Saving” button.

7. Click the “Save Load Cell # Pre-Test Data?” button for each load cell. Each green light will turn on.
8. Change the Pre-Test options to “Read Display”. (Each load should be zeroed now)

Testing

1. Apply a pre-load to the sample by moving the actuators with the Instron controllers on the table.
2. Click the Start button in WaveMatrix (“Instron Control”).
3. Click “Continue” in the “System Errors and Warnings” pop-up window (“Instron Control”).
4. Change the Pre-Test Options to “Wait for Testing to Start?” (“6 DOF Load Cell Control”).
5. Click the “Save Axis # ___ Pre-Test Data?” button for each load cell. Each green light will turn off (“6 DOF Load Cell Control”).
6. Wait for the “Done Saving Pre-Test Data” button to turn light blue for each load cell (“6 DOF Load Cell Control”).
7. Click “Stop Pre-Test Data Saving...” (“6 DOF Load Cell Control”).
8. Click “Wait for Instron to Start” in Labview (“6 DOF Load Cell Control”).
9. Click “OK” in “Confirm Test Start...” pop-up window in WaveMatrix (“Instron Control”).

!!| WARNING If you have loaded the wrong test protocol or amplitude, the load cells may be damaged if they hit any object on the table. This will invalidate the calibration. Keep your hand on the “STOP” button in WaveMatrix (“Instron Control”) and press it if anything is wrong.
10. Wait for the test to run and finish.
11. Click the “Save Axis # ___ Data...” button for each load cell. Each green light will turn off (“6 DOF Load Cell Control”).
12. Wait for the “Done Saving Test Data...” indicator to turn light blue for each load cell (“6 DOF Load Cell Control”).
13. Click “Stop Test Data Saving...” (“6 DOF Load Cell Control”).

14. Click “STOP TEST” in Labview (“6 DOF Control”) when the test is finished to stop data recording.

15. Click “Stop live charts” (“6 DOF Load Cell Control”).

NOTE: If an Labview error message appears after step 12, your data has saved, but the computer will need to be restarted if you want to run another test.

Sample Removal

1. Loosen the set screw on grip #1.
2. Loosen the front screw on grip #1.
3. Repeat steps 1 and 2 for each grip.
4. Remove the sample from the grips, keeping any saline away from the load cells and other electrical components.

Testing additional samples?

Close Labview completely, reopen the vi, and repeat from section “Instron Test Method Setup”.

Data Transfer

Load cell data are saved in C:\Documents and Settings\Tina\Data. Remove data from the folder by flash drive or email. Data not removed from the folder in one month will be deleted.

Grip Removal

1. Remove the screws in grip arm #1, and remove the grip arm.
2. Remove the screws in the load cell block (Figure AC.4), and remove the load cell block.
3. Loosen the screws in load cell #1 (Figure AC.4), while holding the load cell. Remove the load cell, and carefully place load cell #1 in load cell box #1.
4. Remove the screw in the actuator block, and remove the actuator block.
5. Disinfect the grip arm with bleach solution, rinse with DI water, and dry completely. If the grip arm is not cleaned properly, future users could be exposed to biohazards.
6. Put grip #1 back together without the load cell. This will ensure no parts are lost.
7. Repeat steps 1-6 for the remaining grips.
NOTE: If you used a saline bath, carefully remove the bath from the table now. Dispose of the saline in the sink, disinfect the bath with bleach solution, rinse with DI water, and leave to dry on the drying rack.
8. Replace the 5N load cells and connecting plates on the corresponding arms.

Computer Shutdown

“6 DOF Load Cell Control” Computer

1. Click “File” -> Click “Exit”.
2. Click “Don’t Save” in the pop-up window”
3. Logout of the computer.

“Instron Control” Computer

1. Click “X” to close WaveMatrix.

2. Click double arrow (at bottom of console) -> Click "X".
3. Logout of the computer.
4. Flip the ON/OFF switch on the Instron tower to OFF.

5. Post-Processing

At the end of testing, you will have four force files, one for each load cell. Each file has six columns: Fx, Fy, Fz, Mx, My, and Mz. If the testing protocol was followed, the first line of each file corresponds to when the actuator protocol began.

5. Troubleshooting

This section will detail how to respond to problems with the equipment.

Physical Damage to the Load Cells

Problem: One of the load cells was dropped or one of the load cells hit an object during the test.

Action: Contact the TML Supervisor immediately (4-0259) to report the situation. No further testing can be performed until the load cell is checked for damage and calibration.

Saline Contact with Electrical Components

Problem: Saline contacted the load cells or electrical cords.

Action: Quickly dry off any contacted equipment, avoiding any further contact with electrical connections. Then, contact the TML Supervisor immediately (4-0259) to report the situation. No further testing can be performed until the load cell is checked for damage and calibration.

Labview

Problem: The program won't start to view live loads before the test protocol starts.

Cause: The PLC board was not properly closed during previous use.

Action: Click the stop button at the top left and close Labview. Double click on the JR3 icon on the desktop. Type 3114 into the Device ID box. Click the box with two horizontal arrows. Click "OK" in the pop-up window. Click the start button. You will see a live display of the loads and moments. Click the stop button. Close the window. Reopen Labview.

Problem: The program won't show live loads during the test protocol.

Cause: No commands or incorrect commands were entered to send a GPIB signal.

Action: In WaveMatrix ("Instron Control")

1. Click "Method" -> Click "Test" -> Click "Resources".
2. Expand "Left" -> Click on "Digital Output 4" -> Click the right arrow ("Digital Output 4 (Left)" will appear in the right panel).
3. Click "Sequence" under "Test".
4. Insert one step before the protocol starts.
5. Click in the Step 1, Digital Output 4 (Left) box -> Select "Set State to Low".
6. In subsequent method steps, select "Set State to High" in the Digital Output 4 (Left) boxes.
7. Insert one step after the end of the protocol.
8. Click in the last step, Digital Output 4 (Left) box -> Select "Set State to Low".
9. Click in the last step, Axis 1 Left box -> Click the "Hold" box -> Enter 10 seconds.

Problem: One load cell won't show live loads. The other load cells are working fine.

Cause #1: The cords connecting the load cell to the sensor box and the sensor box to the power box may be loose.

Action #1: Check that the cord from the load cell to the sensor box is securely connected on both ends. Check that the two cords on the back panel of the sensor box are securely connected.

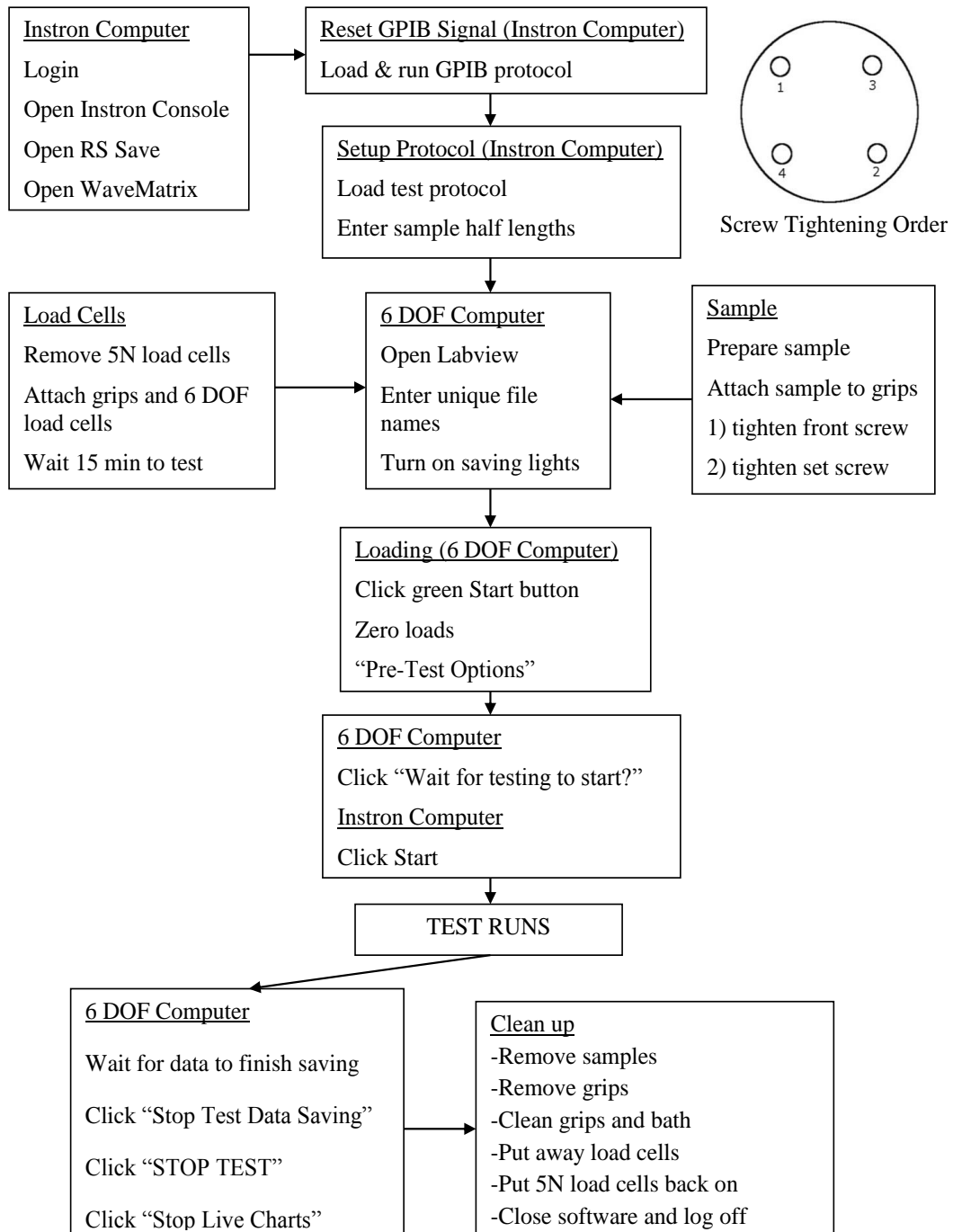
Cause #2: The cord connecting the load cell to the sensor box is connected to the wrong sensor box.

Action #2: Ensure each sensor box is connected to the correct load cell. (i.e. Axis 1 Left Load cell #1 to Axis 1 Left sensor box)

6. Summary

This page gives a brief description of the essential information.

This summary is not intended to replace complete user instructions. The entire manual should be read before any equipment is used.

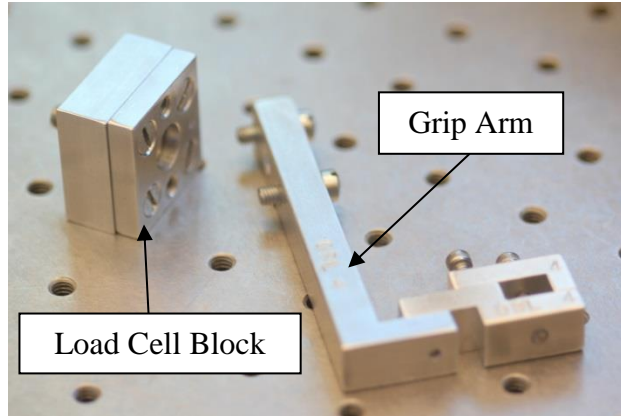


7. Date

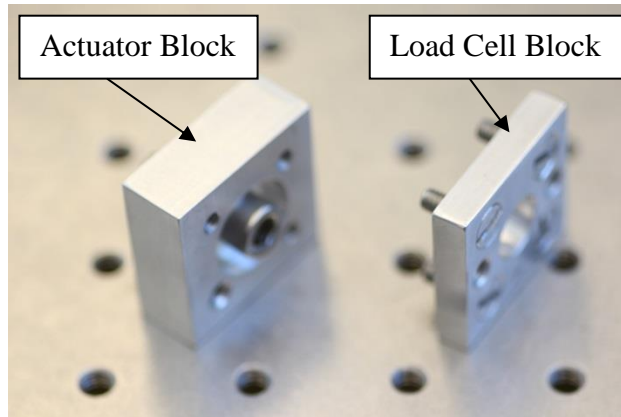
Created June 2013 by Tina M. Nagel.

Section A. Pictorial Load Cell and Grip Attachment

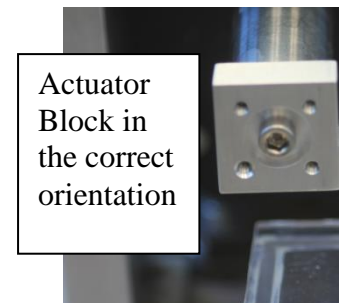
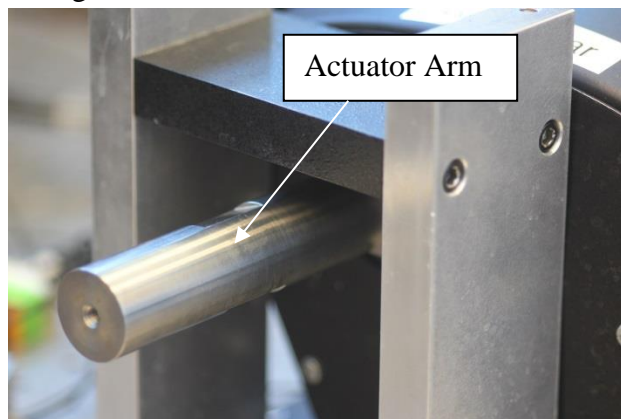
1. Remove the 5N load cells and connecting plate from each actuator.
2. Take grip #1 and remove the grip arm from the load cell block (Figure AC.3).



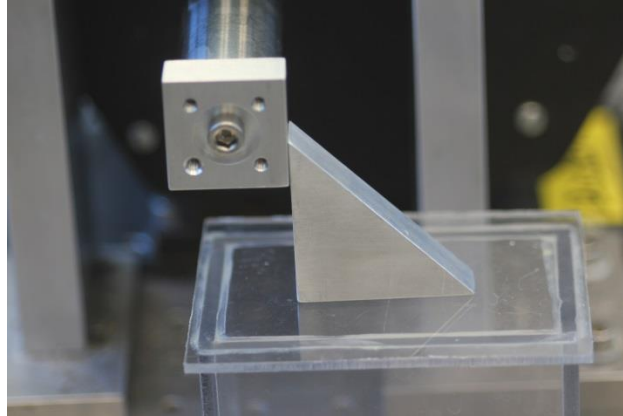
3. Then, remove the load cell block from the actuator block.



4. Loosely screw the actuator block into the actuator arm with the indented surface facing outwards.

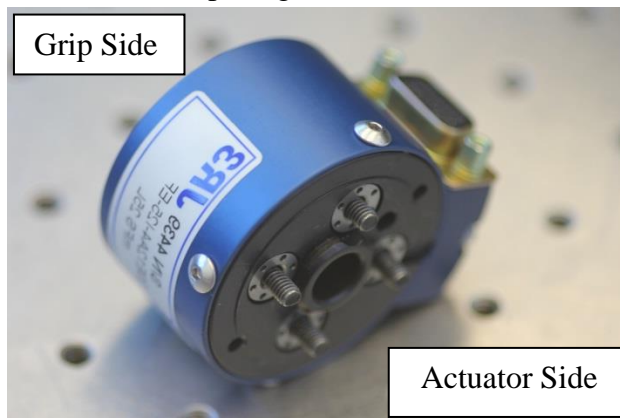


5. Screw the actuator block in tightly using a square.



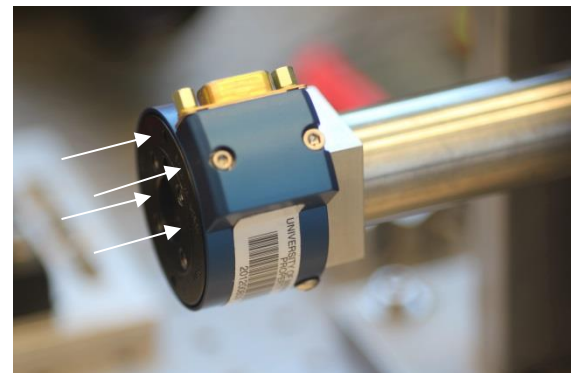
!! CAUTION If the actuator block is not square with the table, the grips may not line up to attach the sample and/or unwanted forces and moments will be introduced to the test.

6. Carefully remove load cell #1 from its box.
7. Place the load cell against the actuator block with the cord connector facing up and the screw tips aligned with the four holes on the actuator block.



8. Tighten the screws using the torque limiting Allen wrench (Figure AC.4).

!! CAUTION If the screws are not tightened in this order, moments are imposed on the load cell, which can damage the sensor.



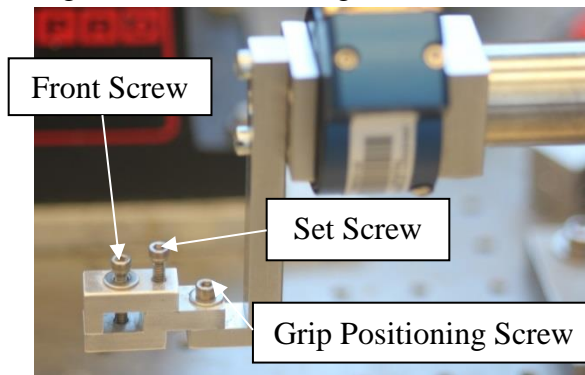
9. Place the load cell block against the load cell with the two screw holes oriented vertically. If they are not oriented vertically, the grip will not be attached in the correct orientation.

10. Tighten the screws using a screw driver (Figure AC.4).

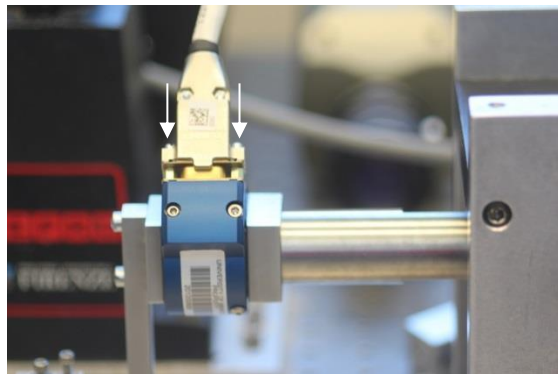


11. Place the grip arm against the load cell block.

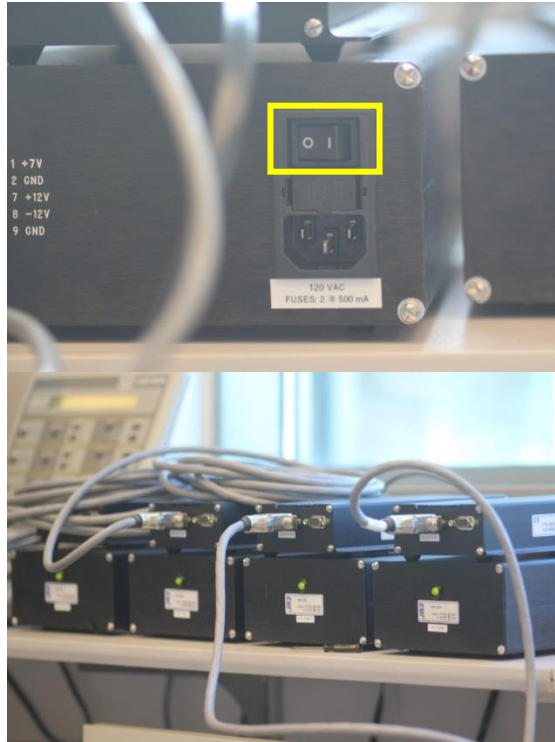
12. Tighten the screws using a screw driver.



13. Connect the cord from sensor box #1 to load cell #1 and tighten the screws.



14. Flip the ON/OFF switch to ON on the back panel of power box #1. This will turn on a green light on the front panel of the power box.



Appendix D – Quantitative T2* (T2 star) Relaxation Times Predict Site Specific Proteoglycan Content and Residual Mechanics of the Intervertebral Disc Throughout Degeneration

In collaboration with Dr. Arin Ellingson, I quantified the biochemical content of the tissue analyzed within this work. Quantifying biochemical content in this study provided a useful opportunity to learn the assays before utilizing them within my dissertation work.

Work described here is reprinted with permission.

Ellingson et al. “Quantitative T2 (T2 star) relaxation times predict site specific proteoglycan content and residual mechanics of the intervertebral disc throughout degeneration” Journal of Orthopaedic Research. 2013. 32. 1083-1089.*

Introduction

The intervertebral disc (IVD) affords the spine its extensive multidirectional motion due to the complex interaction between two morphologically, biomechanically, and biochemically distinct regions: the annulus fibrosus (AF) and the nucleus pulposus (NP). The AF consists of highly organized, concentric rings of fibrocartilaginous material surrounding the NP, which is composed of a hydrated, disorganized matrix of collagen and proteoglycans (Roughley 2004). When a load is applied to the spine, the hydrated NP acts like a pressure vessel, placing the AF in tension (Michael A Adams and Roughley 2006). This unique system allows the disc to absorb and dissipate large compressive loads applied to the spine.

Degeneration of the intervertebral disc is a progressive phenomenon that occurs in response to age, injury, pathology, or more likely a combination of these (Michael A Adams and Roughley 2006; JP and S 2003). Increased or abnormal mechanical loading leads to alterations in the discs' biochemical composition (Michael A Adams and Roughley 2006). These changes lead to diminished mechanical competency resulting in the discs' inability to maintain its structure and function potentially causing discogenic pain or pain due to cord occlusion, neural compressive lesions, or nerve root pinching, from altered spinal stability (M. A Adams 2004). It is of critical interest to detect these changes early in the degeneration process in order to cease the progression with the development of new therapeutics including biologics and other treatments.

Direct measurement of the discs' biochemical content is not possible *in vivo*; therefore magnetic resonance imaging (MRI) is used to evaluate disc health. Unfortunately, current clinical imaging techniques do not adequately assess degeneration, especially in the early stages (Luoma et al. 2001). New quantitative MRI techniques are being developed to overcome the subjectivity in interpreting imaging findings. These techniques include T1 ρ , magnetization transfer, T2 mapping, and T2* mapping. Although some of these are promising, quantitative T2* (T2 star) is a multi-echo gradient-echo technique, rather than a multi-echo spin-echo technique of traditional T2 mapping. The relaxation time is a combination of the inherent "true" T2 relaxation and additional relaxation due to magnetic inhomogeneities ($1/T2^* = 1/T2 + 1/T2'$, where T2' is the relaxation due to magnetic field inhomogeneities) (Chavhan et al. 2009). Therefore T2* has the capability of measuring ultrashort relaxation times; providing the added benefit of a short acquisition time, high signal-to-noise ratio, along with three-dimensional capabilities (Welsch et al. 2011; Krause et al. 2010; Mamisch et al. 2012). T2* is a clinically available scan approved by the FDA. Traditional T2 mapping has been shown to correlate with hydration, but to a lesser degree with proteoglycan and collagen concentration and organization (Weidenbaum et al. 1992; Terti et al. 1991; Marinelli et al. 2009). T2* relaxation times provide information regarding the biochemical properties of the tissue, specifically interrogating water mobility within the

macromolecular network, and has been shown to be beneficial in cartilage imaging (Goetz Hannes Welsch et al. 2011; Krause et al. 2010; Mamisch et al. 2012; Goetz H Welsch et al. 2010; Williams et al. 2010; Bittersohl et al. 2012; Williams, Qian, and Chu 2011; Marik et al. 2012; Miese et al. 2011). Recent studies have expanded T2* imaging to the intervertebral disc (Goetz Hannes Welsch et al. 2011; Hoppe et al. 2012). Welsch et al. reported a significant correlation between T2* relaxation time and the degree of degeneration based on Pfirrmann grades in subjects with low back pain (Goetz Hannes Welsch et al. 2011). Hoppe et al. utilized axial T2* maps and also found a significant correlation between T2* relaxation time and Pfirrmann grade (Hoppe et al. 2012).

Intervertebral disc degeneration typically begins in the nucleus pulposus with the breakdown of hydrophilic proteoglycans (Roughley 2004; Antoniou et al. 1996). This leads to a loss of hydration resulting in a decrease in the hydrostatic pressure, as well as the compressive residual stress and strain of the disc (Pearce, Grimmer, and Adams 1987; Buckwalter 1995; Ellingson and Nuckley 2012; Johannessen and Elliott 2005). The loss of hydration affects the interactions between the NP and AF, resulting in a diminished ability to properly absorb loads. Later stages of degeneration include modification in collagen synthesis and degradation and eventually disc collapse. Altogether the degradation in biochemical content affects the mechanical response and structural integrity of the disc. Noninvasive evaluation of the biochemical composition of the intervertebral disc potentially has a profound impact on the assessment of degeneration.

Although T2* has been shown to be correlated with disc degeneration, the relationship between T2* relaxation time and the intervertebral disc constituents has yet to be established. The objective of this study was to determine the relationship between regional quantitative T2* measures and corresponding sulfated-glycosaminoglycan, total collagen content, and residual mechanical properties. The hypotheses tested in this study are that T2* relaxation time is able to

predict the following site-specific parameters (i) sulfated-glycosaminoglycan content, (ii) hydroxyproline content, (iii) water content, (iv) residual stress, and (v) and excised strain.

Methods

Eighteen human cadaveric lumbar (L4-L5) intervertebral discs (53.2 ± 15.5 yrs; range: 21-71 yrs) were imaged using a Siemens 3T MRI scanner (Magnetom Trio; Siemens Healthcare, Erlangen, Germany), Figure AD.1. Each specimen was placed in the prone position inside a brain coil where traditional T2 weighted and quantitative T2* MR images were acquired in the Sagittal plane. The scans were performed consecutively. To provide context for the relative disc health, Pfirrmann grade was assessed independently by 7 spine surgeons and 3 experienced spine researchers based on the T2 weighted MRI (Pfirrmann et al. 2001). These scores were averaged and rounded to the nearest integer. The graders are all either established neurosurgical / orthopedics surgeons or Ph.D. level trained researchers. Quantitative T2* relaxation maps (MapIt, Siemens Healthcare, Erlangen, Germany) were obtained using the following imaging parameters [TR(ms): 500; TE(ms): 4.18, 11.32, 18.46, 25.60, 32.74, 39.88; Voxel Size(mm): 0.5x0.5x3.0, Slices: 33]. Five test sites were isolated across the transverse plane of the IVD and mean T2* relaxation time was recorded using Osirix Imaging Software at each region of interest (ROI) (Figure AD.2A). The sites, displayed in Figure AD.2, included one in the center nucleus pulposus (NP) and four in the annulus fibrosus (AF), including three outer AF areas: anterior (aAF), posterior (pAF), and lateral (oAF), as well as one inner lateral region (iAF). The lateral test sites were randomized left or right based on a block design based on Pfirrmann grade. A correlational study design was used to examine the relationship between quantitative T2* relaxation time and IVD constituents and residual mechanics properties.

Following imaging, local mechanical properties were measured, including the residual stress and strain, at each location using a hybrid confined/*in situ* indentation methodology (Figure AD.2B) (Ellingson and Nuckley 2012). This technique utilizes the cartilaginous endplate as a

porous indenter by releasing a 3 mm diameter portion of the endplate, while leaving the superior endplate contiguous with the IVD inferiorly. Following excision of the endplate, the released section increased in height, indicating the presence of an internal residual stress. The height increase was used to calculate the excised strain (ϵ_R) by dividing the change in height increase by the original site-specific disc height, calculated from the T2 weighted MR images using the linear measurement tool in Imaging Software (Osirix Imaging Software) to measure the distance between endplates at each ROI.

Stress relaxation tests were performed using an Instron microtester (5548 Instron, Norwood, MA) equipped with a 3 mm diameter indenter tip. The endplate was re-positioned back to its original height with the indenter and allowed to equilibrate for 900 seconds; the equilibrium residual stress was determined by dividing the applied equilibrium force over the 3mm indenter tip area.

Subsequent biochemical analysis was performed at each of the test site investigating sulfated-glycosaminoglycan (s-GAG) and hydroxyproline content. A sharp 3 mm punch was used to remove the endplate-disc-endplate construct at each test site (Figure AD.2C). Both endplates were then removed and the cylindrical disc sample was divided in half along the transverse axis. In a randomized fashion, the superior or inferior section was used to quantify either s-GAG or hydroxyproline content. To determine s-GAG content, disc samples were dried at 60°C to constant dry weight, and a commercially available 1,9 dimethylmethylene blue assay was used (Astart Biologics Rheumera, Proteoglycan Detection Kit, Redmond, WA), and s-GAG content was normalized by dry weight ($\mu\text{g}/\mu\text{g}$) (FARNDALE, BUTTLE, and BARRETT 1986). Total protein content was determined as described previously (Starcher 2001). Hydroxyproline content was determined as described previously, omitting lyophilization (Stegemann and Stalder 1967). Hydroxyproline content was normalized by total protein content ($\mu\text{g}/\mu\text{g}$). Dry weights were not available for the hydroxyproline sections. Water content ($\%\text{H}_2\text{O}$) was also calculated as (wet weight-dry weight)/wet weight at each location.

While Pfirrmann grading provided a categorical value for each sample's independent variable, it was used to contextualize the findings and all results were assessed as continuous data without grouping. Pearson's correlation tests were performed between regional T2* relaxation time (ms) and corresponding biochemical content and residual stress and strain to define the relationship between imaging parameters and the discs' constituents. Each of the hypotheses was tested and acceptance was established based on an alpha of 0.05.

Results

Eighteen L4-L5 discs were imaged, and T2* relaxation times were recorded in five regions. Each test site was then tested mechanically and biochemical composition was measured. Following grading of disc health, the cohort was determined to be from the entire degenerative spectrum (Pfirrmann grades: 3 grade I; 2 grade II; 9 grade III; 2 grade IV; 2 grade V). Pfirrmann grade was found to be significantly correlated with average T2* relaxation time (ranged from 9.1 to 91.6 ms) in the NP ($r=-0.891$; $p<0.001$) and iAF ($r=-0.749$; $p<0.001$) but not pAF ($r=-0.460$; $p=0.055$), oAF ($r=-0.387$; $p=0.113$), or aAF ($r=-0.297$; $p=0.232$).

Correlations were found between the imaging parameters and the discs' constituents. The mean T2* relaxation time was positively correlated with sulfated-glycosaminoglycan normalized by dry weight in all five regions of interest shown in Table AD.1. This relationship was particularly strong in the NP ($r=0.944$; $p<0.001$) and inner AF ($r=0.782$; $p<0.001$). Figure AD.3 displays the correlations between T2* relaxation time and s-GAG (3A), excised strain (3B), and residual stress (3C) for both NP (black) and inner AF (gray). T2* relaxation times of the NP, inner AF, and outer AF were significantly correlated with both excised strain and residual stress. The posterior AF T2* time was also correlated with residual stress. Hydroxyproline, a relative measure of collagen content, normalized to total protein was only significantly correlated with the outer AF ($r=-0.568$; $p=0.014$). Water content (%H₂O) was significantly correlated with T2* value

in the posterior AF region only. All metrics were found to be significantly correlated with the corresponding T2* relaxation time when all locations were grouped.

Discussion

Quantitative T2* MRI is a multi-echo gradient-echo technique where the relaxation time is a combination of the inherent “true” T2 relaxation and additional relaxation due to magnetic inhomogeneities ($1/T2^* = 1/T2 + 1/T2'$, where T2' is the relaxation due to magnetic field inhomogeneities). T2* mapping has been shown to be beneficial in cartilage imaging providing information regarding the spatial macromolecular architecture and interaction with water mobility (Krause et al. 2010; Mamisch et al. 2012). T2* relaxation times were found to be related to histological grades of degeneration in the hip joint, where a decrease in T2* relaxation time was found to be significantly correlated with a higher degree of cartilage degeneration. Also, a significant correlation was determined between T2* relaxation time and disc health assessed via Pfirrmann grade (Krause et al. 2010; Hoppe et al. 2012). This study expands upon these principals and utilizes the T2* technique to investigate the relationship between T2* relaxation times and the corresponding biochemical composition and mechanical competency of the intervertebral disc.

The loss of proteoglycans is an early stage of disc degeneration marker; therefore it is of critical interest to be able to estimate the proteoglycan content of the intervertebral disc noninvasively. As hypothesized, the present study found T2* relaxation time at all five locations (NP, iAF, oAF, aAF, pAF) were significantly and positively correlated with the sulfated-glycosaminoglycan content. An especially strong linear relationship was discovered in the NP ($r=0.944$; $p<0.001$) and inner AF ($r=0.782$; $p<0.001$). Interestingly, there was not a strong correlation between T2* relaxation time and the water content, as hypothesized at individual test sites, other than the oAF. Though there was weak correlation observed on the whole disc and a

trend in the NP that approached significance. This suggests T2* may be able to detect the proteoglycans of the disc based on their interactions with water, not just the hydration level alone.

The results herein are contrary to previous work investigating the relationship between proteoglycan content of the disc and imaging parameters from various MRI techniques, such as T2 mapping, T1, and T1 ρ . Weidenbaum et al. reported a lack of significant correlation between 1/T2 and proteoglycan content, however the scans were performed in a low strength (0.5 tesla) magnet (Weidenbaum et al. 1992). Marinelli et al. reported a moderate correlation between T2 relaxation time and proteoglycan content in the nucleus pulposus ($r^2=0.73$; $p=0.06$), but not in the annulus fibrosus ($r^2=0.45$; $p=0.21$) (Marinelli et al. 2009). Each of these studies did report a significant correlation between T2 and water content (Weidenbaum et al. 1992; Marinelli et al. 2009). It is important to note Marinelli et al. was limited to a low sample size of human disc material ($n=5$). Benneker et al. conducted a similar study with a larger sample size from the entire degenerative spectrum and found a significant relationship between T2 values and water as well as the proteoglycan content (Benneker et al. 2005). The inconsistent data surrounding T2 weighted MRI led to the development of other imaging protocols, such as T1 ρ .

Johannessen et al. reported a correlation coefficient of $r=0.67$ ($p<0.01$) between T1 ρ value and s-GAG per dry weight in non-degenerative discs with a Pfirrmann grade of 3.5 or less (Johannessen et al. 2006). They also found a significant correlation between T1 ρ and water content. Other studies have also established the relationship between T1 ρ and proteoglycans in both articular cartilage and the disc (Auerbach et al. 2006; Blumenkrantz and Majumdar 2007; Wheaton et al. 2005). Nguyen et al. aimed to evaluate the functionality of T1 ρ in more degenerative discs and determine the relationship between T1 ρ values and the mechanics of the NP (Nguyen et al. 2008). The previous relationships with proteoglycans ($r=0.69$; $p<0.05$) and water content ($r=0.53$; $p<0.05$) were confirmed, but were not significant when corrected for the

intercorrelations within the same spine. They did find a significant correlation with the swelling pressure ($r=0.59$; $p<0.05$) of the NP.

T2* relaxation times were hypothesized to be correlated to both the residual stress and excised strain. As postulated, this study found T2* values to be significantly correlated with the residual stress in all test locations except the anterior AF. The excised strain was also found to be significantly correlated with T2* relaxation time in the NP, inner AF, and outer AF. In particular, the NP displayed a very strong correlation with residual stress ($r=0.857$; $p<0.001$) and excised strain ($r=0.816$; $p<0.001$), indicating T2* mapping's ability to detect changes in the mechanical behavior of the disc. The discs' excised strain ranged from a 30% increase in height following release of the endplate to no change, while the residual stress ranged from 0.20 to 0 MPa as discs progressed from healthy to severely degenerated. These values are similar to previously published work using this technique, as well as those reported for pressures *in vitro* and *in vivo* (Ellingson and Nuckley 2012; Nguyen et al. 2008; Andersson, Ortengren, and Nachemson 2014; Wilke et al. 2001). Representative T2* MR images of a healthy, moderately degenerated, and severely degenerated discs are displayed in Figure AD.4 with their respective T2* relaxation time, s-GAG content, and residual stress values overlaid at each test location. These plots provide a glimpse into the progression of disc degeneration as it affects the biochemistry and biomechanics in a site-specific fashion.

The limitations of the present study include the use of cadaveric tissue, where imaging was conducted without any external soft tissue of a motionless specimen at room temperature. Although care was taken to minimize the effect from the adjacent test sites on the current test site during the indentation protocol, this interaction was not characterized. Dry weights were not available for the samples used to quantify hydroxyproline content, therefore they were normalized by total protein, which is less reported and more difficult contextualize and compare against other studies. Multiple freeze-thaw processes necessary for other aspects of the entire

study could have affected the hydration levels of the disc although attempts were made to standardize hydration protocols.

The inclusion of discs from the entire degenerative spectrum allows for the evaluation of the T2* technique. This sequence seems to be sensitive in detecting the early changes in the NP, which is reflected by the large differences in relaxation times at the 'healthier' end of the spectrum. The absolute changes become less for the more degenerative tissues, while still maintaining the observed linear relationship. In other words, the T2* relaxation time drastically decreases early in the degeneration process, similar to the proteoglycan content, then slows down during later stages. It is especially important to note that the majority of the discs included in the study are healthy to moderately degenerated (Pfirrmann Grades I-III) and this technique was able to stratify these discs. Since there was no a priori knowledge of these relationships, a linear fit was first attempted. Future studies should explore the possibility of more complex interactions or equations. Furthermore, since these correlations do not reveal causality, future research should examine the molecular mechanisms whereby T2* relaxation is affected by proteoglycan content. However, a potential explanation of this relationship is the T2* signal is not only influenced by the true T2 relaxation, but also the inhomogeneities of the local magnetic field. The disorganized matrix of the hydrophilic proteoglycans in the disc cause disturbances in the local magnetic field and thus impacts the T2* signal.

The strong correlations obtained in this study between T2* relaxation time and s-GAG, residual stress, and excised strain highlight this technique's ability to predict the health of the disc on a biochemical and mechanical level. T2* relaxation time may serve as a biomarker of both proteoglycan content and mechanical function in the detection of disc degeneration using a currently available technology. T2* mapping is fast, reliable, and available on all clinical 3T MRI systems and may serve as a biomarker for disc health, thus improving patient stratification allowing for more specifically targeted strategies with the development of new therapeutics.

Source of Funding

Funding was provided through NIH/NIAMS grants T32 AR050938 and T32 AR056950.

Table AD.1. Correlations Between T2* Relaxation Time (ms) and s-GAG, Hydroxyproline, Water Content, and Residual Mechanics (r: Pearson's correlation coefficient; p: p-value * represents significance at p=0.05).

		T2* Relaxation Time (ms)					
		NP	iAF	oAF	aAF	pAF	All
sulfated-Glycosaminoglycan	r	0.944	0.782	0.647	0.569	0.474	0.586
	p	<0.001*	<0.001*	0.004*	0.014*	0.047*	<0.001*
Hydroxyproline/Total Protein	r	0.071	0.322	-0.568	-0.153	0.226	-0.217
	p	0.778	0.193	0.014*	0.543	0.368	0.040*
Excised Strain	r	0.816	0.516	0.485	-0.040	0.405	0.412
	p	<0.001*	0.028*	.041*	0.874	0.095	<0.001*
Residual Stress	r	0.857	0.535	0.668	0.242	0.527	0.347
	p	<0.001*	0.022*	0.002*	0.332	0.025*	0.001*
Water Content	r	0.465	0.330	0.341	0.032	0.572	0.427
	p	0.052	0.181	0.166	0.900	0.013*	<0.001*

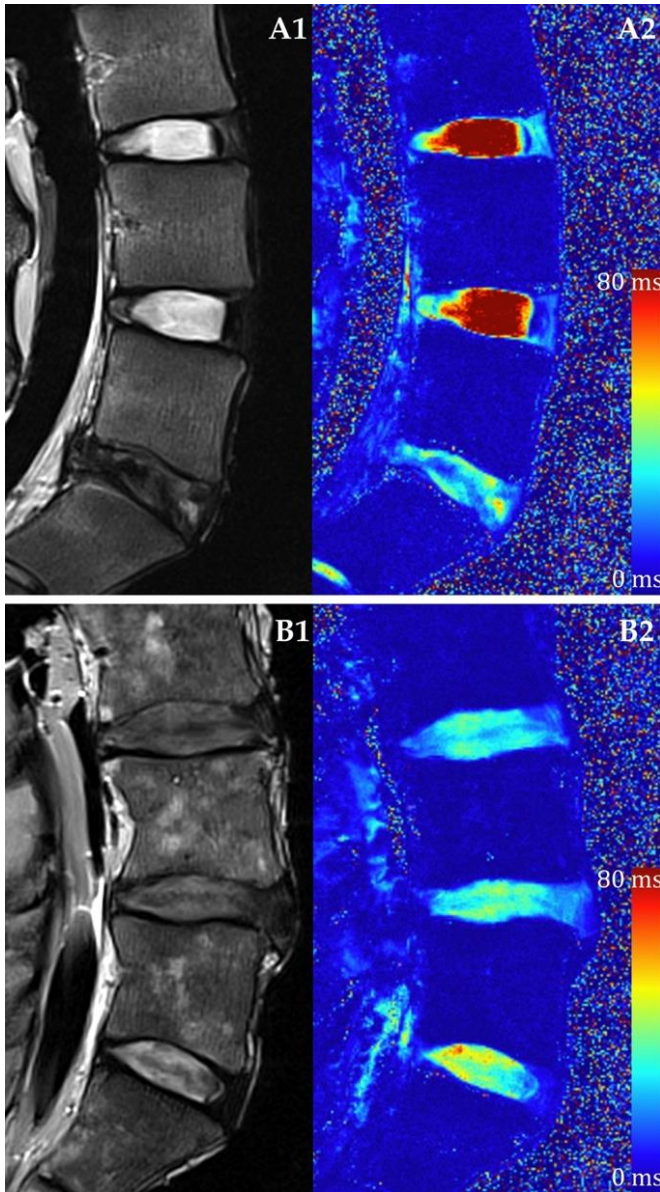


Figure AD.1. Representative T2 weighted MRI and T2* Relaxation Time Mapping. (A) Healthy lumbar intervertebral discs and (B) degenerated discs using a (1) conventional T2 weighted imaging sequence and (2) quantitative T2* mapping techniques.

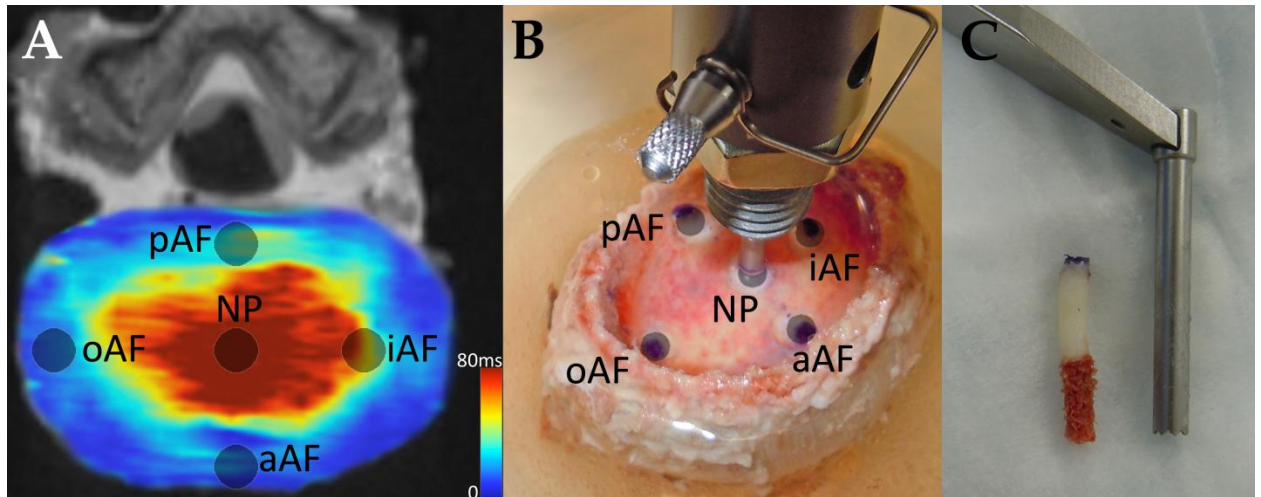


Figure AD.2. Intervertebral disc test sites (NP: nucleus pulposus, AF: annulus fibrosus, o: outer, i: inner, a: anterior, p:posterior). A. Site locations on a transverse slice of a quantitative T2* map. The average T2* relaxation time was measured at each site. B. Same test locations on a specimen undergoing stress relaxation tests using hybrid confined/*in situ* indentation methodology to compute the residual stress and excised strain of the tissue. C. A 3 mm punch was used to remove a plug of tissue at the same locations where indentation tests were performed, and where MRI relaxation times were recorded. The endplate and inferior trabecular bone were removed prior to biochemical quantification. In a randomized fashion, the superior or inferior section was used to quantify either s-GAG and water content or hydroxyproline content.

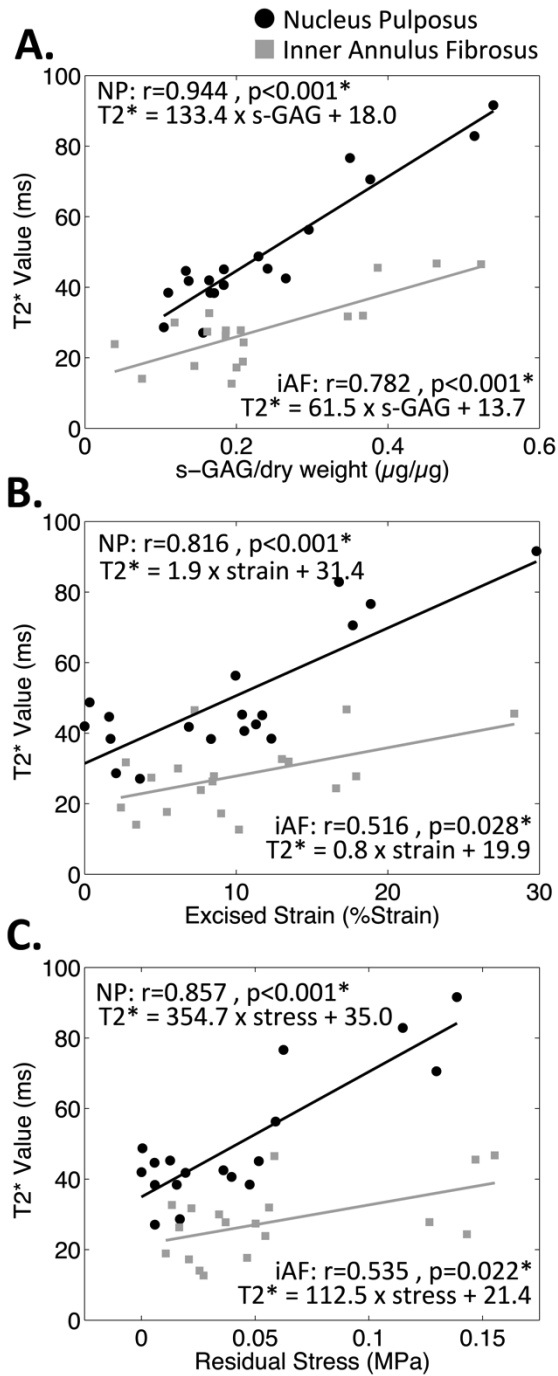


Figure AD.3. T2* Relaxation Time Correlational Plots of the Nucleus Pulposus and Inner Annulus Fibrosus Regions. Nucleus pulposus data is shown in black and inner annulus fibrosus data is shown in gray. Pearson’s correlational coefficient, r , and p -value, p , are displayed on corresponding plots along with the linear regression equation. A- T2*

vs. s-GAG content (% dry weight). B- T2* vs. excised strain (%strain). C- T2* vs. residual stress (MPa).

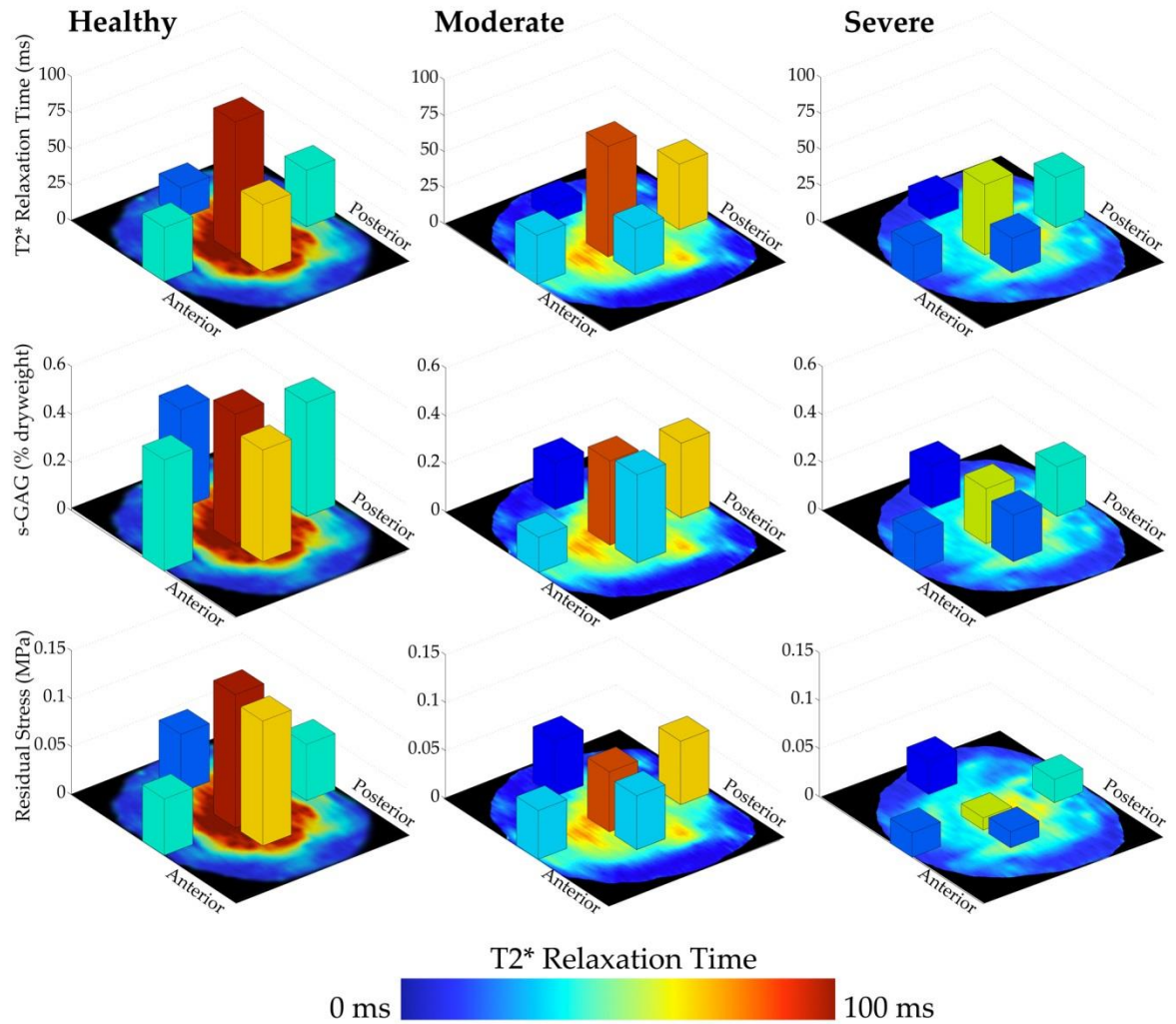


Figure AD.4. Representative Transverse T2* MR Images of a Healthy, Moderate, and Severely Degenerated Intervertebral Disc with Corresponding T2* Relaxation Times, s-GAG Content, and Residual Stress. Bars displayed atop each MR image denote T2* Relaxation Time, s-GAG Content, and Residual Stress at representative test locations: NP, anterior AF, posterior AF, lateral outer AF, and lateral inner AF. The color of the bar is dictated by the T2* relaxation time according to the scale. Healthy: Pfirrmann Grade 1. Moderate: Pfirrmann Grade 3. Severe: Pfirrmann Grade 5.